TEMPERATURE PREDICTION OF INDUCTION MOTORS FROM ESTIMATED PARAMETERS AND LOSSES

Thesis submitted by

Mr. Diptarshi Bhowmick

Doctor of Philosophy (Engineering)

Department of Electrical Engineering
Faculty Council of Engineering & Technology
Jadavpur University
Kolkata, India

2024

Index No. 123/17/E

Title of the Thesis:	**Temperature Prediction of Induction Motors from Estimated Parameters and Losses**
Name, Designation & Institution of the Supervisor:	**Name: Prof. Suparna Kar Chowdhury** Designation: Professor Department: Electrical Engineering Institution: Jadavpur University, Kolkata, West Bengal, India Pin 700032

List of Publications:

1. **D. Bhowmick**, M. Manna and S. K. Chowdhury, "Estimation of Equivalent Circuit Parameters of Transformer and Induction Motor from Load Data," in *IEEE Transactions on Industry Applications*, vol. 54, no. 3, pp. 2784-2791, May-June 2018, doi: 10.1109/TIA.2018.2790378.

List of Patents: Nil

List of Presentations in National/ International/Conferences/Workshops:

1. **D. Bhowmick** and S. K. Chowdhury, "Sensor Less Performance Estimation of Induction Motor," *2022 IEEE Calcutta Conference (CALCON)*, Kolkata, India, 2022, pp. 133-138, doi: 10.1109/CALCON56258.2022.10059605.

2. **D. Bhowmick** and S. K. Chowdhury, "Performance and Temperature Estimation of Induction Motor from Transient Measurement," *2020 IEEE International Conference on Power Electronics, Drives and Energy Systems (PEDES)*, Jaipur, India, 2020, pp. 1-6, doi: 10.1109/PEDES49360.2020.9379709.

3. **D. Bhowmick**, D. Maiti, S. KarChowdhury and S. K. Biswas, "Performance Estimation of an Inverter Fed Three Phase Induction Motor at Reduced Flux Condition," *2020 IEEE International Conference on Power Electronics, Smart Grid and Renewable Energy (PESGRE2020)*, Cochin, India, 2020, pp. 1-6, doi: 10.1109/PESGRE45664.2020.9070513.

4. **D. Bhowmick** and S. K. Chowdhury, "Sensorless Prediction of Equivalent Circuit Parameters and Losses of a Squirrel Cage Induction Motor using PSO," *2019 IEEE Region 10 Symposium (TENSYMP)*, Kolkata, India, 2019, pp. 553-558, doi: 10.1109/TENSYMP46218.2019.8971027.

5. **D. Bhowmick** and S. K. Chowdhury, "Estimation of Losses and Performance Parameters of Three Phase Induction Motor using Particle Swarm Optimization and H – G Diagram," *2018 IEEE International Conference on Power Electronics, Drives and Energy Systems (PEDES)*, Chennai, India, 2018, pp. 1-6, doi: 10.1109/PEDES.2018.8707590.

6. **D. Bhowmick** and S. K. Chowdhury, "Parameter and Loss Estimation of Three Phase Induction Motor from Dynamic Model using H - G Diagram and Particle Swarm Optimization," *2018 IEEE 8th Power India International Conference (PIICON)*, Kurukshetra, India, 2018, pp. 1-5, doi: 10.1109/POWERI.2018.8704353.

7. **D. Bhowmick**, M. Manna and S. K. Chowdhury, "Improved equivalent circuit parameter estimation of induction motor using H-G diagram and PSO," *2017 IEEE Calcutta Conference (CALCON)*, Kolkata, India, 2017, pp. 443-447, doi: 10.1109/CALCON.2017.8280772.

8. **D. Bhowmick**, M. Manna and S. K. Chowdhury, "Estimation of equivalent circuit parameters of transformer and induction motor using PSO," *2016 IEEE International Conference on Power Electronics, Drives and Energy Systems (PEDES)*, Trivandrum, India, 2016, pp. 1-6, doi: 10.1109/PEDES.2016.7914531.

9. **D. Bhowmick**, M. Manna and S. K. Chowdhury, "Online estimation and analysis of equivalent circuit parameters of three phase induction motor using particle swarm optimization," 2016 IEEE 7th Power India International Conference (PIICON), Bikaner, India, 2016, pp. 1-5, doi: 10.1109/POWERI.2016.8077256.

FACULTY OF ENGINEERING & TECHNOLOGY

JADAVPUR UNIVERSITY

"Statement of Originality"

I, **Sri Diptarshi Bhowmick** registered on **7th March, 2017** do hereby declare that this thesis entitled **"Temperature Prediction of Induction Motors from Estimated Parameters and Losses"** contains literature survey and original research work done by the undersigned candidate as part of Doctoral studies.

All information in this thesis have been obtained and presented in accordance with existing academic rules and ethical conduct. I declare that, as required by these rules and conduct, I have fully cited and referred all materials and results that are not original to this work.

I also declare that I have checked this thesis as per the "Policy on Anti Plagiarism, Jadavpur University, 2019", and the level of similarity as checked by iThenticate software is 5 %.

Signature of the Candidate: Diptarshi Bhowmick.

Date: 19/02/2024

Certified by Supervisor:
(Signature with date & seal)

19/02/2024

Professor
Electrical Engineering Department
JADAVPUR UNIVERSITY
Kolkata-700 032

FACULTY OF ENGINEERING & TECHNOLOGY
JADAVPUR UNIVERSITY

CERTIFICATE FROM THE SUPERVISOR

This is to certify that the thesis entitled "**Temperature Prediction of Induction Motors from Estimated Parameters and Losses**" submitted by **Sri Diptarshi Bhowmick**, who got his name registered on **7th March, 2017** for the award of Ph.D. (Engineering) degree of Jadavpur University is absolutely based upon his own work under the supervision of me, **Prof. Suparna Kar Chowdhury**, Professor, Electrical Engineering Department, Jadavpur University and that neither his thesis nor any part of the thesis has been submitted for any degree/diploma or any other academic award anywhere before.

SKarChowdhury 19/02/2024

Prof. Suparna Kar Chowdhury
(Signature of the Supervisor with date & Office Seal)
Professor
Electrical Engineering Department
JADAVPUR UNIVERSITY
Kolkata-700 032

Dedicated to

My Parents

ACKNOWLEDGEMENT

As I approach the final stages of completing my thesis, I am deeply grateful for the support and contributions of numerous individuals who have supported and guided me on this journey. While it is challenging to acknowledge each person individually, their collective efforts have been invaluable in shaping the outcome of this work. I am grateful to all those who have offered their encouragement, expertise, and assistance along the way. Though it is impossible to fully express my gratitude, I wish to extend my heartfelt gratitude to each and every one of them for their immense support and encouragement.

I am extremely grateful to my research guide, ***Prof. Suparna Kar Chowdhury***, for her invaluable mentorship, untiring support, and profound wisdom throughout this journey. Her guidance has not only shaped my research but has also deeply impacted my personal and professional growth. I am obliged to her for her dedication, encouragement, and expertise, which have been instrumental in helping me navigate challenges and achieve success in every part of this journey. I am truly fortunate to have had the privilege of working under her guidance, and I am immensely thankful for her invaluable contributions to my academic and personal development.

I would like to extend my gratitude to, ***Prof. Sujit K. Biswas***, for his constant guidance, invaluable suggestions, and endless encouragement throughout my journey. Prof. Biswas's enthusiasm, boundless energy, and unparalleled passion for the engineering have been a constant source of inspiration for me. Despite facing personal challenges, he has consistently supported me, and helped me shaping my academic and professional career. The lesson I learned from him, not only about the subject, but also about life is going to remain with me for rest of my days.

I would like to thank ***Late Prof. Nirmal K. Deb*** with utmost respect. His knowledge about electrical machines and machine design helped me understand the geometrical intricacies of induction motor. May his soul rest in peace.

I am extremely thankful to ***Prof. Debashis Chatterjee***, ***Dr. Arindam Kumar Sil***, ***Dr. Debangshu Dey***, ***Dr. Susanta Ray***, ***Dr. Arpan Kumar Pradhan***, ***Dr. Krishna Roy*** and ***Mr. Dipten Maity*** for their continuous encouragement, valuable insights, guidance and support

in every aspect throughout my research. I am obliged to them for always being my inspiration and contributing to my overall academic growth.

I am also thankful to all faculties and staffs especially, ***Dipankar Naskar***, ***Jayanta Bhattacharya***, and ***Indrajit Naskar*** of the Machines and Drives Laboratory of the Electrical Engineering Department for their assistance while performing the laboratory experiments.

I want to extend my gratefulness to ***Dr. Arunava Chatterjee***, ***Dr. Soumyajit Ghosh***, ***Dr. Subhendu Bikas Santra***, ***Dr. Samrat Paul, Dr. Saptarshi Chatterjee, Mr. Koustuv Sarkar***, ***Mr. Subhajit Myur***, ***Mr, Biswajit Chakraborty*** and my other fellow research scholars, who was always there by my side, motivated me and helped me overcoming challenges with their valuable wisdom.

I am deeply grateful for the untiring moral support and sacrifices made by my parents and other family members, which encouraged and motivated me to work harder towards completing my thesis. Their steadfast presence provided me with strength and comfort to overcome obstacles and continuing my research journey.

February 2024

Jadavpur University

Kolkata- 700032

Name of Candidate: Diptarshi Bhowmick

ABSTRACT

Induction motors are valued for their reliability and cost-effectiveness in industries. However, they face potential catastrophic failures under harsh conditions, such as high temperatures, humidity, and overloads. This leads to increased downtime and maintenance costs, which in turn invites high financial losses for industries. Thus, to avoid these unwanted situations and maintaining smooth industrial operation, monitoring motor health is imperative.

In industries now a days, inverter-fed motors, particularly those utilizing Pulse Width Modulated (PWM) inverter supply, became popular because of their high dynamic performance and precise speed control, especially in low-speed region. However, they are susceptible to insulation risks due to high DC voltage applied across the windings. High switching frequency of inverters also increase the core loss of the motor, which increase motor temperature. This higher temperature imposes thermal stress on insulation, leading towards incipient insulation failures. Therefore, continuous monitoring of induction motor becomes essential for seamless operations.

The behavior and performance of electrical machines, including induction motors, are intricately tied to their equivalent circuit parameters. An equivalent circuit is a simplified representation of the electrical characteristics of a machine, encapsulating the essential electrical elements and their interconnections. Accurate estimation of these equivalent circuit parameters is crucial because they serve as a window into the inner workings of the machine. Think of these parameters as the unique fingerprints or signatures that characterize how the electrical machine responds to different operating conditions. By precisely determining these parameters, valuable insights into the health and overall performance of the machine are possible. In practical terms, accurate parameter estimation allows to assess the efficiency of the machine, predict its response under different operating conditions, and identify potential issues or deviations from the expected performance. Monitoring these parameters over time provides a means for proactive maintenance, enabling the detection of abnormalities or deterioration in the machine's health before they escalate into critical failures. Therefore, estimating the equivalent circuit parameters of electrical machines provide a comprehensive diagnostic tool for assessing their health and performance. This knowledge is instrumental in optimizing operations, ensuring reliability, and facilitating

timely maintenance interventions to prevent unexpected failures and minimize downtime in industrial settings.

Understanding thermal dynamics within induction motors is pivotal for predictive condition monitoring. A comprehensive thermal model, integrating thermal resistances, capacitances, and heat sources, aids in developing effective monitoring strategies. However, the task is not without challenges, particularly in obtaining detailed dimensional data, which is crucial for accurate thermal modeling. This difficulty arises from various factors, including intellectual property concerns and the practical problems of physically obtaining the motor dimension by completely dismantling the motor. Nevertheless, overcoming these challenges is pivotal for advancing the accuracy of thermal model-based condition monitoring schemes.

The research is focused on integrating various aspects of motor analysis, such as parameter estimation, loss analysis, and temperature prediction, especially for Totally Enclosed Fan Cooled (TEFC) induction motors. By combining these elements, the research aims to provide a more generalized and accurate temperature estimation scheme for precise thermal analysis of TEFC induction motors. This methodology uncovers the intrinsic relationship between the characteristics of an induction motor, it’s losses during operation, and how these factors are influenced by temperature changes, ultimately affecting motor's overall behavior. Moreover, the research introduces an innovative estimation scheme aimed at accurately predicting the internal dimensional values of the motor. This scheme works with the motor's performance data and external dimensions to reverse-engineer the internal structure. This approach overcomes the challenges related to intellectual property and the intricate nature of motor construction, adding a layer of depth to understanding the motor's inner geometry.

The anticipated outcome of this research is to make a substantial contribution to the field of temperature – based predictive condition monitoring. By enhancing the accuracy and comprehensiveness of thermal analysis, the research aims to reinforce the reliability and efficiency of induction motor operations. This improvement is not limited to specific industrial applications but extends across diverse applications and operating conditions, ensuring the longevity and optimal performance of induction motors. Ultimately, the research seeks to lay the groundwork for more robust and effective temperature based predictive maintenance strategies, thereby reducing downtime, minimizing operational risks, and maximizing the overall lifespan of induction motors in industrial settings.

Contents

List of Figures

List of Tables

List of Abbreviation

2-D	Two Dimensional
3-D	Three Dimensional
A	Ampere
AC	Alternating Current
BRB	Broken rotor bar
DC	Direct Current
DOL	Direct Online
d-q / D-Q	Direct - Quadrature
DTC	Direct Torque Controlled
EMF	Electro Motive Force
FE	Finite Element
FEM	Finite Element Method
GA	Genetic Algorithm
hp	Horsepower
Hz	Hertz
IEEE	Institute of Electrical and Electronics Engineers
IRP	Instantaneous Reactive Power
kg	Kilogram
kW	Kilowatt
LM	Levenberg–Marquardt
LP	Lumped Parameter
MRAS	Model Reference Adaptive System
NEMA	National Electrical Manufacturers Association

N-m	Newton-meter
PI	Proportional Integral
PSO	Particle Swarm Optimization
PWM	Pulse Width Modulation
RLS	Recursive Least Square
RMS	Root Mean Square
rpm / RPM	Revolutions Per Minute
TEFC	Totally Enclosed Fan Cooled
V	Volt
VSI	Voltage Source Inverter
VVVF	Variable Voltage Variable Frequency

CHAPTER 1

Introduction

Induction motors are the backbone of industrial operations. Despite their robustness, environmental factors can impact their performance, leading to potential catastrophic failures, prompting the need for continuous health monitoring. Inverter-fed induction motors, popular for precise speed control, introduce insulation challenges, emphasizing the need for predictive condition monitoring. These issues can be addressed by proper understanding of motor behavior, which can be achieved through precise motor modeling by exploring equivalent circuit. In modern AC drive systems accurate estimation of equivalent circuit parameters is fundamental.

The integration of a "Thermal Model" offers comprehensive analysis of temperature distribution. This integrated technique plays a pivotal role in developing temperature-based predictive condition monitoring strategies. Together, these aspects form a general approach, empowering industries to optimize motor performance and ensure longevity in diverse operating conditions.

1.1 Overview

Induction motors find extensive use in industries due to their robustness, reliability, cost-effectiveness, and self-starting capability. Ensuring the reliable operation of induction motors is essential for maintaining uninterrupted process chain and smooth industrial operations. The behavior and performance of electrical machines are characterized by their equivalent circuit parameters. Hence, accurate estimation of these parameters provides significant information about the condition and performance of the machine.

In the area of state-of-the-art modern AC drive systems, machine modeling is particularly important. As for example, in vector control, the determination of rotor flux linkage estimation is crucial, requiring precise prediction of motor equivalent circuit parameters.

However, the industrial requirements often force these motors to operate under unfavorable conditions, such as high temperatures, high humidity, frequent overload, and voltage unbalance, which can lead to catastrophic failure. Repeated motor failures result in excess maintenance costs and substantial fiscal losses due to unscheduled downtime. Hence, health monitoring of induction motors has always been a significant concern for engineers.

Inverter-fed induction motors are widely employed in industry for their robustness and precise speed control. Power electronic control schemes, like Pulse Width Modulated (PWM) Inverter supply, offers advantages over commercial sinusoidal supply, in terms of dynamic response and speed control. This improvement in dynamic response allows for good speed response, including very low-speed operation of induction motors. Nevertheless, the use of PWM Inverter supply introduces

challenges. Peak DC voltage is applied to the stator windings during inverter-fed motor operation, resulting in a high $\frac{dV}{dt}$. This imposes considerable stress on the winding insulation, increasing the risk of insulation failure. Therefore, health monitoring of inverter-fed induction motors becomes crucial for ensuring uninterrupted industrial processes.

Understanding the thermal dynamics within an induction motor is fundamental for predictive condition monitoring. The "Thermal Model" designed to emulate the temperature distribution within the motor, providing a comprehensive analysis of heat flow. The interconnected network of thermal resistances, capacitances, and heat sources in thermal model mirrors the complex interplay of heat dynamics in the induction motor. By representing temperature-related aspects of the motor in form of an electrical circuit, this model enables a detailed analysis of how heat propagates through different components during operation.

In a broader context, the thermal model can be a key factor in the development and implementation of predictive condition monitoring strategiesfor induction motors. It provides a clear and measurable way to understand how the motor's temperature changes. This helps operators and maintenance teams to anticipate potential issues. This, in turn, enhances the overall reliability and longevity of induction motors in diverse industrial applications.

For the thermal model to be accurate, precise calculation of thermal resistances, thermal capacitances, and motor losses is crucial. However, obtaining detailed dimensional data for motor components poses challenges due to intellectual property issues. Physical measurements,

especially of inner dimensions, can be difficult without removing the windings, and even then, rewinding may alter motor properties and performance.

1.2 Literature review

Based on the survey for 0.75 kW to 150 kW induction motors, faults can be categorized as broken rotor bar (BRB) faults (7%), stator winding faults (21%), bearing faults (69%), and shaft/coupling and other faults (3%). Therefore, stator and rotor related faults consist of more than 25% of total motor failure in industries, which is a significant amount and cannot be ignored. [6]. Existing literatures show that the following methods can be used for health monitoring of the induction machine

- Current signature analysis [7], [8]
- Vibration analysis [9], [10]
- Thermal monitoring [11], [12].

In current signature analysis, the current signals are analysed to identify the harmonics, and detects the cause of abnormality in the machine. It is complex, involves high computational burden and requires huge dataset to train the algorithm [7], [8]. Hence, it is used as a specialized tool for fault detection.

Other monitoring schemes i.e., acoustic, thermal and vibration monitoring involves sensors which, requires expertise for placing the sensors inside the motor. Besides, for proper placing of the sensors inside the motor, special design of induction motor is required such as hollow shaft machine. The sensors have to be placed inside the induction machine during its manufacturing which is a big issue for the existing machine.

In order to eliminate this issue, researchers have focused on developing the health monitoring methods which are data driven, such as voltage, current, speed etc. that can be acquired by external instruments. Having proper knowledge about the equivalent circuit parameters of induction motors plays an important role under these circumstances. The survey results, presented in [6], also confirms that parameter -based condition monitoring can be an effective way to reduce downtime. As performance of induction motor can be characterized by its equivalent circuit parameters, accurate determination of induction motor parameter is capable of predicting any deviation from its expected performance, which in turn portrays the health of the induction motor.

The equivalent circuit parameters of electrical machines can be determined from the standard test procedures, as per IEEE guidelines [13], which includes dc resistance test, blocked rotor test and no-load test. Being offline, the technique cannot be employed for the machines which are in operation. To conduct these tests, the motor needs to be disconnected from the existing system which increase the downtime and may affect the economy.

In practice, the equivalent circuit parameters are not provided by the manufacturer. They usually provide nameplate data, related to motor operation [17]. Keun Lee, Stephen Frank, Pankaj K. Sen, Luigi Gentile Polese, Mahmoud Alahmad, Clarence Waters [14] proposed a parameter estimation scheme of three phase induction motor from available name-plate data using Gauss-Seidel algorithm. But these methods suffer from selection of proper boundary conditions, as well as change of parameters with environmental condition, ageing and rewinding. Nameplate data, which is provided by the manufacturer, is

basically a representation of motor performance under certain specified condition. There are several factors that can alter the motor performance under actual operating condition.

- Alteration in ambient temperature can change the winding resistance which can affect the motor performance.
- Rewinding of the machine may also bring changes in its resistance, leakage reactance or magnetizing reactance as well as flux distribution.
- Ageing is also a factor which has a huge influence on motor performance.

Therefore, determination of induction motor parameters from nameplate data may not be a good option always, especially for aged machines those operate under adverse environmental condition. Hence, the researchers are oriented towards development of advanced techniques which can estimate the parameters while the motor is in operation [15].

Induction motor parameter estimation problem is tackled normally using three methods [16].

- Numerical Analysis.
- Estimation under standstill condition.
- Estimation under running condition.

Numerical analysis generally relies on dimensional data of the motor, along with measured electrical data [17] – [20]. However, the limitation of this method is, the geometrical or dimensional data is not always available to the user. Therefore, the machine should be dismantled and measurements should be conducted manually to obtain these data. On

the other hand, in this method, the estimation of parameters is done through finite element or finite difference method which are highly complex computational techniques.

For Estimation under standstill condition, external known signal is applied to the motor terminals and corresponding response currents are measured [2], [15], [21]. These response signals are analyzed to find out the equivalent circuit parameters. While these techniques can accurately estimate the parameter values, the drawback of the technique is that the machine needs to be taken offline during the testing procedure.

For estimation under running condition, the motor is rotated by a prime mover at required speed and corresponding line currents are measured [22], [23]. Thereafter, the current is analyzed for estimating the parameters. However, this method requires special experimental setup with dedicated instrumentation which is costly.

D. M. Reed, H. F. Hofmann and J. Sun [23], proposed an offline method for parameter estimation by fitting measured current data to the circular stator current locus in d-q reference-frame by varying steady-state slip frequencies. Being an offline method, this scheme is not capable of estimating motor parameters without disturbing the system harmony. In [21], authors proposed a current injection based off line identification method of rotor time constant and magnetizing inductance of three phase induction motor. In [24], authors proposed an off-line method for parameter estimation of induction motor using genetic algorithm from current and torque measurement. On the other hand, S. R. P. Reddy and U. Loganathan [15] proposed a recursive offline parameter estimation technique using Kalman filter. This method requires standstill operation of induction motor which has been achieved by shorting two motor

terminals and providing a single-phase supply. Therefore, in this method, the data acquisition requires special connection which involves disconnection of the motor from system. M. Perin, L. A. Pereira, L. F. A. Pereira and G. Nicol [25] proposed parameter identification method of five phase induction motor using step voltage at standstill condition. This method can be replicate for a three-phase machine too. However, it needs disconnection of the machine from the existing system to apply step voltage in the stator winding.

In order to overcome the limitations of the above-mentioned methods, the researchers have proposed equivalent circuit parameter estimation techniques under variable load using different algorithms [26-28]. In [26], authors proposed a parameter identification method from transient voltage, current and speed measurements using least-square technique. In [27], the parameters of a field oriented controlled induction motor have been identified from current and speed measurement using genetic algorithm. Masoumi et al [28] proposed another method of induction motor parameter identification technique from transient voltage, current, and speed measurement under an unspecified load. Authors in [28] used extended Kalman filter for this purpose. This technique uses DC test for stator resistance measurement which again requires to disconnect the machine from AC supply. This method also involves complex mathematical calculations as well as disregards the estimation of core loss resistance. In [29], authors proposed a scheme for estimating rotor resistance and the mutual inductance online by designing MARS based observer. In [30], J. Benzaquen, J. Rengifo, E. Albánez and J. M. Aller presented a parameter estimation scheme for deep bar induction motor from instantaneous measurement during a DOL starting. This scheme mainly focuses on estimating the mechanical parameters i.e.,

developed electromagnetic torque and motor inertia from measured voltage, current, speed and stator resistance. In [31], a back-EMF based stator resistance and rotor time constant estimation approach along with an error correction technique was proposed. In [32], the authors proposed a technique to estimate motor resistance, inductance, inertia and friction coefficient using cuckoo search method and Steiglitz–McBride algorithm. This estimation process requires current and speed measurement however, this technique is incompetent for estimating all the electrical equivalent circuit parameters separately. Whereas, in [33], authors described the importance of accurate parameter estimation in stator flux estimation as well as field-oriented control technique used for induction motor drive. G. B. Reddy, G. Poddar and B. P. Muni in [34] proposed an online estimation of rotor time constant using least square method. In [35], M. Reza Feyzi and M. Sabahi have proposed an online dynamic parameter estimation technique using recursive least square (RLS) algorithm. Koubaa [36] also proposed a recursive least square algorithm-based parameter estimation scheme for induction motor. Zhang Hu, Gong Shu-juan, Dong Zi-zhao [37] also proposed an on-line parameter identification scheme of induction motor based on Recursive Least Square (RLS) algorithm. They have solved the Butterworth digital filtering equation with improved Euler's numerical solution to increase the accuracy of the scheme. In [38], Bigdeli and Rahimpour proposed a scheme to estimate transformer parameters for fault detection and power network analysis based on geometrical dimension. But this method suffers from dimensional data unavailability for old machines.

Though the above-mentioned online techniques are capable of monitoring the induction motor reliably, however, there are certain limitations of each of the methods. The techniques proposed in [29]

involves high computational burden, whereas, in [30], the estimated method assumes the stator resistance value which may not always be correct or available. As mentioned above, some of the litrature are not able to estimate all the equivalent circuit parameters separately which may somehow limit the results towards the correct assessment.

Use of soft computing method for diagnosis of electrical devices was first proposed by Szczepaniak and Rudnicki in [39]. Mehdi Bigdeli, Ebrahim Rahimpour [40] proposed another model for transient analysis of transformer using genetic algorithm (GA). S. Subramanian and S. Padma [41] proposed a method for parameter estimation of three winding transformer based on bacterial foraging algorithm.

In [42], Mohamed I. Mossad, Mohamed Azab, and A. Abu-Siada used particle swarm optimization (PSO) for estimation of the transformer parameters from name plate data without conducting any offline tests. They also provided comparative study of the proposed method with GA and showed significant improvement with PSO. Nangsue, Pillay and Conry [43] proposed a parameter estimation technique of induction motor using genetic algorithm (GA). In [44], authors presented a scheme for induction motor parameter estimation using chaotic ant swarm algorithm and showed that the errors are minimized than that of GA. Burak Tekgun, Yilmaz Sozer and Igor Tsukerman [45] have proposed a technique to estimate the parameters of split phase induction motor by Levenberg–Marquardt (LM) algorithm.

In [46], the authors proposed a PSO based evolutionary optimization technique for parameter identification of induction motor. They added a constriction factor with classical PSO to identify the parameters of induction motor. In [47], Hassan M. Emara, Wesam Elshamy and A.

Bahgat proposed a modified PSO technique named Clubs-based PSO technique to identify the parameters of induction motor. However, most of the literature till discussed, ignore the core loss equivalent resistance during parameter estimation. In classical dynamic model of induction motor, core loss has been considered as a constant loss and hence the core loss resistance can be ignored. However, in precise machine modelling, core loss resistance plays a significant role. As the machine gets heated up with prolonged runtime, the resistance of the eddy current path increases. On the other hand, with increased temperature, B-H curve of iron shows a tendency to downshift which also indicate the increase in core loss equivalent resistance. With constant voltage supply, as the core loss resistance increases with temperature, the core loss itself reduces. That's why, if the core loss of induction motor is calculated under thermal equilibrium condition, the loss characteristics shows a bit down shift with increase in load. This phenomenon becomes more prominent in PWM inverter fed induction motors. As in inverter fed machines, switching frequency is very high, therefore core loss in those machines is always on a higher side, hence, core loss resistance cannot be ignored there. Therefore, core loss resistance has to be considered in equivalent circuit model of induction motor for precise machine modelling.

Accurate knowledge of equivalent circuit parameters is vital for several applications, including speed estimation in sensor-less motor drives [1], [2], designing efficient induction motors [3], [4], and predicting incipient faults [5] in induction motors. Inverter-fed induction motors, particularly Pulse Width Modulated (PWM) Inverter supply, widely used in industries. However, while sinusoidal supply ensures a pure sinusoidal flux with low dV/dt, inverter-fed machines, with their high

dV/dt during switching, stress winding insulation, posing a risk of failure. Health monitoring of inverter fed induction motors is of immense importance for continuing the industrial processes in an uninterrupted manner [48]. It is possible to continuously monitor the health of an induction motor and protect it from incipient faults by accurately determining induction motor equivalent circuit parameters with losses. Some research work has already been done on parameter estimation of inverter fed induction motor in this decade. In [49], authors proposed a technique of parameter identification of a three-phase induction motor connected with a single-phase supply from stator voltage and current measurement under standstill condition. A recursive least square technique-based parameter estimation scheme for a voltage source inverter fed three phase induction motor is proposed in [50] under standstill condition. Parameter identification method for a VSI fed five phase induction motor both under standstill and running condition has been proposed in [51]. A parameter estimation technique of inverter fed induction motor has also been proposed [2] by identifying inverse-Γ equivalent circuit at standstill.

Several researches have been carried out on temperature estimation of induction motor for predictive condition monitoring, for different applications. In [52], rotor temperature estimation technique for induction machines using a lumped-parameter thermal network and dual kalman filtering was proposed. It combines a lumped-parameter thermal network and dual kalman filtering with stator windings temperature measurements. This approach, facilitates real-time estimation of rotor temperature evolution and thermal model parameters. In [53] authors suggest rotor temperature estimation method based on parameter identification. A combination of recursive

least squares (RLS) and model reference adaptive system (MRAS) has been used. RLS identifies motor inductance parameters, and MRAS achieves online rotor resistance identification through instantaneous reactive power (IRP) and a proportional integral (PI) regulation adaptive law. In [54], authors suggested an innovative way of predicting winding temperature from current measurement, especially for induction motors running with unbalanced supply. They proposed a polynomial equation, derived from experimental data, to evaluate the temperature of induction motors. [55] confirms that model-based temperature estimation has better applicability than signal injection-based estimation in terms of being non-invasive as well as free from harmonic interference. Boglietti, Cavagnino, Lazzari and Pastorelli [56] proposed a thermal model-based temperature estimation technique for variable speed TEFC (Totally Enclosed Fan Cooled) induction motor. In [57] authors investigated the correlation between supply frequency changes and the accuracy of rotor temperature estimation based on rotor resistance identification. It analyzed a complex voltage vector derived from poly-phase voltage measurements, filters out harmonics and interference, and adjusts the phase to align with the voltage signal, providing a more accurate estimation of rotor temperature amid supply frequency fluctuations. [58] observed the temperature changes in motors under different load condition. The researchers developed a model to predict the power loss in the motor under diverse conditions and used a simple thermal resistance model to calculate the temperature increase in the motor. [59] proposed a signal injection-based temperature estimation scheme for Direct Torque Controlled (DTC) induction motor from stator resistance. Authors in [60] proposed a rotor temperature estimation scheme based on the change in input impedance

of the machine. Instead of real value of input impedance, here, authors identified the absolute input impedance value from measured input voltage and current. From the change of this input impedance, rotor temperature is calculated. [61] proposed a temperature estimation technique based on induction motor's load-ability curve. In this work, the authors identified the parameters of the first-order thermal model for any arbitrary overload condition. Authors in [62] proposed a non-invasive, high frequency signal injection-based rotor temperature estimation technique for doubly fed induction motor. Being a signal injection-based method, this technique offers accuracy and precision, however, it suffers from limited applicability, especially with singly excited induction motors. In [63], authors investigated the temperature distribution in a fan-cooled motor employing 3D coupled-field FEM. This model calculates motor losses and their distribution and accordingly calculates temperature, considering the effect of rotor rotation on airflow through the motor. In [64], authors compared four different thermal models starting from fourth order to first order for their accuracy in temperature prediction. From the comparison, it can be concluded that, increase in order improve the accuracy of estimation to a small extent, but it also increases the complexity of the model progressively. Authors in [65], used infrared thermograph for bearing fault detection. They used two-dimensional discrete wavelet transform for diagnosing inner and outer race defects and lack of lubrication and to remove noise in thermal images. Then machine learning algorithms such as principal component analysis and support vector machine were used for feature extraction and fault classification. [11] introduced a method for assessing the thermal parameters of induction motors used in industrial applications. It built a short-time thermal transient

identification method and extended it to address the more complex scenario of multiple three-phase machines. The generalized model considered mutual heat exchange between windings and potential causes of temperature mismatch. [66] analyzed thermal characteristics of induction motors working under adverse environment at food and beverages industries. For this analysis, they evaluated the equivalent thermal resistance between stator winding and the lamination and proposed use of epoxy resin as potting material to the end winding for increased thermal conductivity, in an enclosed machine, designed to work under wash-down area. Another study [67] investigates the impact of the transient starting process on the temperature distribution and rise in electric motors. Here the authors developed a 3-D fluid-solid coupling transient model considering motor's actual physical structure to analyze the transient temperature distribution during the starting process with different loads. Moon and Lee [68] focused on predicting temperatures in electrical machines by allocating stray load loss (SLL) with calculated losses under rated-load conditions using 2-D transient finite-element analysis of induction machines. These synthesized losses are then incorporated into thermal-flow analysis for accurate temperature estimation. [69] introduced a practical method for modelling and analyzing transient thermal effects in air-cooled electric traction motors, especially for the critical motor parts, such as windings and bearings. It combines numerical and analytical modelling to achieve precise hot spot temperature estimation. Computational fluid dynamics simulations are employed to model air flow, providing heat transfer data as inputs to the combined finite-element (FE) and lumped parameter (LP) thermal models for fast transient calculations. [70] studied the thermal impact on induction motors due to overload and

voltage unbalance. In this research, authors induced various overloads and voltage unbalance levels, monitored their thermal impact on the stator winding, created a time-overload curve, determined the thermal levels based on this curve and the overload thermal profile, and finally, estimated the parameters of the time-unbalance model using the thermal levels obtained and the unbalance thermal profiles.

1.3 Research gaps

Therefore, from the discussed literature in the field of parameter estimation of induction motor, following research gaps have been identified:

i. Highly complex analytical techniques increase computational burden.

ii. Sensor dependent methods require costly sensors and highly skilled professionals to install and monitor them.

iii. Offline estimation techniques interrupt the ongoing motor operation which may introduce financial loss to industry.

iv. Most of the literature do not include all the equivalent circuit parameters into estimation. They often discard core loss equivalent resistance considering core loss as constant loss. However, closer observation reveals that core loss changes slightly with load, which should be taken into consideration for accurate loss and temperature estimation of induction motor.

v. The effect of temperature on motor parameters has not been widely studied.

vi. Often, the available literature does not consider the variation of motor parameters under running condition due to the temperature change.

vii. Most of the available literature use the complex Finite Element Technique for temperature prediction.

Therefore, from this discussion, a requirement to develop an integrated equivalent circuit parameters and loss estimation technique, coupled with a lumped parameter thermal model is recognized, which can provide a significant leap forward in the field of induction motor condition monitoring. The proposed work should address the critical need for temperature-based monitoring, and offer a comprehensive solution that takes into account both electrical and thermal aspects of motor operation.

1.4 Objective of the work

The primary objective of this research is to develop an advanced and generalized thermal analysis technique for Totally Enclosed Fan Cooled (TEFC) induction motors by seamlessly integrating two critical aspects:

- Estimation of parameters and loss from performance data
- Temperature estimation through thermal modeling.

This comprehensive approach aims to enhance the understanding of the thermal dynamics of induction motors, which can provide a detailed and accurate depiction of machine behavior under varying operating conditions.

The first tier of the objective involves the estimation of parameters and losses from performance data. Traditional methods face challenges,

such as, interruption of ongoing process, injection of external signals, requirements of specialized design, internal sensor placement and sophisticated instrumentation, high computational complexity or incapability of predicting all the equivalent circuit parameters at a time. This work seeks to establish a scheme that exploits the inherent relationships between motor performance and its parameters.

Simultaneously, this work integrates a lumped parameter thermal model into the analysis process. The thermal model, represented as an equivalent electrical circuit, provides a detailed analysis of temperature distribution and heat flow within the motor. Thermal model-based temperature estimation technique using predicted losses aims to offer a comprehensive understanding of the motor's thermal dynamics. This approach identifies the inherent connection between motor parameters and losses and their dependence on temperature variations which influence motor behavior.

However, development of accurate thermal model for induction motors face challenges, because detailed dimensional data is inaccessible due to intellectual property constraints. Hence this work also includes the development of an estimation scheme, which is capable of accurately predicting motor inner dimensional values from motor performance data and motor external dimensions. The predicted dimensional data, along with estimated parameters and losses can provide a precise estimation of temperature at various parts of the motor with the help of the developed thermal model.

The integration of equivalent circuit parameters and loss estimation, with the developed thermal model collectively aims to contribute towards the comprehensive temperature-based condition monitoring of

induction motors. This technique is anticipated to contribute significantly to the development of more robust, efficient, and reliable induction motors operation by early addressing of potential issues, and ensuring the longevity and reliability of induction motors across diverse industrial applications.

1.5 Organization of the thesis

This thesis is organized as follows:

Chapter 2: Describe the scheme for estimating equivalent circuit parameters of three phase induction motor from steady state motor performance data under various load condition, utilizing steady state motor model.

Chapter 3: This chapter digs into the innovative approach employed to estimate parameters and losses in three-phase induction motors by combining dynamic models with steady-state data.

Chapter 4: This study focuses on the critical task of estimating parameters and losses in the equivalent circuit of an induction motor from transient data.

Chapter 5: This section investigates the performance characteristics of an inverter fed three-phase induction motor operating particularly under reduced flux conditions.

Chapter 6: This chapter addresses a critical aspect of induction motor health monitoring by proposing a novel temperature estimation scheme. Focused on utilizing estimated losses, this work seeks to develop an accurate and practical method for assessing the temperature profile within an induction motor.

Chapter 7: This study specifically explores the critical domain of estimating inner dimensions of an induction motor from motor performance data, aimed towards development of an innovative thermal model for temperature prediction of induction motor.

Chapter 8: Conclusion and scope of future work.

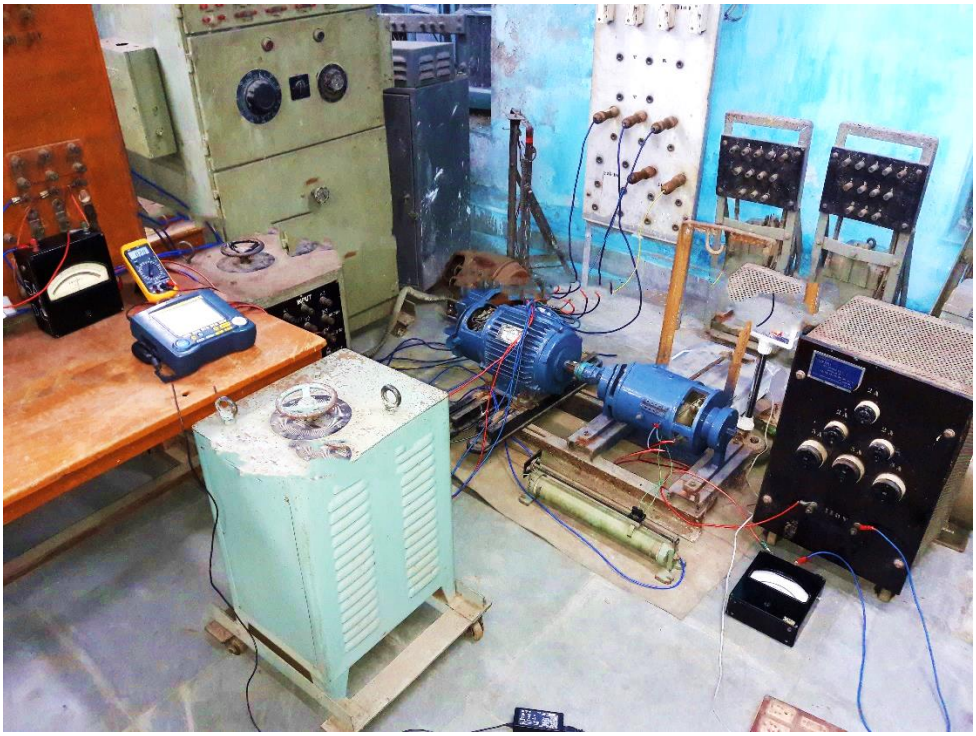

CHAPTER 2

Estimation of Equivalent Circuit Parameters of Induction Motor from Load Data

Equivalent circuit parameters are the key factors for determining the behavior of electrical machines. These parameters include winding resistances, leakage reactances, core loss equivalent resistance and magnetizing reactance. Determination of accurate parameters are important for performance prediction, efficiency estimation or health monitoring of induction motor. This chapter proposes a novel scheme for estimating equivalent circuit parameters of three phase induction motor from motor performance data under various load condition.

2.1 Introduction

The determination of equivalent circuit parameters, such as, winding resistances, leakage reactance, core loss equivalent resistance, and magnetizing reactance, is critical for comprehending and predicting the behavior of induction motors. They are essential in various aspects of motor analysis, including performance prediction, efficiency estimation, and health monitoring. However, induction motor models are complex and nonlinear in nature. The parameters also hold complex interactions between themselves. Therefore, heuristic optimization techniques are often required for estimation of motor parameters. Heuristic optimization techniques, such as Genetic Algorithms (GA), Particle Swarm Optimization (PSO), or Simulated Annealing (SA) have the following features which make them suitable candidate for estimating the parameter of induction motor.

- Induction motors have nonlinear, complex models with many interacting parameters, making traditional analytical methods inefficient for parameter estimation.
- These models often involve nonlinear equations with multiple local minima or maxima.
- Heuristic optimization techniques are effective in such cases, as they explore the solution space globally and stochastically, often finding good solutions faster than traditional methods.
- They are also adaptable to various motor types and operating conditions, offering flexibility for real-world scenarios.
- Since traditional analytical solutions often don't exist for these models, heuristic methods provide an iterative approach to approximate the parameters.

This chapter introduces a technique, aimed at estimating the equivalent circuit parameters of a three-phase induction motor. The proposed scheme utilizes motor performance data acquired under different load conditions. Based on these acquired data, the proposed scheme estimates the precise values of the key parameters that govern the motor's electrical characteristics, with the help of H-G diagram and Particle Swarm Optimization (PSO).

The reasons behind considering PSO as the preferred optimizer are:

i) PSO occupies the biggest optimization capability compared to the other optimization methods.

ii) PSO can handle big search space which is very essential for the development of a generalized parameter and loss estimation scheme for general purpose induction motors.

iii) In the field of parameter estimation of induction motor, PSO provides better results than other optimization techniques [26].

iv) PSO doesn’t require any initialization of parameters for accurate estimation.

v) PSO is less complex and consume less computational time whereas, provide sufficiently accurate results.

The significance of this technique lies in its simplicity, generalized approach and accuracy of the estimation. Traditional methods often rely on complex experimental setups or include mathematical models that increase the computational complexity and cost. Often, they are designed for some special type of machines or a particular kind of operating condition. In contrast, the proposed scheme capitalizes on

actual motor performance data, providing a more realistic, reliable and generalized basis for parameter determination.

The outcomes of this research seem promising in the broader field of induction motor analysis. Accurate equivalent circuit parameters derived from the proposed scheme also lay the groundwork for improved efficiency estimation and proactive health monitoring of induction motors, along with the contribution towards precise performance predictions.

2.2 Steady state equivalent circuit model of induction motor

Fig 2.1 shows the complete equivalent circuit of a three-phase induction motor.

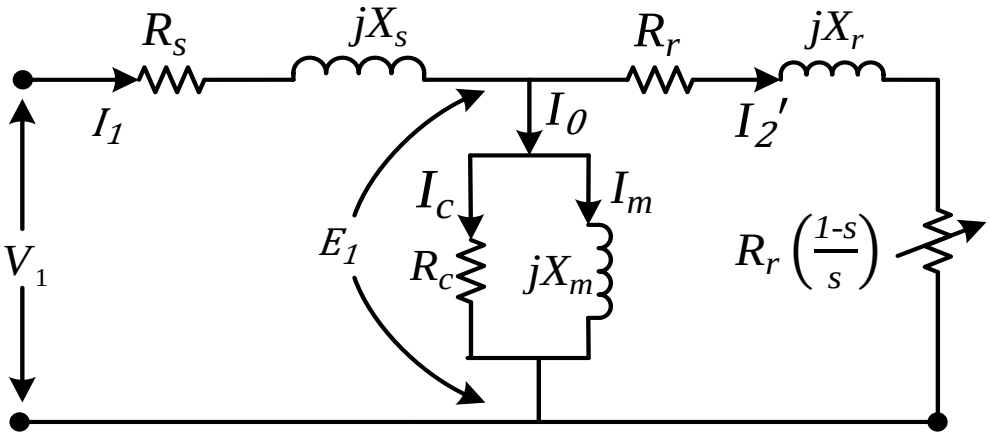

Fig. 2.1. Induction motor steady state equivalent circuit.

Where, symbols have their usual meanings. R_s, X_s, $R_C$and X_m are the stator side resistance, reactance, core loss resistance and magnetizing reactance whereas R_r and X_r are the rotor resistance and reactance referred to stator side. $R_r\frac{(1-s)}{s}$ represents the electrical equivalent of mechanical load of the motor. Here, $Z_1 = R_s + jX_s$ is the stator side

impedance, $Z_2 = R_r + jX_r$ is rotor side impedance referred to stator, $Z_l = R_r \frac{(1-s)}{s}$ represents mechanical load whereas, $Z_p = \frac{(R_c * jX_m)}{(R_c + jX_m)}$ stands for the impedance of the parallel branch.

From the equivalent circuit shown in Fig 2.4, the voltage – current equations can be written as:

$$I_1 = V_1 / Z_{in} \tag{2.1}$$

Where, $Z_{in} = Z_1 + [Z_p \parallel (Z_2 + Z_l)]$

Now, magnetizing current (I_m) and current through core loss branch (I_c)can be calculated as:

$$I_m = E_1 / X_m \quad \text{and} \quad I_c = E_1 / R_c \tag{2.2}$$

Therefore, the currents through the overall no-load current, I_0 can be represented as:

$$I_0 = I_c + jI_m \tag{2.3}$$

Rotor current $I_2{}'$ can be found as:

$$I_2{}' = I_1 - I_0 = \frac{E_1}{(Z_2 + Z_l)} \tag{2.4}$$

These equations were solved for estimation of induction motor parameters.

2.3 Parameter estimation of induction motor

It was found during experimentation that if the parameters of the equivalent circuit were estimated using PSO only, the accuracy becomes low. In the equivalent circuit, the output of three phase induction motor is defined as $R_2 \times \frac{(1-s)}{s}$. As in this case, speed is a measured quantity,

hence slip is known. Therefore, estimation of rotor resistance is quite accurate when the load current is dominant. But under no load condition or lightly loaded condition, magnetizing current is predominant. This introduces error in the estimation using particle swarm optimization technique. Again, PSO operates as a global optimization algorithm. Hence, it might encounter a scenario where the global best particle is a local optimum in the optimization problem. This can create a challenge for PSO to break free from this local optimum. As in this problem, motor equivalent circuit parameters are estimated from performance data, therefore, in the above-mentioned circumstances, PSO can get stuck into some local minima (set of parameters) which may differ from the actual parameters of the experimental machine, however, produce the same motor performance. Therefore, using only PSO proves to be problematic in accurately approximating all six motor equivalent circuit parameters $(R_s, R_r, X_{eq}, R_c and X_m)$ and it requires some more information to reduce the estimation error. To address this limitation, various hybrid optimization techniques have been introduced [74]. Some researchers have suggested using modified PSO methods to enhance parameter estimation accuracy and mitigate the issue of converging to local optima [75], [76]. Some literature suggests a combination of both hybridization and modification [77]. However, these modifications and hybrid approaches introduce higher computational complexities and time consumption. Hence H-G diagram-based resistance estimation technique [78], [79] was utilized in this problem to determine the stator and rotor resistances ($R_s and R_r$). The remaining parameters i.e., leakage reactance (X_{eq}), core loss resistance (R_c) and the magnetizing reactance (X_m) were estimated using PSO.

2.3.1. Stator and rotor resistance estimation using H – G diagram

H – G diagram basically represents a two-dimensional plane consist of horizontal axis $H(\omega_{sl})$ and vertical axis $G(\omega_{sl})$ having the dimension of inductance. The parameters H and G are the function of slip frequency ω_{sl} and are associated with the reactive (Q) and active (P) power consumption of the motor, respectively. Once the H_i and G_i can be found out for each operating point $'i'$ of induction motor, the rotor and stator resistance can be found out as described by (2.5) – (2.12). Fig 2.2 depicts the step-by-step representation of the H – G Diagram algorithm, whereas, the equivalent circuit of an induction motor is shown in Fig. 2.3.

Let us consider the steady state, stator and rotor voltage equation as:

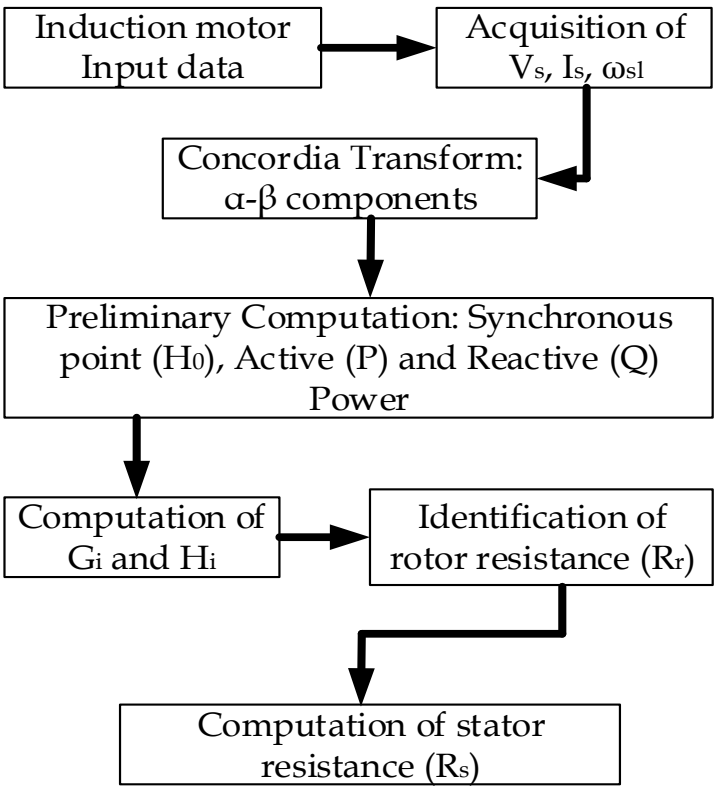

Fig. 2.2. Flowchart of H – G Diagram algorithm.

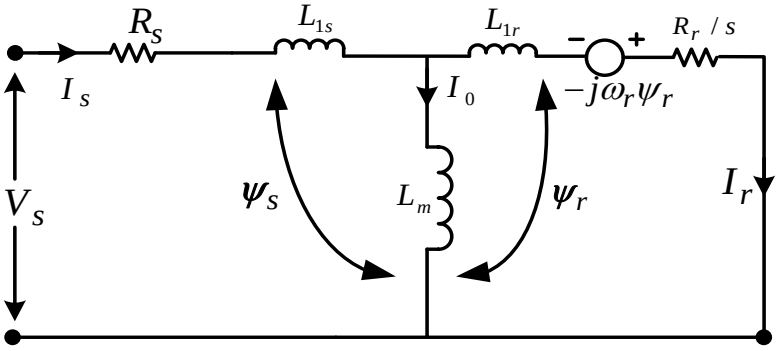

Fig. 2.3. Complex static reference frame induction motor equivalent circuit.

$$\overline{V_s} = (R_s + j\omega_s L_s)\overline{I_s} + j\omega_s M\overline{I_r} \tag{2.5}$$

$$0 = \left(\frac{R_r}{s} + j\omega_s L_r\right)\overline{I_r} + j\omega_s M\overline{I_s} \tag{2.6}$$

As the induction motor, rotor is short circuited (either by end ring or by external resistance), steady state rotor voltage has been considered as $\overline{V_r} = 0$. Here, 'ω_s' is the supply frequency, 's' is the slip, '$L_s(L_r)$' is the cyclic stator (rotor) inductance, '$R_s(R_r)$' represents the stator (rotor) resistance and 'M' stands for the stator-rotor mutual inductance.

The complex input impedance $\overline{Z_{in}}$ can be written as:

$$\overline{Z_{in}} = \frac{\overline{V_s}}{\overline{I_s}} = (R_s + j\omega_s L_s) + \left[\left(\frac{R_r}{s} + j\omega_s L_r\right) \parallel (j\omega_s M)\right] \tag{2.7}$$

Or,

$$\overline{Z_{in}} = \frac{\overline{V_s}}{\overline{I_s}} = R_s + \omega_s G(\omega_{sl}) + j\omega_s H(\omega_{sl}) \tag{2.8}$$

Where,

$$\begin{aligned} G(\omega_{sl}) &= \frac{M^2\omega_{sl}R_r}{R_r^2 + L_r^2\omega_{sl}^2} \\ H(\omega_{sl}) &= L_s - \frac{M^2{\omega_{sl}}^2}{R_r^2 + L_r^2\omega_{sl}^2}L_r \end{aligned} \tag{2.9}$$

The $G(\omega_{sl})$ and $H(\omega_{sl})$ have dimension of inductance and they represent the active power consumption generating the motor torque and reactive power consumption generating the magnetizing flux. The active power

and reactive power consumed by the motor given by the following equation [79].

$$P = \overline{V_s} \bullet \overline{I_s} = u_{s\alpha} i_{s\alpha} + u_{s\beta} i_{s\beta} \tag{2.10}$$

$$Q = \overline{V_s} \times \overline{I_s} = u_{s\alpha} i_{s\beta} + u_{s\beta} i_{s\alpha} \tag{2.11}$$

With change in motor load, the active (P) and reactive (Q) power consumption by the motor changes. Hence, $G(\omega_{sl})$ and $H(\omega_{sl})$ also varies for every operating point. Now, for any operating point $'i'$, $G(\omega_{sl})$ and $H(\omega_{sl})$ can be termed as G_i and H_i, hence can be formulated in terms of active (P) and reactive (Q) power as:

$$\begin{aligned} G_i = G(\omega_{sl}) &= \frac{1}{\omega_s}\left(\frac{P}{{I_s}^2} - R_s\right) \\ H_i = H(\omega_{sl}) &= \frac{Q}{\omega_s {I_s}^2} \end{aligned} \tag{2.12}$$

Where, ${I_s}^2 = {I_{s\alpha}}^2 + {I_{s\beta}}^2$ (concordia transform [80], [81])

If the operating point $'i'$ is varied from no-load (H_0) to rated load (H_i) condition, then considering the experimental magnetizing characteristics, rotor resistance can be deduced from (2.13) – (2.16). From (2.9), it can be written that:

$$\frac{\frac{G_i}{1-\frac{H_i}{H_0}}\omega_{sl}}{1-\left(\frac{L_s - \frac{M^2 {\omega_{sl}}^2}{R_r^2 + L_r^2 \omega_{sl}^2} L_r}{L_s}\right)} = \frac{\frac{M^2 \omega_{sl} R_r}{R_r^2 + L_r^2 \omega_{sl}^2}}{1-\left(\frac{L_s - \frac{M^2 {\omega_{sl}}^2}{R_r^2 + L_r^2 \omega_{sl}^2} L_r}{L_s}\right)} \omega_{sl} \tag{2.13}$$

Here, H_0 is the pure synchronous point where $\omega_{sl} = 0$. Hence, from (2.9), at pure synchronous point, $H_i = H(\omega_{sl}) = H_0 = L_s$.

Equation (2.13) can be simplified as follows:

$$\frac{G_i}{1-\frac{H_i}{H_0}}\omega_{sl} = \frac{\frac{M^2\omega_{sl}R_r}{R_r^2+L_r^2\omega_{sl}^2}}{\left(\frac{L_s-L_s+\frac{M^2{\omega_{sl}}^2}{R_r^2+L_r^2\omega_{sl}^2}L_r}{L_s}\right)}\omega_{sl}$$

$$\frac{G_i}{1-\frac{H_i}{H_0}}\omega_{sl} = \frac{\left(\frac{M^2\omega_{sl}R_r}{R_r^2+L_r^2\omega_{sl}^2}\right)\cdot L_s}{\left(\frac{M^2{\omega_{sl}}^2}{R_r^2+L_r^2\omega_{sl}^2}\right)L_r}\omega_{sl}$$

$$\frac{G_i}{1-\frac{H_i}{H_0}}\omega_{sl} = \left(\frac{M^2\omega_{sl}R_r}{R_r^2+L_r^2\omega_{sl}^2}\right)\cdot\left(\frac{R_r^2+L_r^2\omega_{sl}^2}{M^2{\omega_{sl}}^2}\right)\cdot\left(\frac{L_s}{L_r}\right)\omega_{sl}$$

$$\frac{G_i}{1-\frac{H_i}{H_0}}\omega_{sl} = \left(\frac{\omega_{sl}R_r}{{\omega_{sl}}^2}\right)\cdot\left(\frac{L_s}{L_r}\right)\omega_{sl}$$

$$\frac{G_i}{1-\frac{H_i}{H_0}}\omega_{sl} = R_r\cdot\left(\frac{L_s}{L_r}\right)$$

Therefore, simplifying (2.13), it can be written that,

$$\frac{G_i}{1-\frac{H_i}{H_0}}\omega_{sl} = R_r\left(\frac{L_s}{L_r}\right) \tag{2.14}$$

Considering the stator and rotor flux leakages to be equal, $L_s = L_r$, so,

$$R_r = \frac{G_i}{1-\frac{H_i}{H_0}}\omega_{sl} \tag{2.15}$$

The stator resistance can be given by

$$R_s = kR_r \tag{2.16}$$

Where,

$$k = \frac{R_{sn}}{R_{rn}}$$

R_{sn} & R_{rn} are the rated values of stator and rotor resistance respectively. These values can also be determined by performing no-load test, blocked rotor test and DC resistance measurement.

2.3.2. Overview of PSO

Particle swarm optimization technique was first proposed by Kennedy and Eberhart [71]. This method is based on two fundamental concepts: social concept and swarm intelligence concept. It consists of swarm of particles, where each particle symbolizes a potential solution. The swarm is defined as a set:

$$s = \{x_1, x_2, \ldots, x_N\} \tag{2.17}$$

N is number of particles (candidates' solution).

Each particle has a unique position vector and velocity in the search space. Position of particle can be shifted by adding velocity to the current position. Position vector and velocity of each particle is defined as:

$$x_i = \{x_{i1}, x_{i2}, \ldots, x_{in}\}^T \subseteq A \quad \text{where } i = 1,2,\ldots,N \tag{2.18}$$

$$v_i = (v_{i1,} v_{i2}, \ldots, v_{in})^T \subseteq A \quad \text{where } i = 1,2,\ldots,N \tag{2.19}$$

Velocity of particle can be updated using the information obtained from previous step. This is implemented in terms of memory where the particle's best position is stored. This memory can be defined:

$$P_i = (P_{i1}, P_{i2}, \ldots, P_{in})^T \subseteq A \tag{2.20}$$

After each iteration, position and velocity should be updated using following two equations.

$$v_i(t+1) = w \cdot v_i + c_1 R_1 (P_{ibest} - x_i) + c_2 R_2 \left(P_{gbest} - x_i\right)$$

$$x_i(t+1) = x_i(t) + v_i(t+1) \tag{2.21}$$

Where, $'t'$ is the iteration counter, R_1 and R_2 are random variables between 0 and 1, $w$is the particle inertia, c_1 is the cognitive parameter

and c_2 is the social parameter. $p_{ibest}(t)$ and $p_{gbest}(t)$ are local and global best position in the search space.

With the update in position and velocity after every iteration, the best position for each particle should also be updated. If, with the local best position, the function value moves towards convergence, then the local best will be replaced by the new best position. Otherwise, the solution retains the previous position.

The same procedure is followed for the global best. With mathematical equations, this can be represented as:

$$\left.\begin{aligned} P_i(t+1) &= \begin{cases} x_i(t+1) if,\ f\big(x_i(t+1)\big) < f\big(P_i(t)\big) \\ P_i(t) Otherwise \end{cases} \\ P_g(t+1) &= \begin{cases} P_i(t+1) if,\ f\big(P_i(t+1)\big) < f\left(P_g(t)\right) \\ P_g(t) Otherwise \end{cases} \end{aligned}\right\} \quad (2.22)$$

The pseudocode of Particle swarm optimization technique is given in Table 2.1. Whereas, Fig 2.1 represents the general flowchart of particle swarm optimization.

The computation time as well as precision of PSO depends on the defined search space and its internal parameters i.e., size of population, tolerance limit etc. The inertia weight constant was chosen based on the constriction factor approach. The inertia weight is updated dynamically during the optimization process based on the following equation:

$$w = w_{max} - \left((w_{max} - w_{min}) * \frac{Current\ iteration}{Maximum\ iteration}\right)$$

where, w_{max} = Maximum inertia weight = 0.9

w_{min} = Minimum inertia weight = 0.4

Table 2.1. Pseudocode of the operation of PSO [71], [72], [73]

Input	No. of particles: N, Swarm: S, Best particle: P
Step 1	Set $t \leftarrow 0$
Step 2	Initialize$S$and set $P \equiv S$.
Step 3	Evaluate S and P, and define index g of the best position.
Step 4	While (termination criterion not met)
Step 5	Update S using equations (1) and (2).
Step 6	Evaluate S.
Step 7	Update P and redefine index g.
Step 8	Set t ← (t + 1) .
Step 9	End While
Step 10	Print best position.

The cognitive and social coefficient C_1 and C_2 were selected based on the performance analysis, through trial-and-error method. C_1 and C_2 values were kept same as 1.5 to achieve the best result for this specific problem. Based on practical experience and parameter values obtained from classical DC resistance test, no-load test and blocked rotor test. the boundary of search area is kept large enough to increase the practicality of the technique. This ensures that the estimation technique converges towards the actual parameter values despite handling a large boundary condition. On the other hand, the variables of PSO have been selected to maintain a favourable relation between precision and computational time.

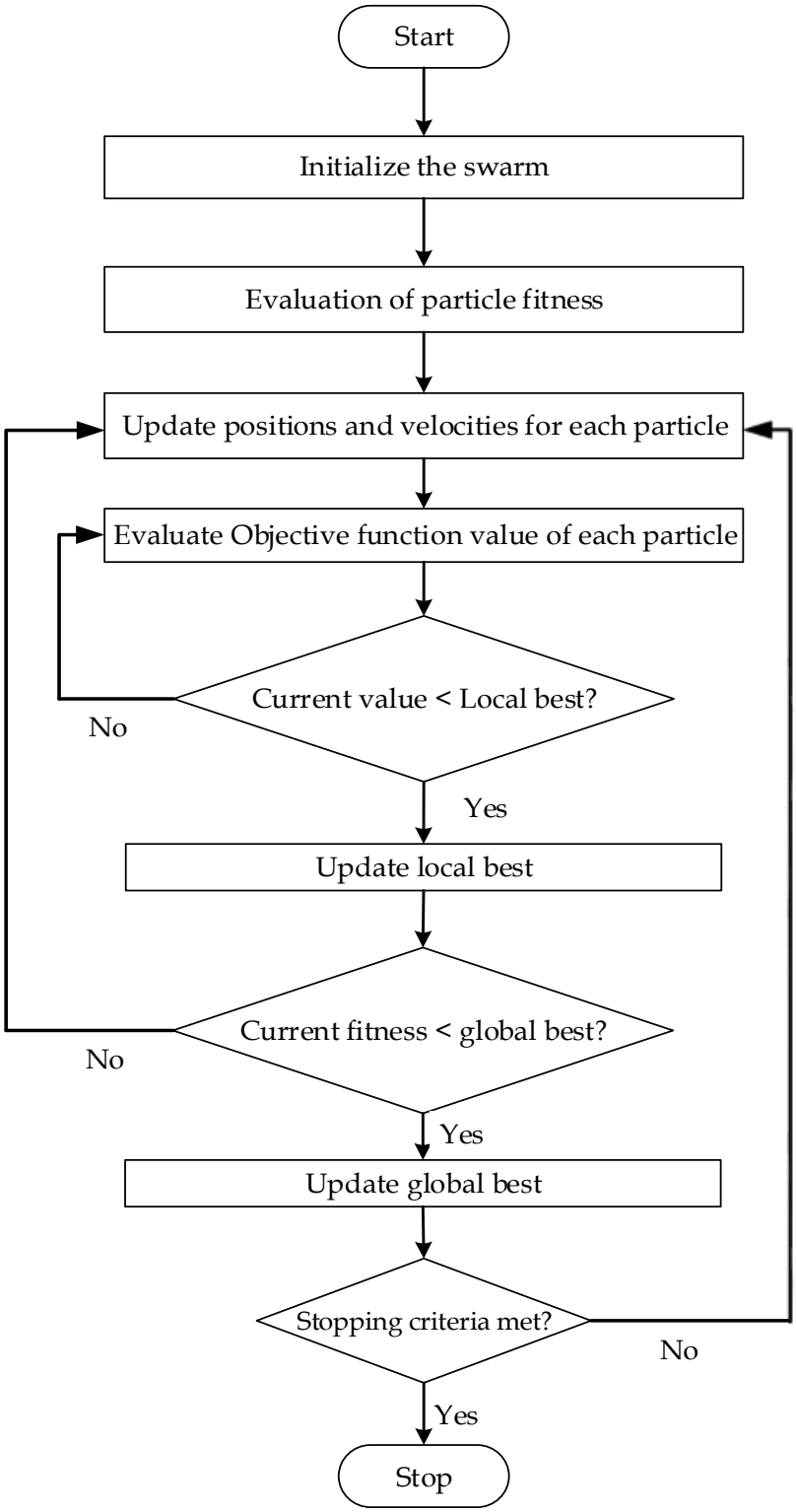

Fig. 2.4. Flowchart of particle swarm optimization (PSO).

2.3.3. Formulation of objective function for PSO

For the estimation of equivalent leakage reactance (X_{eq}), core loss resistance (R_c), and magnetizing reactance (X_m), the objective function was formulated based on the minimization of square error technique as given in equation (2.23).

$$0 = min\left[\left(\frac{I_1 - I_{1est}}{I_1}\right)^2 + \left(\frac{I_0 - I_{0est}}{I_0}\right)^2 + \left(\frac{P_{in} - P_{inest}}{P_{in}}\right)^2 + \left(\frac{P_{out} - P_{outest}}{P_{out}}\right)^2 + \left(\frac{pf_{in} - pf_{inest}}{pf_{in}}\right)^2\right] \quad (2.23)$$

From the experimental observations, it can be concluded that, a large number of sets of parameter values satisfies same nameplate data (i.e., magnitude of current, voltage and efficiency remain near rated value whereas the parameter values are changing a lot). There are various reasons for this. For example, induction motors designed with same current density and flux density, but with different values of actual number of primary and secondary turns (turns ratio being same) will have different parameters. Parameters also depend on the number of stator and rotor slots and their dimension. Even the parameters will differ if the winding arrangement varies, with every other consideration remaining same. Therefore, here all the measurable quantities such as stator current (I_1), input power (P_{in}), input power factor (pf_{in}), output power (P_{out}) are considered in formation of the objective function. Subscript $'est'$ stands for estimated values of corresponding quantities. The above-mentioned quantities are taken into consideration as they change with load and defines machine behavior. Here, the no-load current I_0 plays an important role in accurate estimation of core loss resistance R_c and magnetizing reactance X_m. Hence, I_0 was considered in the objective function. However, it is not possible to measure the no-

load current of the motor under running condition. The no-load current has been considered as 40% of the full-load current in accordance with the guidelines of National Electrical Manufacturers Association (NEMA). No-load test also holds up this consideration. Magnetizing current (I_m) and current through core loss branch (I_c) are not separately used here in the objective function as they are neither the measurable quantity, nor provided by the manufacturer. However, the algorithm could distinguish between I_m and I_c to come up with an estimate of R_c and X_m because, no load current I_0 comprised of I_m and I_c considering them as vectors. Therefore, the algorithm estimates R_c and X_m in such a manner so that estimated no load current I_{0est} is close enough to the prescribed value I_0. On the other hand, the algorithm considers the power factor in the objective function. Therefore, at the same time, it will try to maintain the power factor error value close to zero. This consideration also leads the algorithm to come up with an accurate estimation of R_c and X_m.

The practicality of the PSO technique increases if it converges towards the actual parameter values despite handling a large search space. Therefore, here a large boundary condition has been considered for all the equivalent circuit parameters. Table 2.2 provides the boundary condition of search area. On the other hand, convergence time and accuracy of the technique depends on the variables of PSO e.g., population size, tolerance limit etc. In this work, the PSO variables have been selected in such a way so that an optimum relation between accuracy and convergence time is maintained. Table 2.3 presents variables of PSO which have been considered for the estimation.

Table 2.2. Limit of search area for Particle Swarm Optimization (PSO)

Parameter	X_{eq} $(in\ \Omega)$	R_c $(in\ \Omega)$	X_m $(in\ \Omega)$
Lower Bound	1.00	100.0	1.00
Upper Bound	50.0	50000.0	1000.0

Table 2.3. Variables of PSO considered for estimation

Optimization Technique	Population Size	Max. Iteration	Max. Iteration Stalling	Function Tolerance
PSO	50	600	100	1e-6

2.4 Experimental setup

Fig. 2.5. Experimental setup of induction motor used in the laboratory.

The complete experimental setup is shown in Fig: 2.5. The experimental setup consisted of a three – phase, four pole, 110 V, 2 kW, 50 Hz induction motor (nameplate specifications of the machine has been given in Table 2.4) coupled with an eddy current dynamometer for output power and torque measurement. A resistive load box was used for varying the load of the dynamometer. The supply voltage was kept constant by an autotransformer. A 'YOKOGAWA C240' power analyzer was used for input voltage, input current, power and power factor measurement and a 'MECO-G' optical tachometer was used for speed measurement. A calibrated digital weight machine was used for the load measurement. The eddy current dynamometer used in this experiment is a custom-built device. The eddy current dynamometer has an arm extension connected to its stator. At the farthest end of the arm, a pointer was connected. This pointer was placed on a digital weight machine for torque measurement. When the prime mover of the dynamometer (induction motor under test) rotates with dynamometer field supply turned on, the extended arm exerts a force on the digital weight meter. That force, multiplied by the am length evaluates the shaft torque of the motor. With the knowledge of motor speed, the output power of the motor was calculated.

Table 2.4. Nameplate Data for the Induction Motor Under Observation

Maker's Name	**Frame**	**Type**	**Voltage**	**Current**
General Electric	225	M	110 V	14.4 A
Speed	**Cycle**	**Service Factor**	**Secondary Voltage**	**Secondary Current**
1430 rpm	50	1.15	52 Volt	20.8 Amps

Let us consider that the digital weight meter reading is: 'W' kg. Length of arm extension of the dynamometer is: 'R' meter. Radius of the dynamometer is: 'r' meter. Therefore, shaft torque can be calculated as:

$$T_{sh} = W \times 9.81 \times (R + r) \text{ N-m} \tag{2.24}$$

Hence, shaft power can be calculated as;

$$P_{sh} = T_{sh} \times 2\pi \times \frac{N_r}{60} \tag{2.25}$$

$$P_{sh} = W \times 9.81 \times (R + r) \times 2\pi \times \frac{N_r}{60} \quad \text{watt} \tag{2.26}$$

The field circuit of the dynamometer was connected to a resistive load box. The shaft load of the induction motor was varied by varying the dynamometer field current. Fig 2.6 displays the eddy current dynamometer used for the experiment.

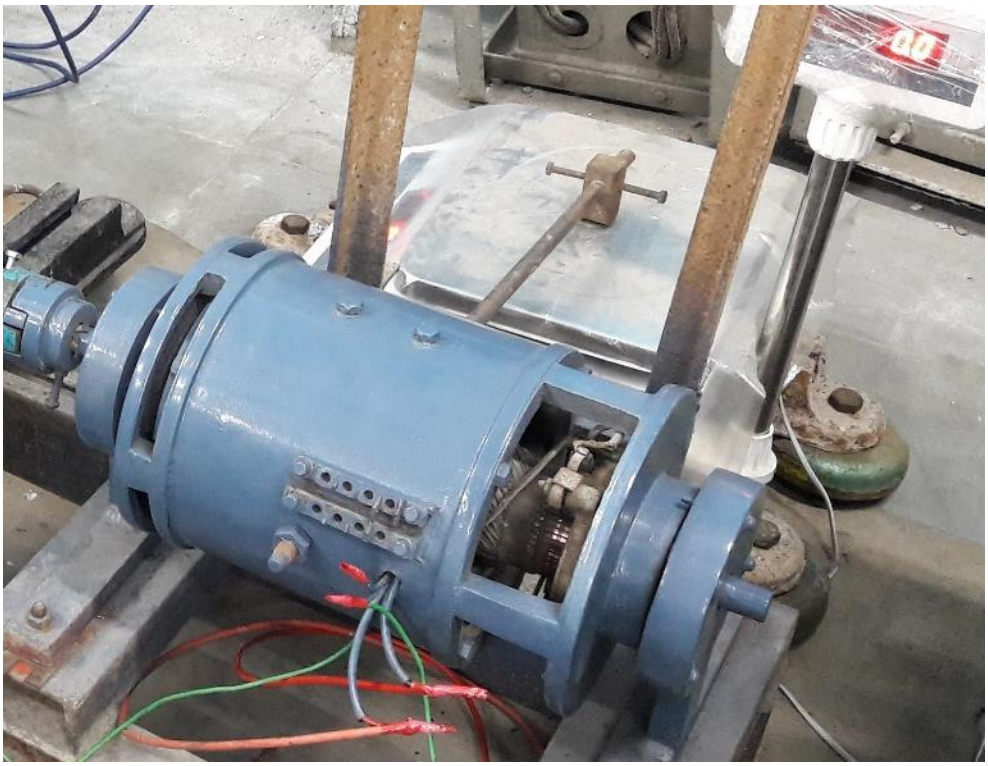

Fig. 2.6. The custom-built eddy current dynamometer.

The following tests were performed initially on the machine for determining equivalent circuit parameters.

- DC resistance test
- No-load test for induction motor
- Blocked rotor test for induction motor

The experimentally obtained parameter values can be used as the references for determining the accuracy of the proposed estimation technique. These test results are shown in Table 2.5.

Here, 'cold' resistance in Table 2.5 signifies the initial resistance, measured at ambient temperature whereas 'hot' resistance implies the resistance measured after the machine reaches thermal equilibrium state, running with rated load. The dc resistances, thus obtained from the test, were then converted into ac resistances by multiplying a factor of 1.2.

Table 2.5. Motor parameter values obtained from conventional experiment as par IEEE standard test procedures [13]

R_s(in Ω)		R_r (in Ω)		X_{eq} (in Ω)	R_C (in Ω)	X_m (in Ω)
cold	**hot**	**cold**	**hot**			
0.7	0.81	1.15	1.33	2.87	158.19	27.61

2.5 Results and Analysis

The proposed algorithm employs steady state circuit model of induction motor for parameter estimation. H – G diagram and Particle swarm

optimization has been assigned to evaluate the best possible parameter set (R_s, $R_r X_{eq}$, R_c and X_m) for the induction motor at any particular load.

First of all, the rms voltage (V_{in}), stator current (I_1), input power (P_{in}) and input power factor (pf_{in}) data were recorded with the help of 'YOKOGAWA C240' power analyzer. Rotor speed (N_r) was recorded with the a 'MECO-G' optical tachometer. The output power (p_{out}) was calculated from the digital weight meter reading as given in (2.26).

Now, the recorded rms voltage (V_{in}), current (I_1) and speed (N_r) data has been fed into the computer programming-based H-G diagram. The computer program performs the concordia transform [80] and computes $G(\omega_{sl})$ and $H(\omega_{sl})$ values for each induction motor operating point at ω_{sl} (slip frequency). Finally, the stator (R_s) and rotor (R_r) resistances at different load were estimated from H-G diagram as discussed in section 2.3.1. The estimated stator and rotor resistances under different load on the machine and their comparison with the corresponding experimentally obtained values are given in Table 2.6.

Table 2.6. Comparison of stator and rotor resistance values: Experimental vs. Estimated from H – G diagram

Parameters (in Ω)	**Experimentally obtained values (in Ω)**		**Parameters estimated from H – G diagram at different load (in Ω)**			
	Cold	**Hot**	**40 % Load**	**75 % Load**	**90 % Load**	**100 % Load**
$\boldsymbol{R_s}$	0.7	0.81	0.706	0.717	0.761	0.8027
$\boldsymbol{R_r}$	1.15	1.33	1.173	1.192	1.264	1.3336

In the second part, as stator (R_s) and rotor (R_r) resistances have already been evaluated for different load condition, therefore, they can be

considered as predefined. Now, the recorded rms voltage data was fed into the computer programming-based steady-state induction motor model. This mathematical model provides motor current $(I_{1_{est}})$, input power $(P_{in_{est}})$, input power factor $(pf_{in_{est}})$, output power $(P_{out_{est}})$ and no-load current $(I_{0_{est}})$ as model output. These estimated quantities $(I_{1_{est}}, P_{in_{est}}, pf_{in_{est}}, P_{out_{est}} and\ I_{0_{est}})$ were compared with the corresponding measured values $(I_1, P_{in}, pf_{in}, P_{out} and I_0)$ using particle swarm optimization to minimize the objective function value as specified in (2.19) and estimate remaining equivalent circuit parameters i.e. magnetizing reactance (X_m), core loss resistance (R_c) and equivalent leakage reactance (X_{eq}).

If the objective function value falls below the tolerance limit, the optimization gets terminated and corresponding parameter set is considered as the best parameter set. Otherwise, the iteration continues till the best parameter set has been found. Table 2.7 presents the comparison of estimated and experimentally obtained values of $X_{eq}, R_c and X_m$ under different load condition.

Table 2.7. Evaluation of estimated parameters and comparison with experimentally obtained data

Parameters (in Ω)	**Experimentally obtained values (in Ω)**	**Estimated parameters (in Ω)**			
		40 % Load	**75 % Load**	**90 % Load**	**100 % Load**
X_{eq}	2.87	3.485	3.46	3.33	2.868
R_c	158.19	165.4	165.1	162.5	160.02
X_m	27.61	28.95	28.80	28.35	27.917

This comparison shows that the estimation algorithm is capable of estimating the parameters without much error.

Table 2.8 compare the estimated motor performance data with the corresponding measured values under different load conditions. The analysis shows that the proposed estimation scheme can predict the performance of the machine in a comprehensive manner with an acceptable degree of precision.

Table 2.8. Motor performance data obtained from estimated parameters

Performance Data		**Loading**			
		40 % Load	**75 % Load**	**90 % Load**	**100 % Load**
Input Current	Measured	7.91	10.07	11.68	13.05
	Estimated	7.870	10.16	11.21	12.606
	% Error	0.500	-0.89	4.048	3.402
Input Power	Measured	870.1	1464.	1689.	1990.7
	Estimated	868	1466	1690	1986.5
	% Error	0.245	-0.11	-0.055	0.208
Input Power Factor	Measured	0.55	0.71	0.76	0.80
	Estimated	0.552	0.711	0.758	0.7993
	% Error	0.554	0.717	0.756	0.7995
Output Power	Measured	606.8	1140	1324	1547.2
	Estimated	606	1141	1323	1551.3
	% Error	0.133	-0.05	0.046	-0.266
Speed	Measured	1468	1436	1420	1396
	Estimated	1467	1437	1418	1396
	% Error	0.041	-0.06	0.120	0

The variation of the parameters with load, are shown in fig 2.7 (a)-(d). From the figures, it is evident that the estimated parameters are within acceptable limit.

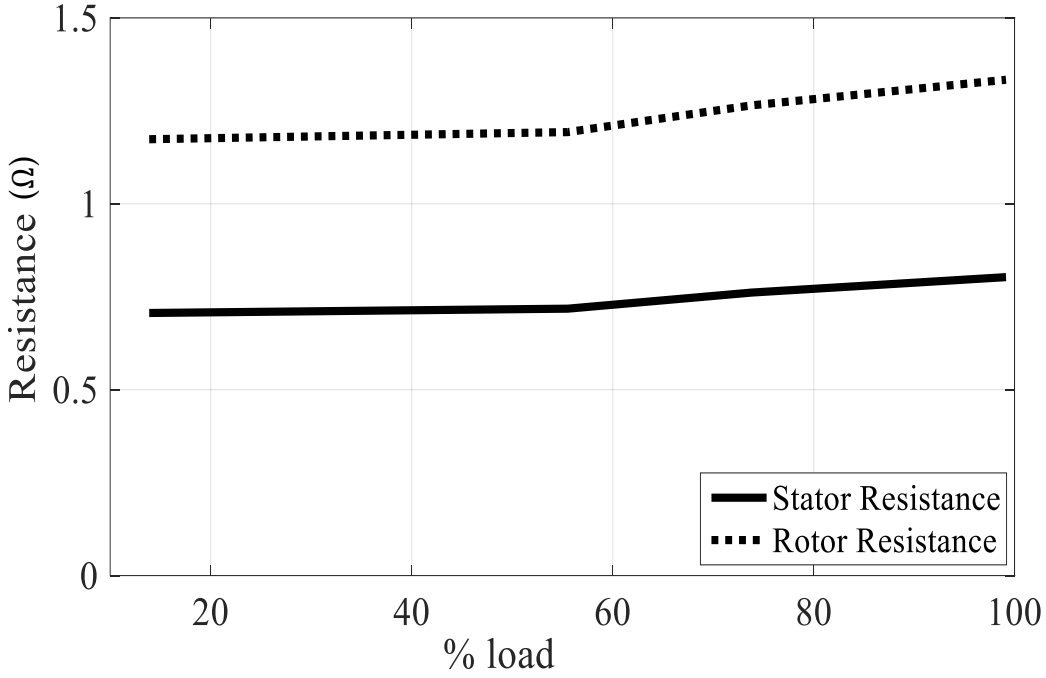

(a)

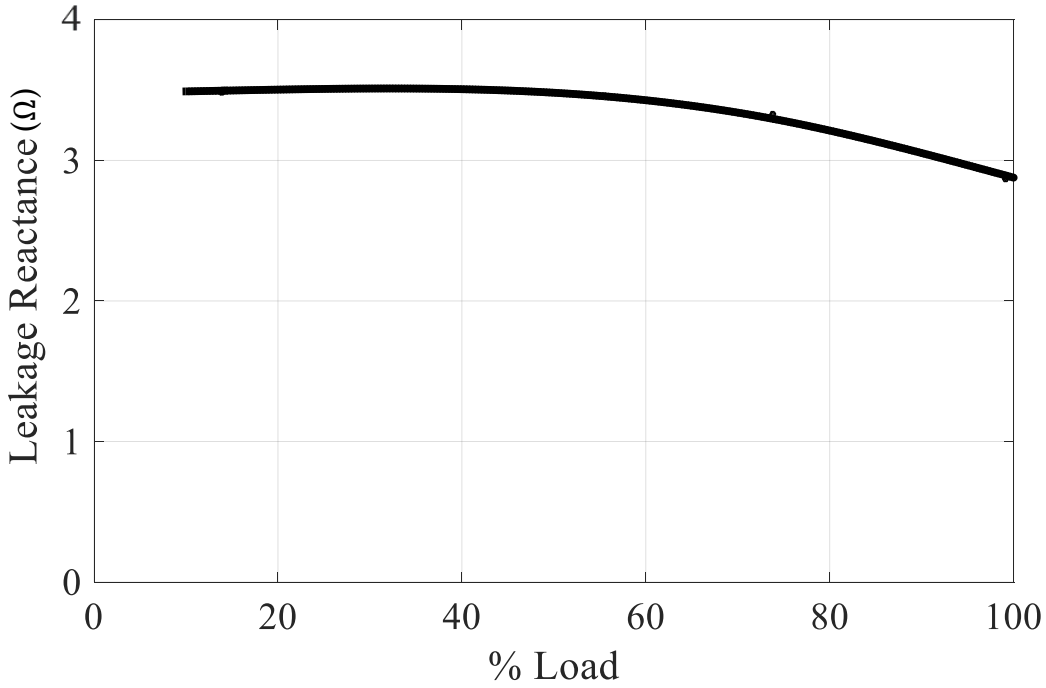

(b)

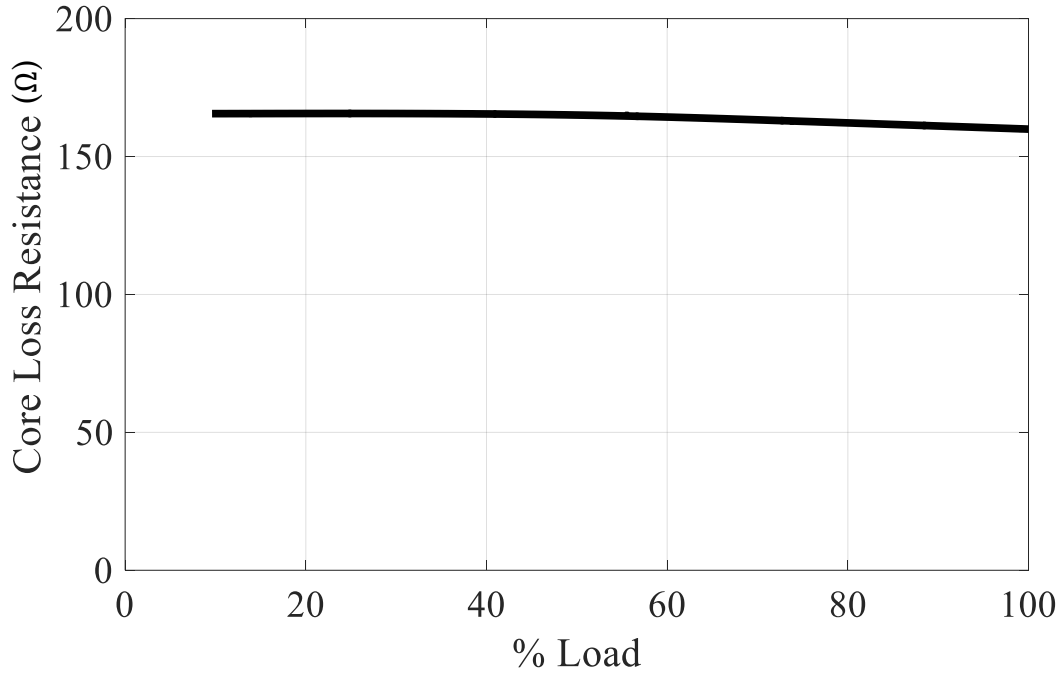

(c)

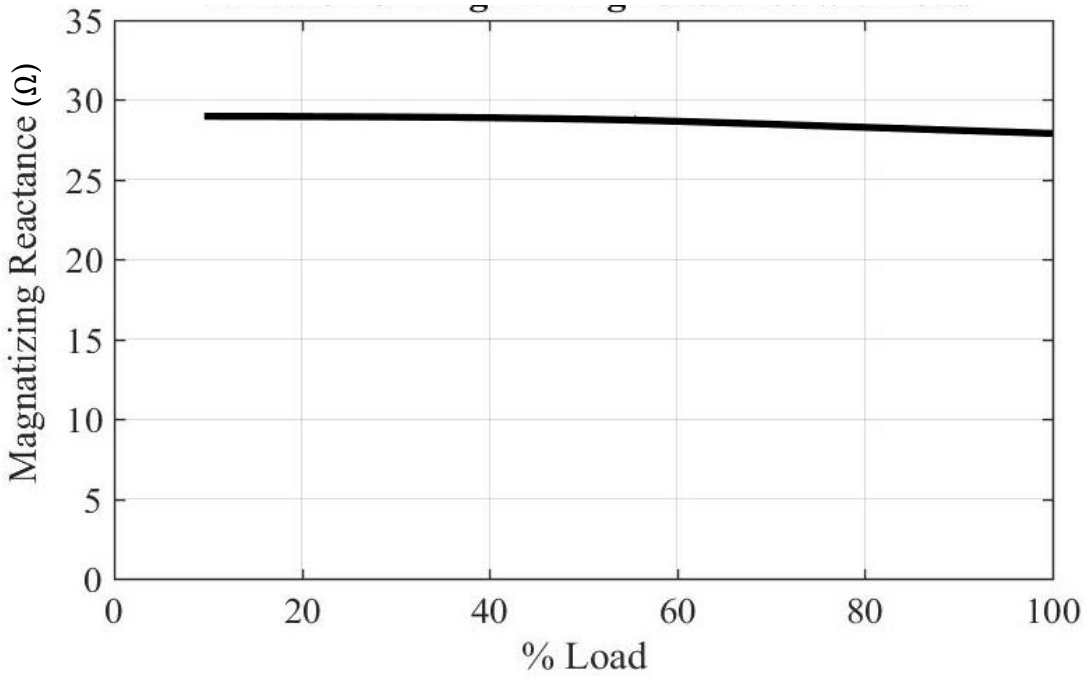

(d)

Fig. 2.7. Variation of (a) stator and rotor resistance, (b) equivalent leakage reactance, (c) core loss resistance and (d) magnetizing reactance with load.

Graphical representation of variation of different losses (measured in Watt) with load is shown in Fig. 2.8.

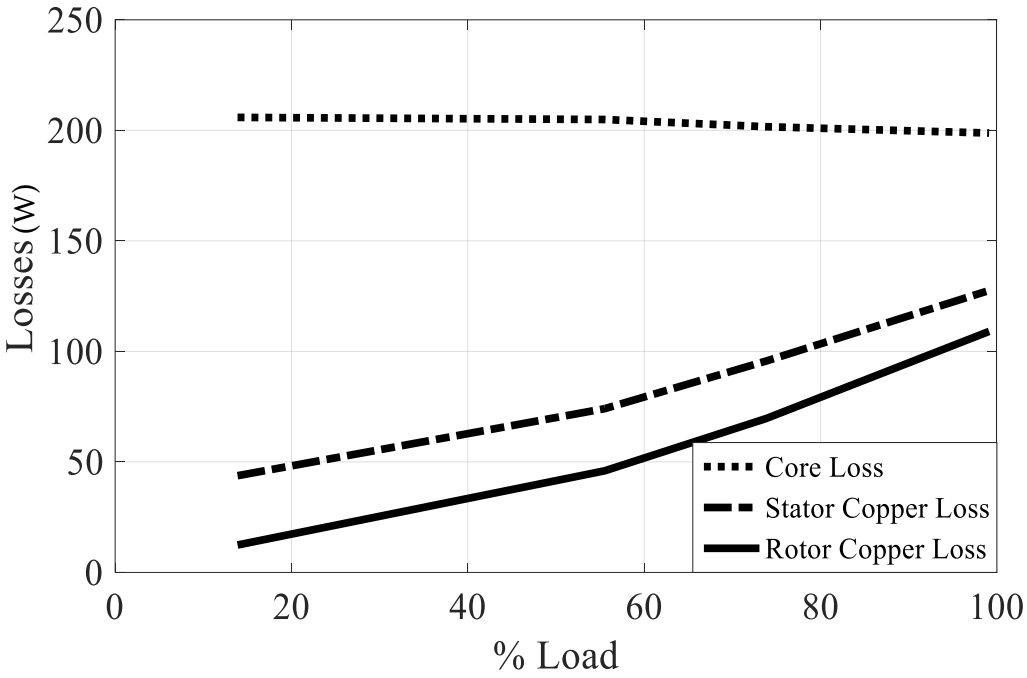

Fig. 2.8. Variation of different losses with load.

2.6 Conclusion

Accurate parameter estimation is essential for vector-controlled drives and fault detection of electrical machines. A simple, and effective technique to estimate the equivalent circuit parameters of a three-phase induction motor from load data has been proposed in this work. The identification process is carried out using a very simple method, which is easy to understand and gives sufficiently good accuracy. The simulation result substantiates this observation. This method is easy to implement and with little modifications it can be adopted for parameter estimation of other machines also. This method can be improved by validating it for Variable Voltage Variable Frequency (VVVF) drive induction motors with different load condition. The losses estimated using the proposed scheme, can be utilized in thermal model of these

machines for temperature prediction so that the machines can be protected from thermal failure too. However, the proposed scheme requires voltage, current, input power, output power, input power factor and speed measurement data along with and no-load current information to pursue the estimation. However, no load current is not a measurable quantity while the motor is under operation. Therefore, here no-load current is assumed from NEMA guideline to maintain any ongoing motor operation uninterrupted. These issues can also be addressed by incorporating some modifications in the proposed scheme.

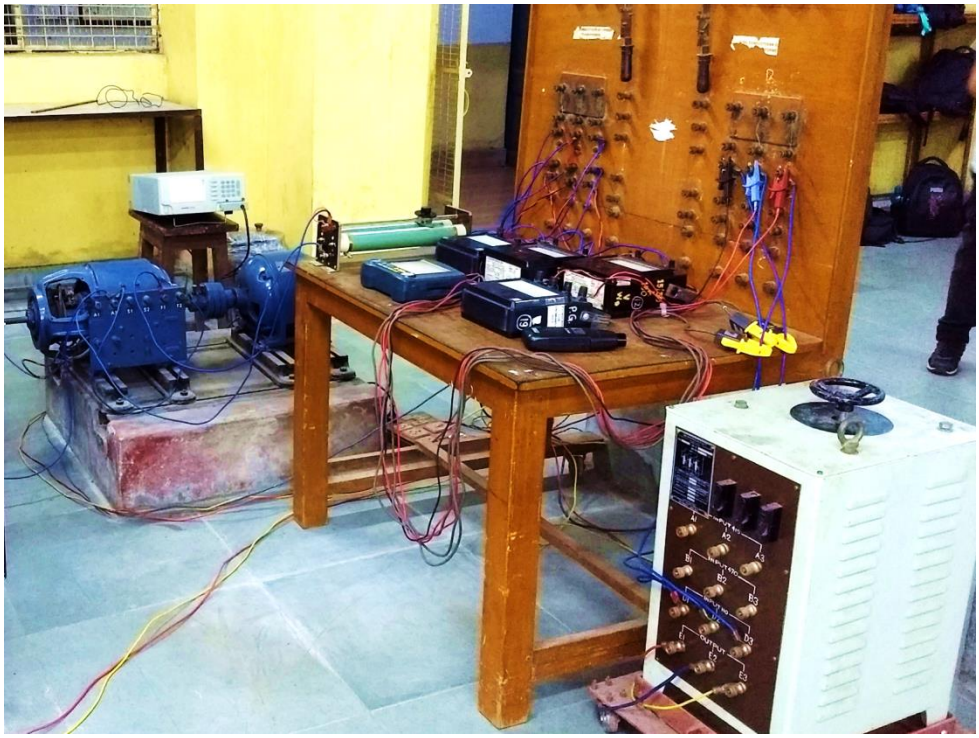

CHAPTER 3

Estimation of Parameter and Losses of a Three Phase Induction Motor from Steady State Performance Data using Dynamic Model

This chapter digs into the innovative approach employed to estimate parameters and losses in three-phase induction motors. Focused on refining motor performance analysis, the proposed approach combines dynamic models with steady-state data. This chapter outlines the methodology, theoretical framework, and key considerations for precise estimation of parameters and losses in three-phase induction motors. This research aims to contributes crucial insights into the field of parameter and loss estimation, enhancing the precision of motor analysis andimproving the efficiency and reliability of induction motors in diverse applications.

3.1 Introduction

This chapter, introduces a method for estimating parameters and losses of three-phase induction motors from dynamic model. This approach utilizes dynamic models, fed with steady-state data. Parameter and loss estimation using steady-state equivalent circuits, requires extensive measurements and assumption of no-load current. To overcome these limitations, this study employs a dynamic motor model, which allows for more accurate parameter and loss estimation without the need to consider the no-load current. By integrating dynamic modeling with steady-state data, this approach offers a more efficient and reliable solution for estimating induction motor parameters and losses.

The aim of this work is to develop a parameter and loss estimation method that is simple, minimal in terms of data acquisition resources and do not disturb the ongoing process during data acquisition for estimation purpose. This work lays the foundation for insight about the working of the motors, leading to more effective and dependable performance in different applications. This is especially useful in industries where, getting the most out of motor performance is very important.

The theory and objective of this work is presented in section 3.2. Section 3.3 describes the software tools and experimental setup used for estimation. Section 3.4 presents a detailed result analysis and validation. Section 3.5 explains necessity of considering the dynamic model and fed it with steady state data. Section 3.6 provide the validation of the proposed scheme with another machine of similar rating but different equivalent circuit parameter values. Section 3.7 concludes the work and enlightens some of the potential future scopes of the work respectively.

3.2 Theory and objective of the work

Accurate parameter values can provide an insight into the health of the induction motor. Successful determination of motor parameter can provide an estimation of induction motor performance and can help reducing the downtime due to failure. It has been observed in chapter 2 that, motor parameter and loss estimation from steady state data considering steady state equivalent circuit requires a lot of measurement for estimation. This increases the measurement burden as well as makes the objective function very bulky. It requires the no load current to be incorporated in the objective function which is neither a directly measurable quantity under running condition, nor provided by the manufacturer. Hence, the no-load current was assumed following NEMA guideline. This technique is applicable for healthy and new motors. However, rewinding or aging may alter this value. introducing error in estimation. To overcome these shortcomings, dynamic model of induction motor has been considered here instead of steady state model for the estimation of motor parameters and losses.

Classical dynamic model, proposed by Krause [82-84], does not consider the core loss resistance in the equivalent circuit considering constant core loss. With increase in loading, the winding temperature increases which in turn, increase the resistance of the stator winding. This phenomenon increases voltage drop across stator winding; therefore, the airgap voltage reduces. Due to temperature rise, lamination resistance also increases. Cumulatively, they affect and alter the core loss value. Hence, the notion of upholding core loss as a constant loss can no longer be considered. Thus, for precise estimation of core loss, the core loss resistance needs to be identified accurately. Hence in this

work, the core loss equivalent resistance (R_c) has been incorporated in the mathematical model of induction motor and the equations have been modified accordingly.

From Fig. 3.1, the d and q axis voltage equations for dynamic model of a three-phase induction motor can be given as:

$$V_{qs}{}^{e} = R_s \times i_{1qs} + \frac{\omega}{\omega_e}\psi_{ds} + \frac{p}{\omega_e}\psi_{qs} \tag{3.1}$$

$$V_{ds}{}^{e} = R_s \times i_{1ds} - \frac{\omega}{\omega_e}\psi_{qs} + \frac{p}{\omega_e}\psi_{ds} \tag{3.2}$$

$$V_{qr}{}^{e} = R_r \times i_{qr} + \frac{(\omega-\omega_r)}{\omega_e}\psi_{dr} + \frac{p}{\omega_e}\psi_{qr} \tag{3.3}$$

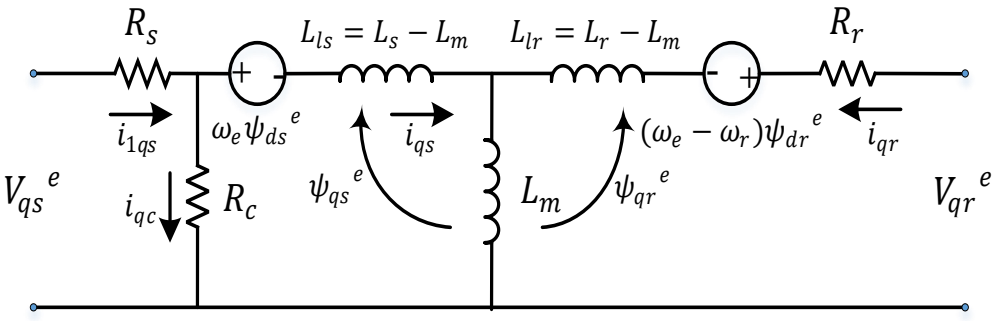

(a)

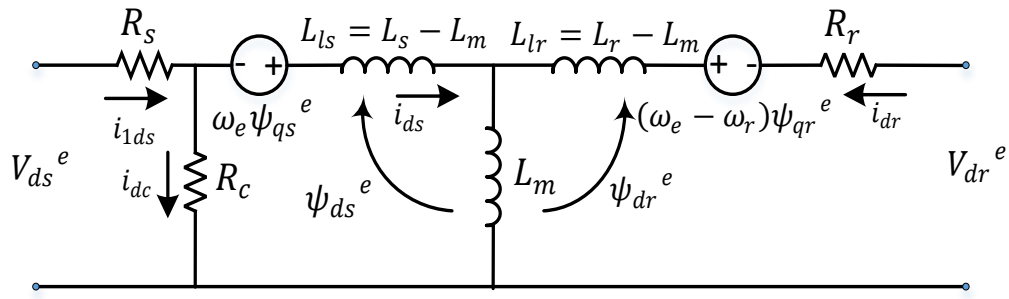

(b)

Fig. 3.1. a) q – axis, (b) d – axis equivalent circuit of induction motor considering core loss resistance in synchronously rotating reference frame.

$$V_{dr}{}^{e} = R_r \times i_{dr} - \frac{(\omega-\omega_r)}{\omega_e}\psi_{qr} + \frac{p}{\omega_e}\psi_{dr} \quad (3.4)$$

Where, p is the derivative operator ($\frac{d}{dt}$).

For induction motor, $V_{qr}{}^{e} = V_{dr}{}^{e} = 0$.

Therefore, flux linkage equations have been written as:

$$\psi_{qs} = X_{ls}i_{qs} + X_m(i_{qs} + i_{qr}) \quad (3.5)$$

$$\psi_{ds} = X_{ls}i_{ds} + X_m(i_{ds} + i_{dr}) \quad (3.6)$$

$$\psi_{qr} = X_{lr}i_{qr} + X_m(i_{qs} + i_{qr}) \quad (3.7)$$

$$\psi_{dr} = X_{lr}i_{dr} + X_m(i_{ds} + i_{dr}) \quad (3.8)$$

$$\psi_{mq} = X_m(i_{qs} + i_{qr}) \quad (3.9)$$

$$\psi_{md} = X_m(i_{ds} + i_{dr}) \quad (3.10)$$

Where, $X_{ls}$is the stator leakage reactance, X_{lr} is the rotor leakage reactance and X_m is the mutual or magnetizing reactance. These quantities have been represented as:

$$X_{ls} = \omega_e L_{ls}$$

$$X_{lr} = \omega_e L_{lr}$$

$$X_m = \omega_e L_m$$

d and q axis current representation in terms of flux linkage have been given as follows.

$$i_{qs} = \frac{1}{X_{ls}}(\psi_{qs} - \psi_{mq}) \quad (3.11)$$

$$i_{ds} = \frac{1}{X_{ls}}(\psi_{ds} - \psi_{md}) \quad (3.12)$$

$$i_{qr} = \frac{1}{X_{lr}}(\psi_{qr} - \psi_{mq}) \tag{3.13}$$

$$i_{dr} = \frac{1}{X_{lr}}(\psi_{dr} - \psi_{md}) \tag{3.14}$$

q and d axis core loss components of current ($i_{qc} and i_{dc}$) in terms of flux linkage have been written as:

$$i_{qc} = \frac{1}{R_c}(\frac{p}{\omega_e}\psi_{qs} + \frac{\omega}{\omega_e}\psi_{ds}) \tag{3.15}$$

$$i_{dc} = \frac{1}{R_c}(\frac{p}{\omega_e}\psi_{ds} - \frac{\omega}{\omega_e}\psi_{qs}) \tag{3.16}$$

The stator current ($i_{1qs} and i_{1ds}$) will be the summation of reactive component and core loss component and hence, can be represented as follows:

$$i_{1qs} = i_{qs} + i_{qc} = \frac{1}{X_{ls}}(\psi_{qs} - \psi_{mq}) + \frac{1}{R_c}(\frac{p}{\omega_e}\psi_{qs} + \frac{\omega}{\omega_e}\psi_{ds}) \tag{3.17}$$

$$i_{1ds} = i_{ds} + i_{dc} = \frac{1}{X_{ls}}(\psi_{ds} - \psi_{md}) + \frac{1}{R_c}(\frac{p}{\omega_e}\psi_{ds} - \frac{\omega}{\omega_e}\psi_{qs}) \tag{3.18}$$

Therefore, (1) can be rewritten as,

$$V_{qs} = R_s \times (\frac{1}{X_{ls}}(\psi_{qs} - \psi_{mq}) + \frac{1}{R_c}(\frac{p}{\omega_e}\psi_{qs} + \frac{\omega}{\omega_e}\psi_{ds})) + \frac{\omega}{\omega_e}\psi_{ds} + \frac{p}{\omega_e}\psi_{qs} \tag{3.19}$$

Similarly, (2), (3) and (4) have also been rewritten as,

$$V_{ds} = R_s \times (\frac{1}{X_{ls}}(\psi_{ds} - \psi_{md}) + \frac{1}{R_c}(\frac{p}{\omega_e}\psi_{ds} - \frac{\omega}{\omega_e}\psi_{qs})) - \frac{\omega}{\omega_e}\psi_{qs} + \frac{p}{\omega_e}\psi_{ds} \tag{3.20}$$

$$V_{qr} = R_r \times (\frac{1}{X_{lr}}(\psi_{qr} - \psi_{mq}) + \frac{(\omega - \omega_r)}{\omega_e}\psi_{dr} + \frac{p}{\omega_e}\psi_{qr} \tag{3.21}$$

$$V_{dr} = R_r \times (\frac{1}{X_{lr}}(\psi_{dr} - \psi_{md}) - \frac{(\omega - \omega_r)}{\omega_e}\psi_{qr} + \frac{p}{\omega_e}\psi_{dr} \tag{3.22}$$

Flux linkage equations, can be written as:

$$p\psi_{qs}{}^{e} = \left(\frac{R_c}{R_c+R_s}\right)\omega_e\left[V_{qs}{}^{e} - \left(\frac{R_s}{R_c}+1\right)\left(\frac{\omega}{\omega_e}\right)\psi_{ds}{}^{e} - \frac{R_s}{X_{ls}}\left(\psi_{qs}{}^{e} - \psi_{mq}{}^{e}\right)\right] \tag{3.23}$$

$$p\psi_{ds}{}^{e} = \left(\frac{R_c}{R_c+R_s}\right)\omega_e\left[V_{ds}{}^{e} + \left(\frac{R_s}{R_c}+1\right)\left(\frac{\omega}{\omega_e}\right)\psi_{qs}{}^{e} - \frac{R_s}{X_{ls}}\left(\psi_{ds}{}^{e} - \psi_{md}{}^{e}\right)\right] \tag{3.24}$$

$$p\psi_{qr}{}^{e} = \omega_e\left[V_{qr}{}^{e} - \left(\frac{\omega-\omega_r}{\omega_e}\right)\psi_{dr}{}^{e} - \frac{R_r}{X_{lr}}\left(\psi_{qr}{}^{e} - \psi_{mq}{}^{e}\right)\right] \tag{3.25}$$

$$p\psi_{dr}{}^{e} = \omega_e\left[V_{dr}{}^{e} + \left(\frac{\omega-\omega_r}{\omega_e}\right)\psi_{qr}{}^{e} - \frac{R_r}{X_{lr}}\left(\psi_{dr}{}^{e} - \psi_{md}{}^{e}\right)\right] \tag{3.26}$$

Where,

$$\psi_{mq} = X_{mq}\left(\frac{\psi_{qs}}{X_{ls}} + \frac{\psi_{qr}}{X_{lr}}\right) \tag{3.27}$$

$$\psi_{md} = X_{md}\left(\frac{\psi_{ds}}{X_{ls}} + \frac{\psi_{dr}}{X_{lr}}\right) \tag{3.28}$$

and,

$$X_{mq} = X_{md} = \left(\frac{1}{X_m} + \frac{1}{X_{ls}} + \frac{1}{X_{lr}}\right)^{-1} \tag{3.29}$$

The developed shaft torque and rotor speed equations are given as:

$$T_e = \left(\frac{n}{2}\right)\left(\frac{P}{2}\right)\left(\frac{1}{\omega_e}\right)\left(\psi_{qr}{}^{e} i_{dr}{}^{e} - \psi_{dr}{}^{e} i_{qr}{}^{e}\right) \tag{3.30}$$

$$p\omega_r = \frac{P}{2J}\left(T_e - T_l\right) \tag{3.31}$$

Here,

ψ= flux linkage, V = voltage,

i = current, R_s = stator resistance,

R_r = rotor resistance, R_c = core loss resistance,

X_l = leakage reactance, X_m = magnetizing reactance,

ω = synchronous speed in rad/sec, ω_r = rotor speed in rad/sec,

ω_e = speed of reference frame in rad/sec, P = no. of poles,

n = no. of phases, T_e = developed electromagnetic torque,

T_l = applied load torque, J = inertia of the motor.

subscript $'s'$ and $'r'$ represents stator and rotor components respectively, subscript $'d'$ and $'q'$ signifies the d-axis and q-axis components in park transformation. Superscript $'e'$ denotes that the analysis was done in synchronous reference frame. $'p'$ is the derivative operator. $'$

3.3 Parameter estimation of induction motor

In this work, the dynamic model of induction motor has been considered for the estimation purpose. H – G diagram and Particle swarm optimization was assigned to evaluate the best possible parameter set for the induction motor at any particular load. The overview of particle swarm optimization (PSO) and H – G diagram has already been discussed in section 2.3.1 and 2.3.2 of Chapter 2. The experimental setup as well as data acquisition procedure remains same as discussed in section 2.4 of chapter 2. The tuning parameters for PSO in this work also remain same as described in the section 2.3.2 of chapter 2. The steady state voltage, current, power and power factor data has been recorded with the help of 'YOKOGAWA C240' power analyzer. Rotor speed has been recorded with the a 'MECO-G' optical tachometer. From the recorded steady state voltage, current and speed data, $G(\omega_{sl})$ and $H(\omega_{sl})$ has been calculated using H – G diagram method and the

stator (R_s) and rotor (R_r) resistances at different load were estimated as discussed in section 2.3.1. The estimated stator and rotor resistances and their comparison with the corresponding experimentally obtained values have been already discussed in Table 2.6.

In the proposed method, rotor inertia (J) of the machine is considered to remains constant throughout the operation. Hence, in the second part of estimation, R_s, R_r and J were considered as predefined.

Now the measured steady state voltage data has been fed into the dynamic model of the induction motor. The objective function given in (3.32), compares the estimated stator current $\left(I_{1_{est}}\right)$, load level (LL_{est}) and input power factor $\left(pf_{in_{est}}\right)$ with their measured values using PSO, to determine equivalent leakage reactance $\left(X_{eq}\right)$, core loss resistance (R_c), and magnetizing reactance (X_m). The 'rng default' command in MATLAB was used for random number generation within the search space provided for PSO. This ensures consistency in estimation results. If the objective function value falls below the tolerance limit, the optimization gets terminated and corresponding parameter set is considered as the best parameter set. Otherwise, the iteration continues till the best parameter set has been found.

$$O = min\left[\left(\frac{I_1 - I_{1_{est}}}{I_1}\right)^2 + \left(\frac{LL - LL_{est}}{LL}\right)^2 + \left(\frac{pf_{in} - pf_{in_{est}}}{pf_{in}}\right)^2\right] \quad (3.32)$$

Subscript $'est'$ stands for estimated values of corresponding quantities. All the measured and estimated performance data have their root mean square (RMS) values.

Table 3.1 portrays the comparative analysis of parameters (X_{eq}, R_c and X_m) estimated using PSO, with measured values and their variation

under different load condition at thermal equilibrium state. From table 3.1, it can be understood that the proposed scheme is competent enough to estimate all the motor parameters with precision.

Table 3.1. Comparison of motor parameter values: Experimental vs. Estimated from PSO using objective function (3.32)

Parameters $(\boldsymbol{in\ \Omega})$	**Experimentally obtained values** $(\boldsymbol{in\ \Omega})$	**Parameters estimated from PSO diagram at different load using objective function (**3.32**)** $(\boldsymbol{in\ \Omega})$			
		40 % Load	75 % Load	90 % Load	100 % Load
$\boldsymbol{X_{eq}}$	2.87	3.324	3.331	3.242	2.8721
$\boldsymbol{R_c}$	158.19	148.8	152.7	154.7	157.22
$\boldsymbol{X_m}$	27.61	28.67	28.54	28.18	27.611

3.4 Result and Analysis

In this section, the estimated motor performance and loss data, have been analyzed, compared and validated with measured values. Table 3.2 shows the comparison of the motor performance data i.e. input current, input power, input power factor, output power and speed, estimated from the proposed scheme, with the corresponding measured values. Whereas, Fig 3.2 depicts the estimated and measured loss comparison.

The complete analysis of the result demonstrates that the proposed technique is capable of estimating the equivalent circuit parameters and losses of induction motor, in a precise manner. This technique requires fewer measurements which are easily obtainable without dedicated installations or specific measuring instruments, ensuring minimal disruption to ongoing motor operations.

Table 3.2. Comparison of motor performance data: Experimental vs. Estimated from PSO

Performance Data		Loading			
		40 % Load	**75 % Load**	**90 % Load**	**100 % Load**
Input Current	Measured	7.91	10.07	11.68	13.05
	Estimated	8.023	10.18	11.59	12.92
	% Error	-1.43	-1.09	0.77	0.99
Input Power	Measured	870.1	1464	1689	1991
	Estimated	884.0	1470	1691	1976
	% Error	-1.6	-0.4	-0.085	0.750
Input Power Factor	Measured	0.55	0.71	0.76	0.80
	Estimated	0.552	0.716	0.750	0.784
	% Error	0.002	-0.66	1.012	1.867
Output Power	Measured	606.8	1140	1324	1547
	Estimated	607.3	1140	1322	1548
	% Error	-0.08	0.05	0.10	-0.08
Speed	Measured	1468	1436	1420	1396
	Estimated	1468.2	1435.8	1418.9	1397.6
	% Error	-0.011	0.011	0.076	-0.114

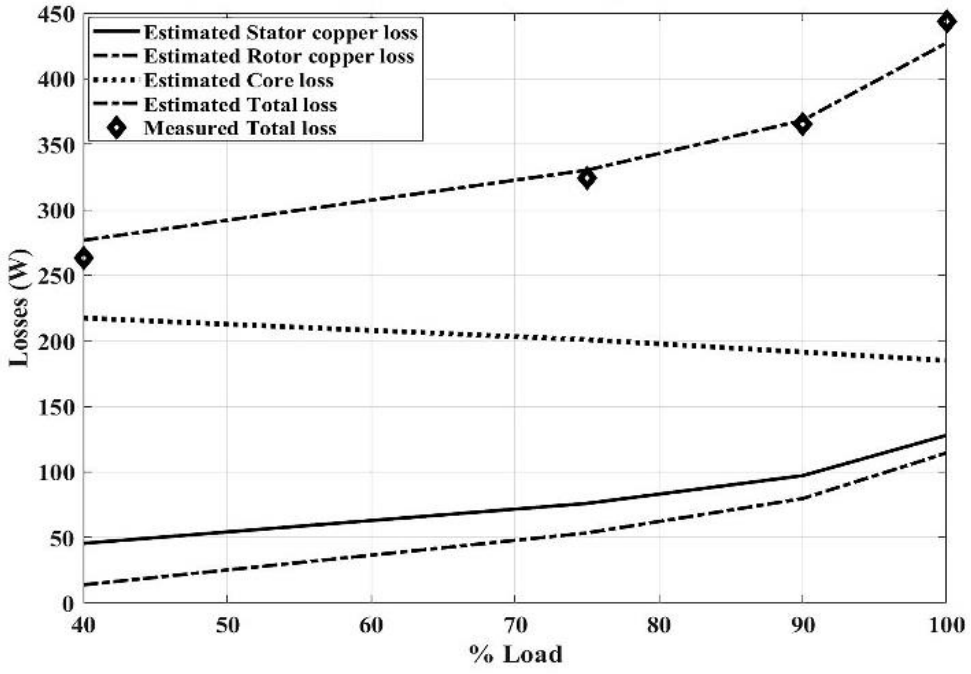

Fig. 3.2. Comparison of estimated motor losses under different load condition and validation with measured values.

This not only reduces the measurement burden but also contributes to a more compact and streamlined system. The key advantage of this technique lies in elimination of the requirement for considering no-load current. Furthermore, the proposed system can reliably predict the performance characteristics of the induction motor under variable load conditions.

3.5 Reason behind consideration of dynamic model and feeding with steady state data

Accurate estimation of motor parameters and losses with steady-state induction motor model requires multiple measurements, including input power, output power, input power factor, no-load current, and speed using steady state equivalent circuit. The complexity is further compounded when incorporating the no-load current as a known quantity into the objective function. The objective function,defined for the estimation purposes was already presented in equation (2.19).

The importance of no-load current I_0 in accurate estimation of core loss resistance R_c and magnetizing reactance X_m, has already been discussed in chapter 2. As, it is not feasible to directly measure the no-load current of a motor during operation, the no-load current was considered as 40% of the full-load current. However, as the machine ages or undergoes rewinding, relying on this assumption may not hold good. Hence, it seems necessary to find out an alternate objective function, without considering the no-load current. Therefore, motor dynamic model is considered here and (3.32) is proposed as the new objective function, free from consideration of no-load current and the results have been discussed in section 3.3 and 3.4. Comparison of Table 2.7 and Table 3.2 establishes that, consideration of dynamic model provides more

accurate results than steady state model when fed with the same steady state data, with reduced measurements burden.

3.6 Validation of proposed scheme with 2nd machine

Extending the examination to another motor, the proposed scheme was validated on a 2nd machine of 2 hp, 110 Volt, 1415 rpm, 50 Hz, squirrel cage induction motor, representing a common industrial configuration. This additional case study reinforces the robustness and generalizability of the proposed dynamic model-based approach utilizing the steady state performance data. The nameplate data of the new machine is listed in Table 3.3. whereas, Fig. 3.3 depicts the laboratory experimental setup for estimation of equivalent circuit parameters of the new 2 hp induction motor.

Table 3.3. Nameplate Data for the New Induction Motor Under Observation

Maker's Name	**Frame**	**Rating**	**Voltage**	**Current**
General Electric	224	2 hp	110 V	12 A
Speed	**Cycle**	**Service Factor**	**Duty**	**Phase**
1425 rpm	50	1.15	Continuous	3

The classical DC resistance test, no-load test and blocked rotor test were performed on this machine as per IEEE guideline [13], prior to the experimentation, to find out the motor parameter values. These experimentally obtained values has been compared with the estimated values to access the accuracy of the proposed scheme. The experimentally obtained parameter values of the new machine is given in Table 3.4

(a)

(b)

Fig. 3.3. Photograph of the experimental setup: (a) Complete arrangement, (b) Induction motor coupled with DC generator.

The parameters of the 2nd machine have been estimated maintaining the same procedure as discussed in section 3.3. The machine was coupled with a DC generator, connected with a resistive load box for load variation and supplied from 110 V ac mains.The 'YOKOGAWA C240' power analyzer was used to record data on steady-state voltage, current, power, and power factor, while the rotor speed was captured using an 'MECO-G' optical tachometer. Under every load condition, the machine was kept in running condition for 120 minutes to achieve thermal equilibrium. During the entire course of experimentation, variation of parameters has been estimated and depicted in Fig 3.4. The results show the accuracy of the proposed estimation technique, whereas, curves align well with the expected pattern, demonstrating the precision of the analysis.

Table 3.4. Motor parameter values obtained from conventional experiment as par IEEE standard test procedures [13]

R_s(in Ω)		R_r (in Ω)		X_{eq}	R_C	X_m
cold	hot	cold	hot	(in Ω)	(in Ω)	(in Ω)
2.00	2.75	1.1	1.2	1.53	127.15	33

The motor's performance data was calculated from estimated parameters and compared with measured values, as illustrated in Fig. 3.5. The comparison reveals that the proposed scheme appropriately predicts motor performance with notable precision. The estimations align closely with the actual measurements, highlighting the scheme's capability to accurately assess motor performance.

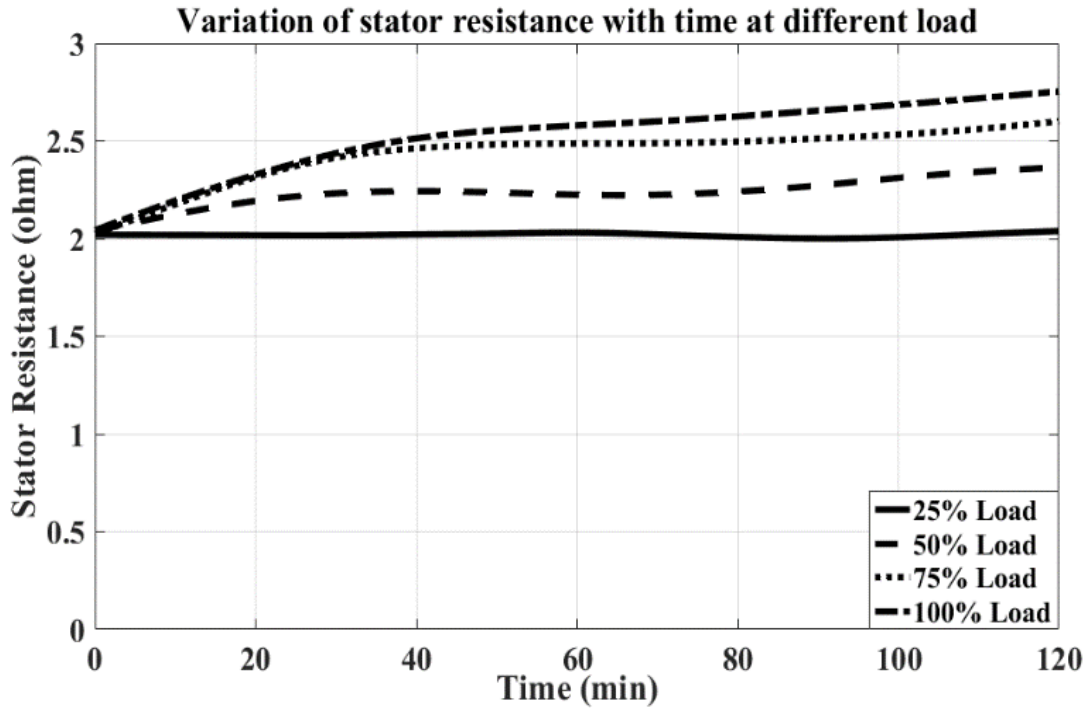
Variation of stator resistance with time at different load
Stator Resistance (ohm)
Time (min)
25% Load
50% Load
75% Load
100% Load

(a)

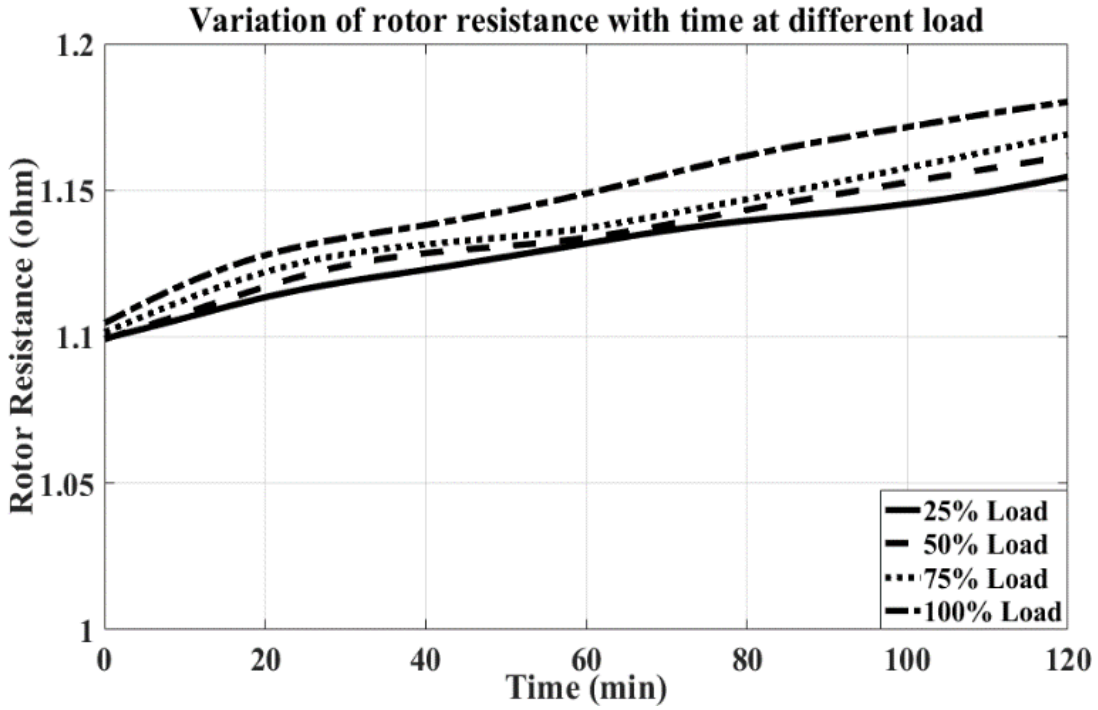
Variation of rotor resistance with time at different load
Rotor Resistance (ohm)
Time (min)
25% Load
50% Load
75% Load
100% Load

(b)

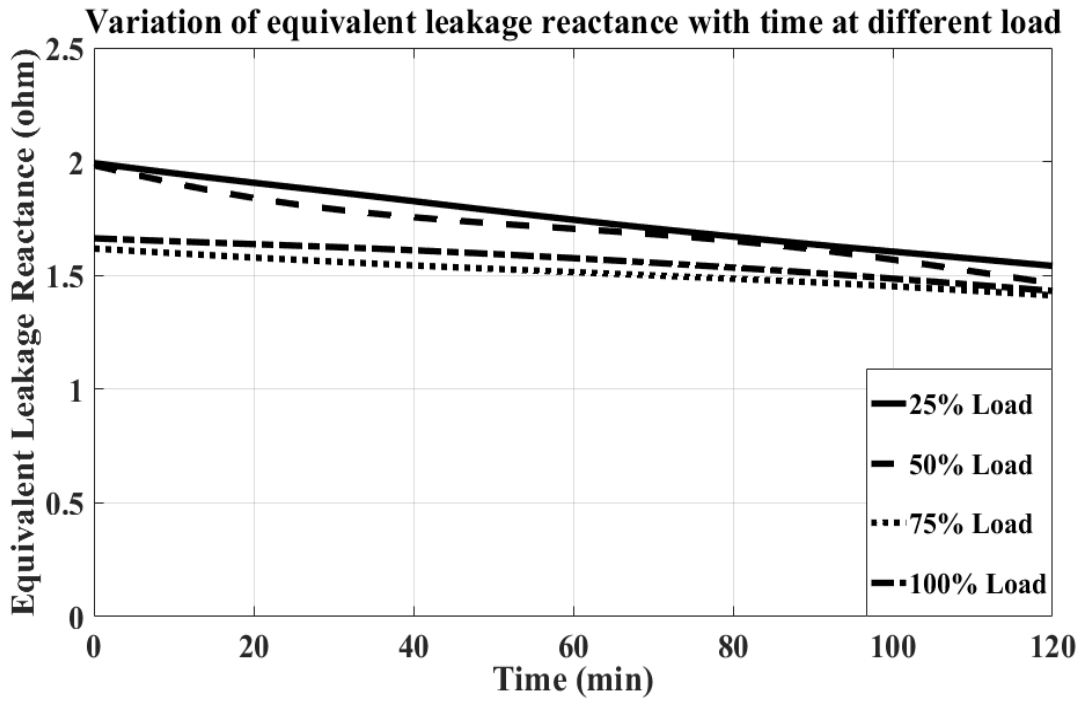
Variation of equivalent leakage reactance with time at different load
Equivalent Leakage Reactance (ohm)
Time (min)
25% Load
50% Load
75% Load
100% Load

(c)

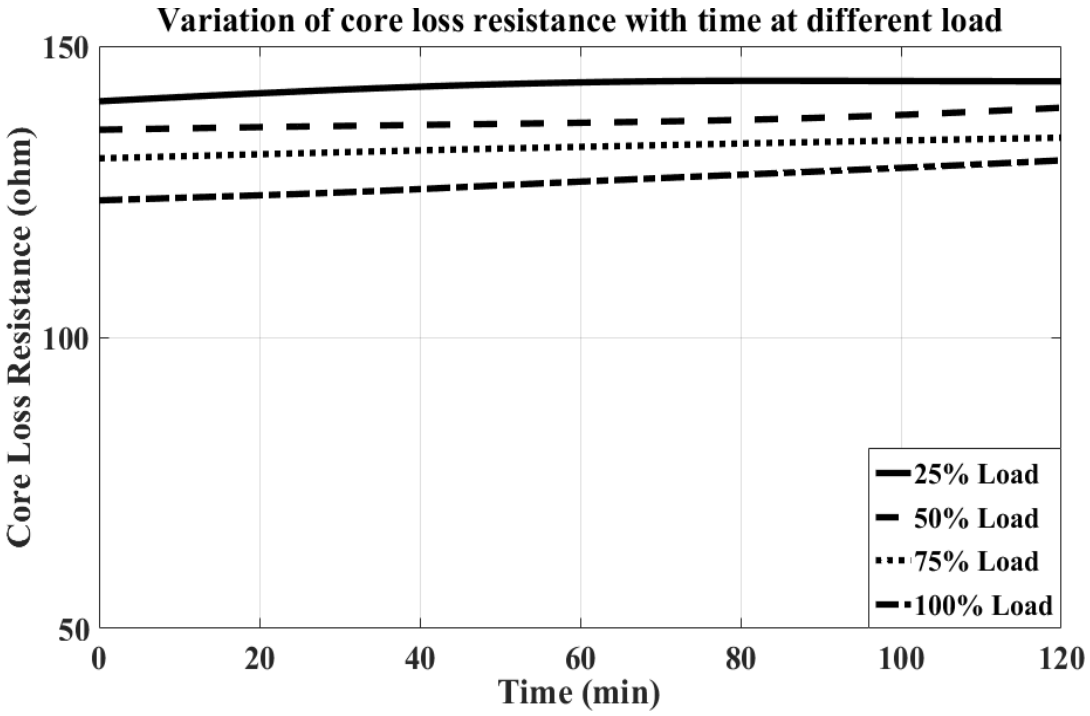
Variation of core loss resistance with time at different load
Core Loss Resistance (ohm)
Time (min)
25% Load
50% Load
75% Load
100% Load

(d)

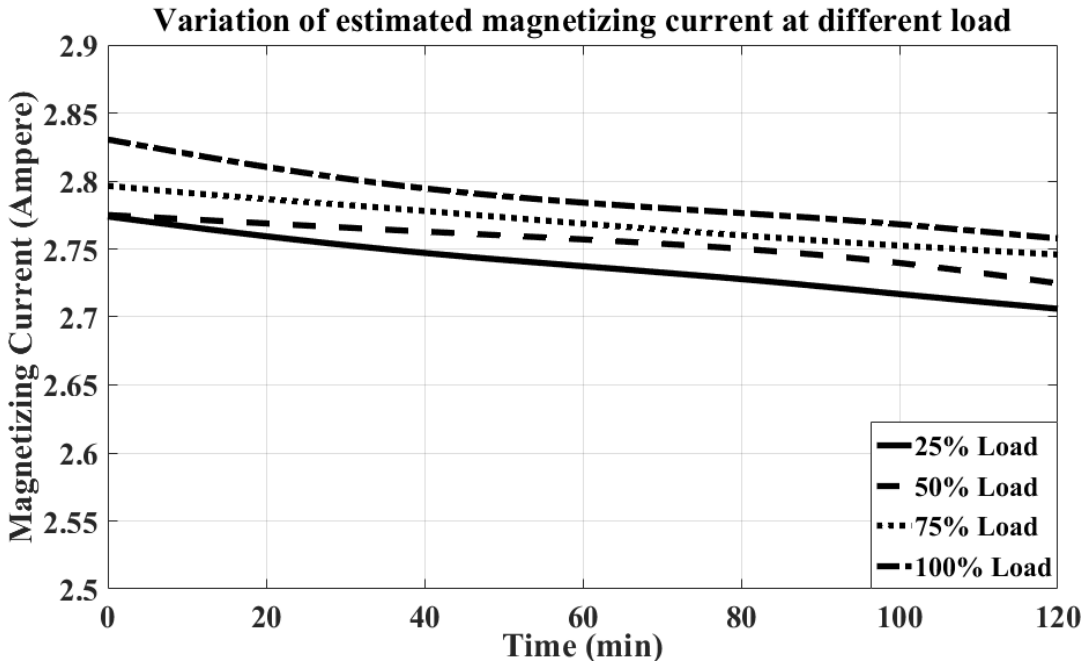

(e)

Fig. 3.4. Variation of motor parameter values with time under different load condition: (a) Stator resistance, (b) Rotor resistance, (c) Leakage reactance, (d) Core loss resistance, (e) Magnetizing current.

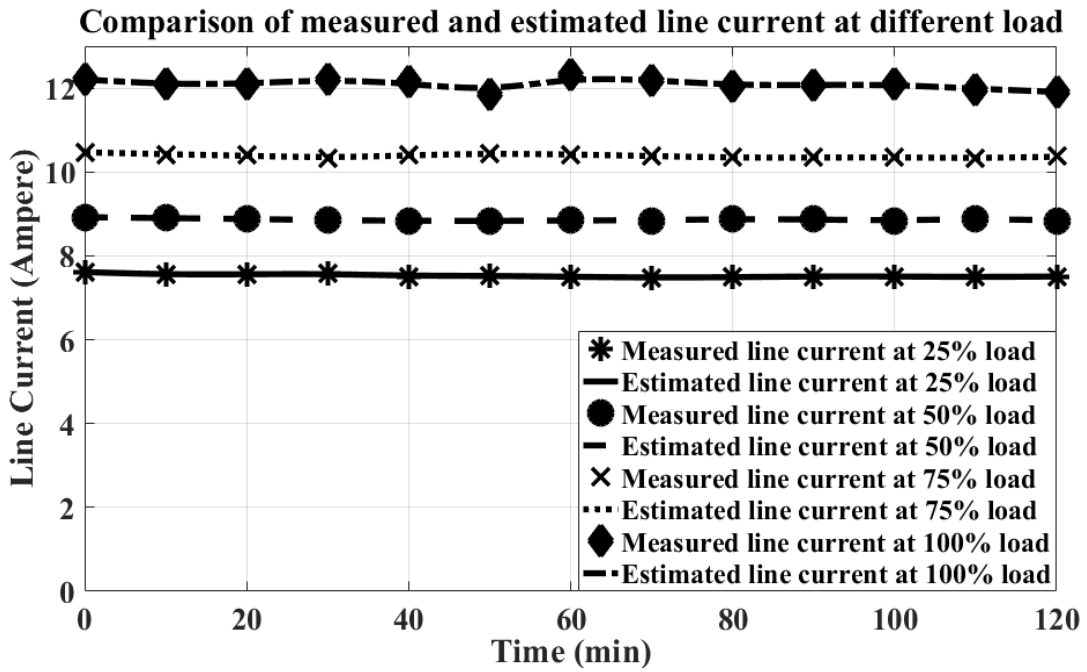

(a)

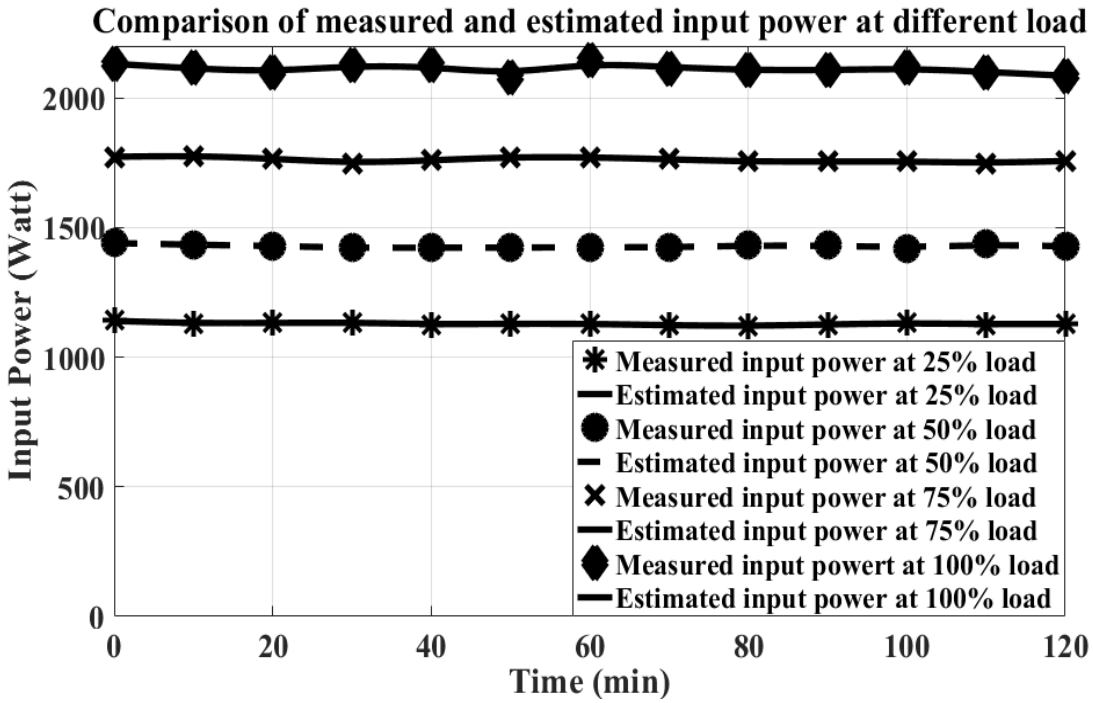
Comparison of measured and estimated input power at different load
Input Power (Watt)
Time (min)
0
500
1000
1500
2000
0
20
40
60
80
100
120
Measured input power at 25% load
Estimated input power at 25% load
Measured input power at 50% load
Estimated input power at 50% load
Measured input power at 75% load
Estimated input power at 75% load
Measured input powert at 100% load
Estimated input power at 100% load

(b)

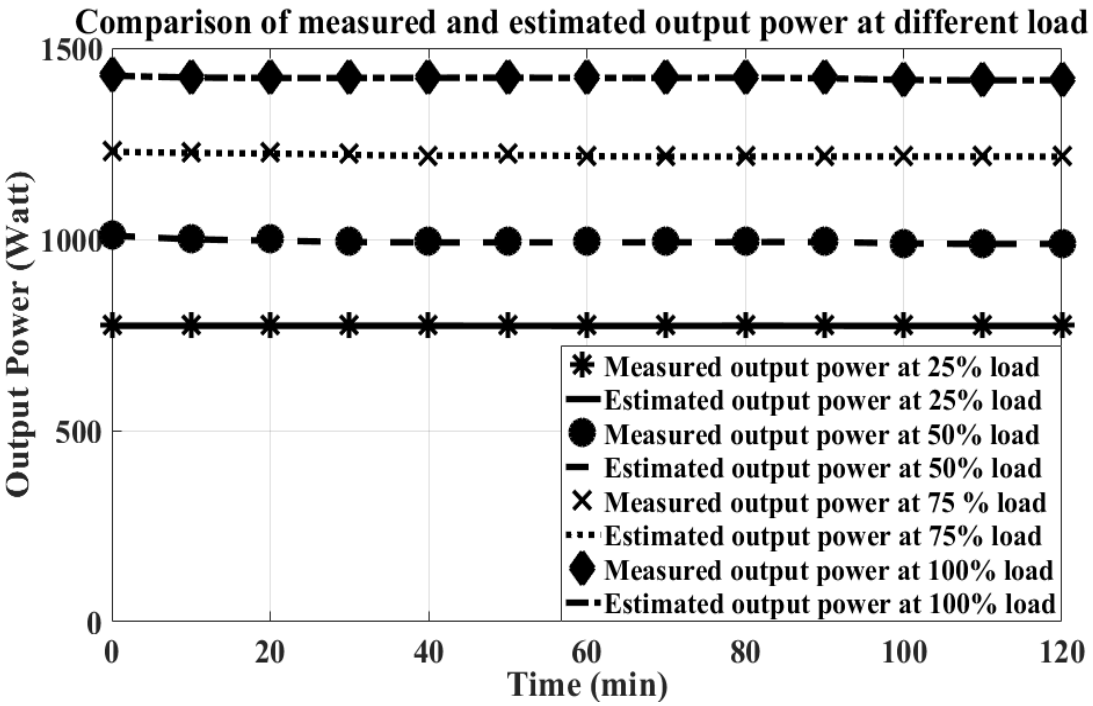
Comparison of measured and estimated output power at different load
Output Power (Watt)
Time (min)
0
500
1000
1500
0
20
40
60
80
100
120
Measured output power at 25% load
Estimated output power at 25% load
Measured output power at 50% load
Estimated output power at 50% load
Measured output power at 75 % load
Estimated output power at 75% load
Measured output power at 100% load
Estimated output power at 100% load

(c)

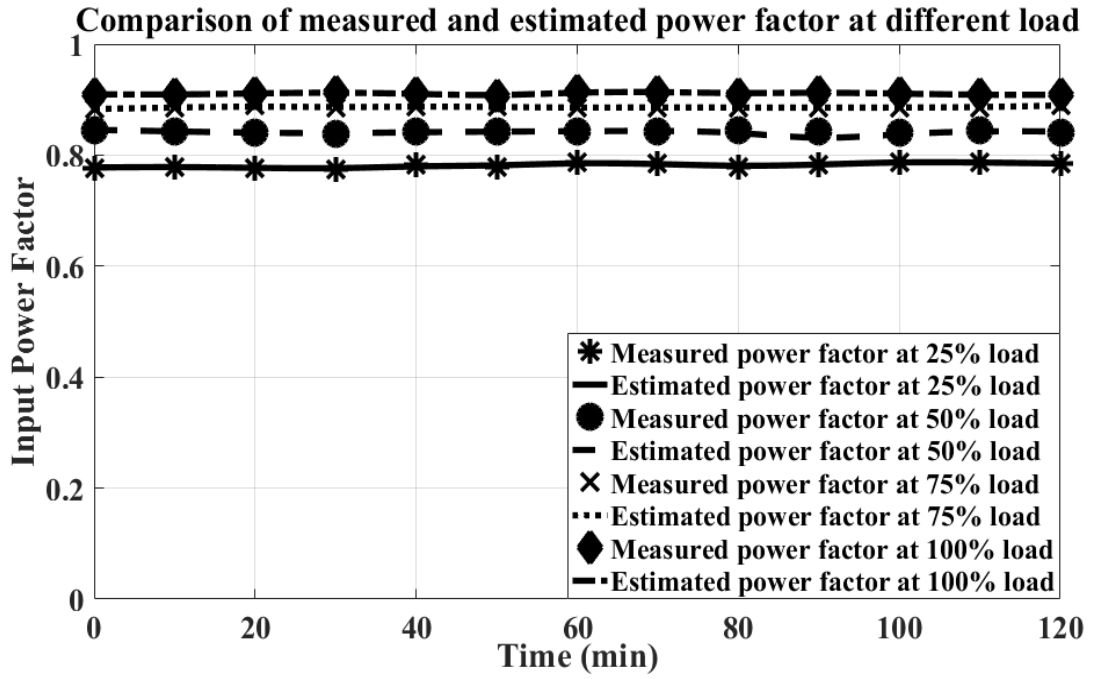

(d)

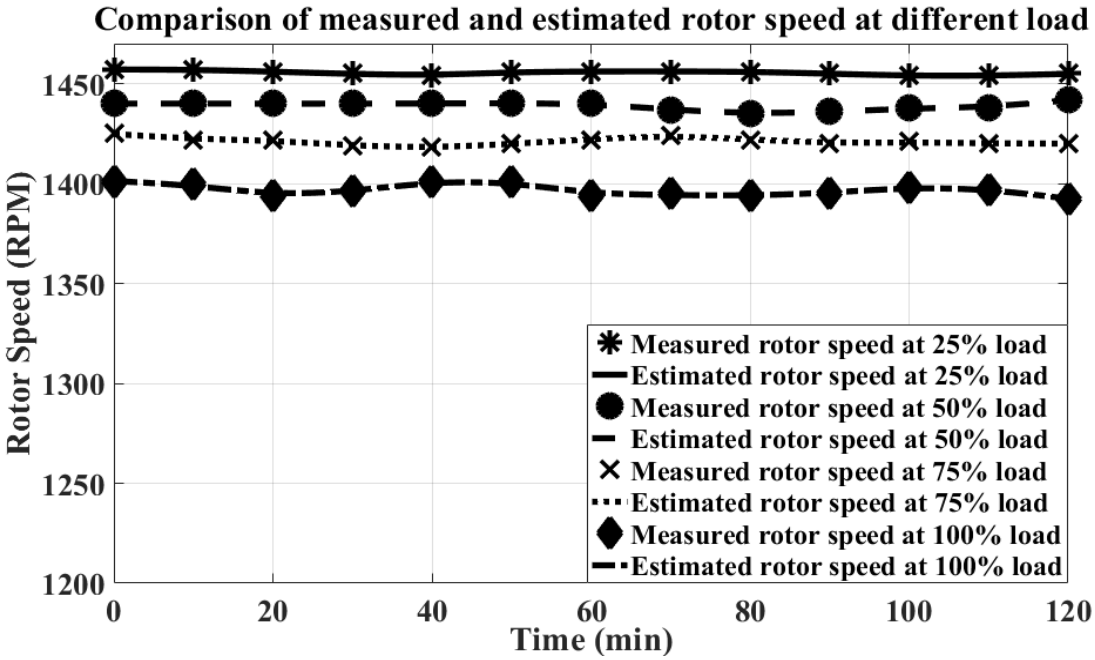

(e)

Fig. 3.5. Variation of motor performance data with time under different load condition: (a) Line current, (b) Input power, (c) Output power, (d) Power factor, (e) Speed.

Fig 3.5 validates the reliability of the proposed methodology in providing a trustworthy estimation of the motor's operational characteristics. This notably accurate estimation develops confidence in its potential applications across various contexts. The resemblance between estimated and measured values in Fig. 3.5 demonstrates the scheme's effectiveness in capturing the essence of motor performance with commendable accuracy.

3.7 Conclusion

In this study, steady-state voltage and speed data were collected and utilized as inputs for the dynamic model of the induction motor. By employing the H-G diagram, the stator and rotor resistances were estimated. Subsequently, utilizing these estimated resistances as predetermined values, the performance data of the motor, including input current, input power factor, and load level, were estimated. These estimated performance parameters were then compared with the corresponding measured values using Particle Swarm Optimization (PSO) to predict the equivalent leakage reactance, magnetizing reactance, and core loss resistance of the induction motor. To validate the effectiveness of the proposed method, it was applied to two different machines. The results of the validation process demonstrated the accuracy and reliability of the proposed scheme. This comprehensive approach utilizes measured performance data, dynamic modeling, H-G diagram and particle swarm optimization technique to estimate key parameters of induction motors, showcasing its potential for enhancing motor performance analysis and predictive maintenance strategies.

The advantages of the proposed work are:

- H-G diagram prevents the proposed technique from getting trapped in local minima.
- The proposed technique gathers all measurements while the motor is in operation, eliminating the need to interrupt ongoing processes.
- It helps reducing downtime as well as financial losses for the industries.
- No initial assumptions for parameters are required.
- The wide parameter boundaries validate the scheme's capability in estimating accurate parameters even within an expanded search space.
- Measurement burden is reduced.
- No-load current need not to be assumed, making this technique applicable for more versatile applications.

As the proposed technique can estimate motor losses accurately, the estimated losses could have been utilized to develop a thermal model. The thermal model can predict the motor temperature at different parts of the motor and together, they can work as a complete temperature-based condition monitoring scheme for induction motor.

CHAPTER 4

Estimation of Induction Motor Equivalent Circuit Parameters and Losses from Transient Measurement

This study focuses on the critical task of estimating parameters and losses in the equivalent circuit of an induction motor from transient data. The transient behavior of the motor offers valuable insights into its dynamic response and operational characteristics. By leveraging advanced measurement techniques, this work aims to accurately identify and quantify key parameters, shedding light on the motor's behaviour. The investigation not only contributes to a deeper understanding of induction motor dynamics but also holds significance for optimizing motor control strategies and enhancing overall system efficiency.

4.1 Introduction

Induction motors are fundamental components in various industrial processes. Accurately characterizing electrical behavior of induction motors is essential for enhancing performance, efficiency, and longevity. Equivalent circuit parameters and losses play a crucial role in understanding the behavior. The precise estimation of equivalent circuit parameters and losses in induction motors is crucial for optimizing their performance and ensuring operational efficiency.

This study is dedicated to the crucial task of estimating the equivalent circuit parameters and losses of an induction motor from transient measurements. Transient behaviour provides invaluable insights into the dynamic response and operational characteristics of the motor. This work proposes a simple, reliable and efficient estimation technique that is capable of estimating the electrical equivalent circuit parameters, applied load torque and rotor inertia of induction motor independently, involving comparatively lesser computational complexity. The proposed scheme utilizes the particle swarm optimization (PSO) technique [71] for estimation as it imposes a lower computational burden, less time consumption and high convergence rate in comparison with other well established optimization techniques [88], [89]. The transient measurement techniques employed in this study allow for a more detailed examination of the motor's behaviour, particularly during dynamic conditions. By shedding light on the internal workings of the motor through precise parameter and loss estimation, this work contributes not only to theoretical knowledge but also to practical applications in real-world industrial scenario.

4.2 Theory and objective of the work

Dynamic model consists of complex differential equations and is capable of reproducing the transient behaviour of the machine. Hence, dynamic model is information rich as well as can deliver information about the rotor speed and rotor inertia. Thus, for the parameter and loss estimation purpose, induction motor dynamic model has been considered, in spite of being relatively computationally complex than the steady state model. In chapter 3, section 3.2, a detailed outline of induction motor dynamic model, along with the necessity of incorporating core loss resistance, has been discussed. The accordingly revised equations were also presented. The modified equivalent circuit of induction motor dynamic model is given in Fig 4.1. The d - q axis voltage equations for stator and rotor in synchronously rotating reference frame is given as:

$$V_{qds}^{e} = R_s \times \left(\frac{1}{X_{ls}} \left(\psi_{qds}^{e} - \psi_{mqd}^{e} \right) + \frac{1}{R_c} \left(\frac{p}{\omega_e} \psi_{qds}^{e} \pm \frac{\omega}{\omega_e} \psi_{dqs}^{e} \right) \right) + \frac{\omega}{\omega_e} \psi_{dqs}^{e} + \frac{p}{\omega_e} \psi_{qds}^{e} \tag{4.1}$$

$$V_{qdr}^{e} = R_r \times \left(\frac{1}{X_{lr}} \left(\psi_{qdr}^{e} - \psi_{mqd}^{e} \right) \pm \frac{(\omega - \omega_r)}{\omega_e} \psi_{dqr}^{e} + \frac{p}{\omega_e} \psi_{qdr}^{e} \right) \tag{4.2}$$

Accordingly, flux linkage equations are given by:

$$p\psi_{qds}{}^{e} = \left(\frac{R_c}{R_c + R_s} \right) \omega_e \left(V_{qds}{}^{e} \mp \left(\frac{R_s}{R_c} + 1 \right) \left(\frac{\omega}{\omega_e} \right) \psi_{dqs}{}^{e} - \frac{R_s}{X_{ls}} \left(\psi_{qds}{}^{e} - \psi_{mqd}{}^{e} \right) \right) \tag{4.3}$$

$$p\psi_{qdr}{}^{e} = \omega_e \left(V_{qdr}{}^{e} \mp \left(\frac{\omega - \omega_r}{\omega_e} \right) \psi_{dqr}{}^{e} - \frac{R_r}{X_{lr}} \left(\psi_{qdr}{}^{e} - \psi_{mqd}{}^{e} \right) \right) \tag{4.4}$$

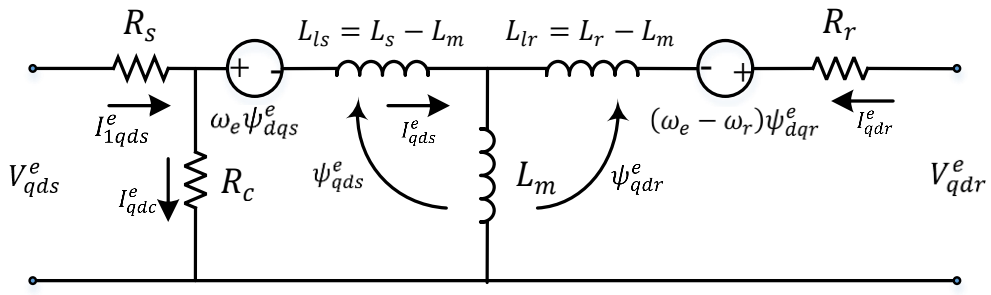

Fig. 4.1. Equivalent circuit of induction motor dynamic model, considering core loss resistance, in synchronously rotating reference frame.

Where,

$$\psi_{mqd}{}^{e} = X_{mqd}\left(\frac{\psi_{qds}}{X_{ls}} + \frac{\psi_{qdr}}{X_{lr}}\right) \tag{4.5}$$

and,

$$X_{mq} = X_{md} = \left(\frac{1}{X_m} + \frac{1}{X_{ls}} + \frac{1}{X_{lr}}\right)^{-1} \tag{4.6}$$

The developed shaft torque and rotor speed equations is given by:

$$T_e = \left(\frac{n}{2}\right)\left(\frac{P}{2}\right)\left(\frac{1}{\omega_e}\right)\left(\psi_{qr}{}^{e} I_{dr}{}^{e} - \psi_{dr}{}^{e} I_{qr}{}^{e}\right) \tag{4.7}$$

$$p\omega_r = \frac{P}{2J}(T_e - T_l) \tag{4.8}$$

Here, the symbols have their usual meaning as discussed in section 3.2. In this work, the equivalent circuit parameters $(R_s, R_r, X_{ls}, X_{lr}, R_c, X_m)$, rotor inertia (J) as well as the applied load torque (T_l) of the induction motor were estimated considering the equations described in (4.1) – (4.8) (detailed derivation is available in section 3.2). The estimation process was conducted using PSO (a brief overview of PSO has been presented, in section 2.2).

4.3 Experimental setup and procedures

The experimental setup consists of a 415 V, 0.75 kW, 50 Hz, three phase, squirrel cage, totally enclosed fan cooled (TEFC) induction motor coupled to a 315 V, 1 kW dc generator. Fig 4.2. Shows the photograph of the experimental set up and Fig 4.3 shows the schematic diagram of the proposed scheme. The nameplate data of the motor has been given in Table 4.1. The coupling was done through a torque transducer of 'KISTLER' make (model number '4520A'). The torque transducer was used to measure the output torque of the induction motor for validation purpose. A 'OC 351-4 set point controller' manufactured by 'Orbit Control AG' was used to display of shaft torque. This torque transducer was calibrated to provide 'zero' torque output when the machine runs under no-load condition. The output terminals of the dc generator were connected to load box for changing the load of induction motor. In the data acquisition system, a 'Pico 4824 Eight Channel Oscilloscope' was used to record the transient three phase supply voltage and currents. This oscilloscope was configured at a sampling frequency of 4000 samples per second for all the active channels. To measure the rms voltage, rms current, input power, input power factor and supply frequency, a 'YOKOGAWA C-240 Power Analyzer' was used. An optical tachometer was employed for speed measurement. Supply to induction motor was given through a variac for smooth voltage change as well as for maintaining a constant supply voltage. It is to be mentioned here that, the experiment was conducted under thermal equilibrium condition.

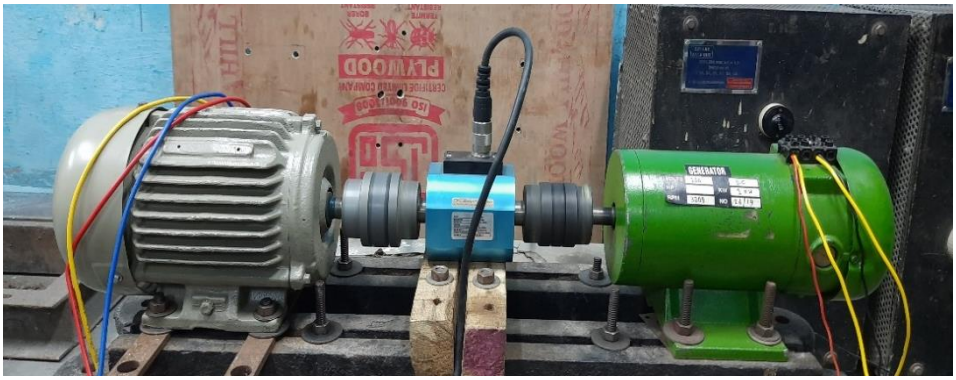

(a)

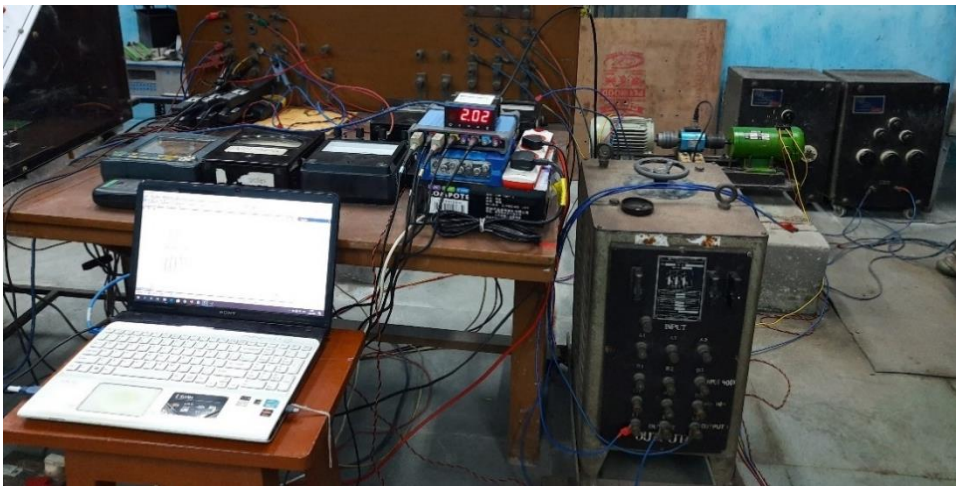

(b)

Fig. 4.2. Complete experimental setup in laboratory: (a) Motor-Generator set coupled with torque transducer. (b) Complete Data acquisition system.

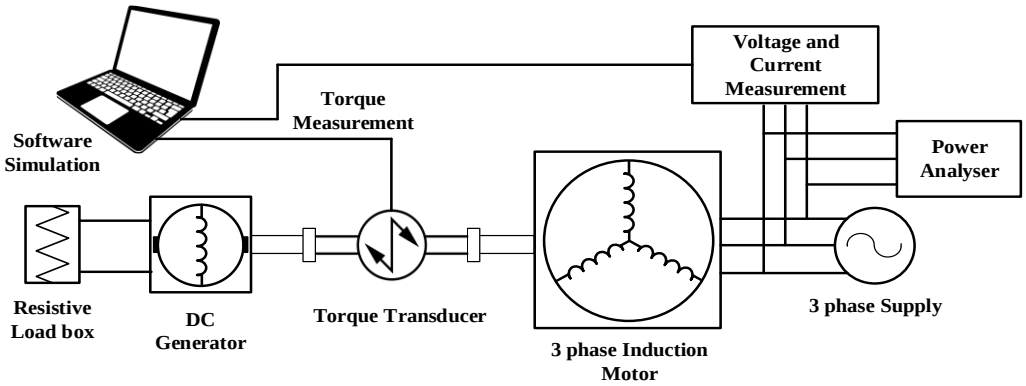

Fig. 4.3. Schematic diagram of the proposed parameter estimation process.

Table 4.1. Motor nameplate data

Machine Nameplate Data	***Values***
Voltage (volt)	**$415 \pm 10\%$**
Power (HP)	**1.00**
Current (A)	**1.62 (Y Connected)**
Frequency (Hz)	**$50 \pm 5\%$**
Speed (RPM)	**2875**

4.4 Results and Analysis

4.4.1 Result analysis

The acquired applied voltage and transient current data of the induction motor have been shown in Fig 4.4. Based on the acquired voltage and transient current, the parameters of the induction motor equivalent circuit have been estimated by the developed PSO based software. The objective function has been developed considering only the motor input current given by equation (4.9).

$$O = min\left[sum\left(\frac{(I_s - I_{s_{est}})}{I_s}\right)^2\right] \tag{4.9}$$

Where, I_s is the measured stator current, $I_{s_{est}}$ is the estimated stator current. The boundary of search area and the variables of PSO, are presented in Table 4.2 and Table 4.3 respectively. The boundary of search area is kept large enough to increase the practicality of the technique. This ensures that the estimation technique converges towards the actual parameter values despite handling a large boundary condition. On the other hand, the precision as well as computation time of PSO depends on its internal parameters i.e., size of population, tolerance limit etc. Therefore, here the variables of PSO have been

selected to maintain a favourable relation between precision and computational time. The steps followed for the estimation have been shown by the schematic diagram depicted in Fig 4.5.

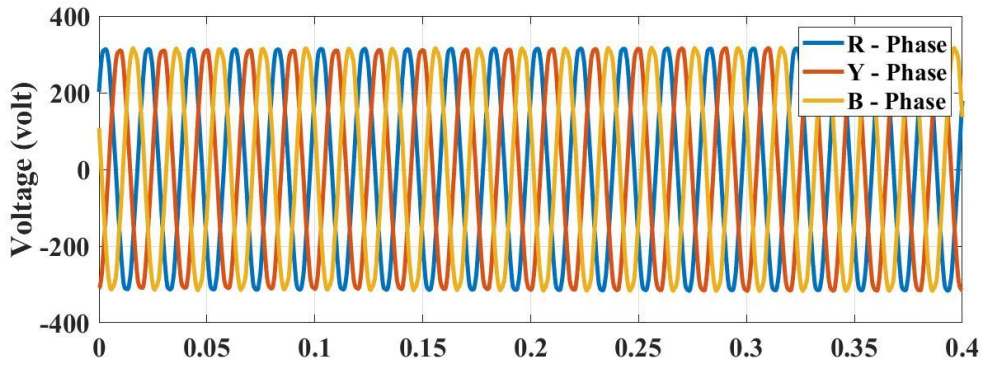

(a)

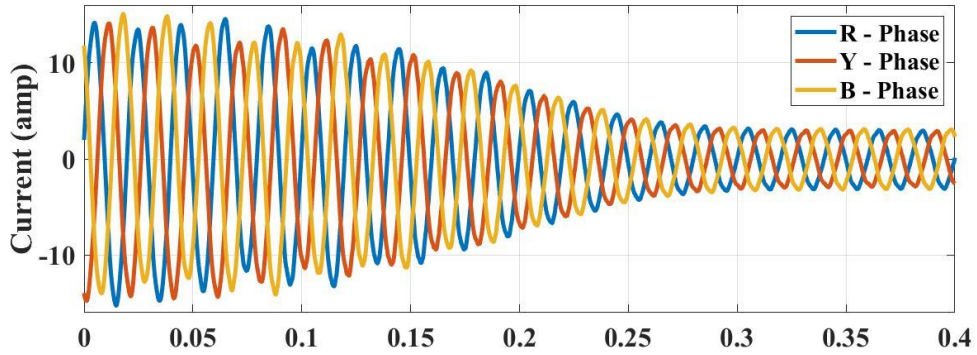

(b)

Fig. 4.4. Measured (a) voltage and (b) current profiles.

Table 4.2. Limit of search area for PSO

Parameters	R_s **(in**Ω**)**	R_r' **(in**Ω**)**	X_{eq} **(in**Ω**)**	R_c **(in**Ω**)**	X_m **(in**Ω**)**	J **(in**Kgm^2**)**
Lower Bound	1.00	1.00	1.00	100.0	1.00	0.00
Upper Bound	50.0	50.0	50.0	5000.0	500.0	1.00

Table 4.3 Variables of PSO considered for estimation

Optimization Technique	Population Size	Max. Iteration	Max. Iteration Stalling	Function Tolerance
PSO	50	600	100	1e-6

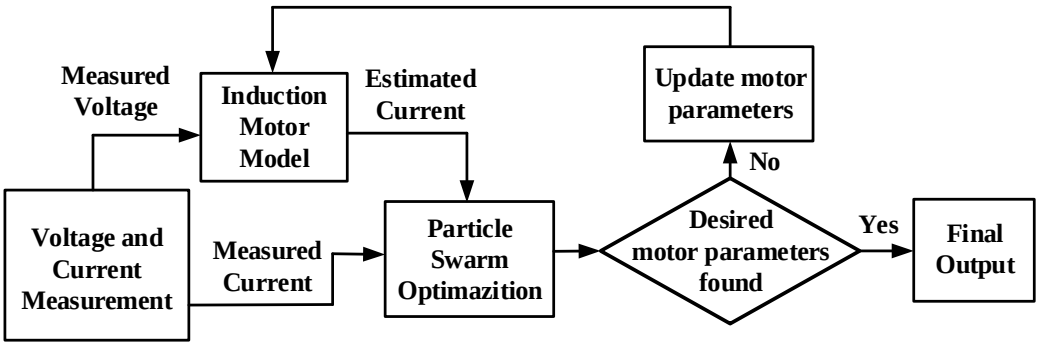

Fig. 4.5. Detailed schematic diagram of the proposed software.

The proposed scheme estimates the motor equivalent circuit parameters, rotor inertia and applied load torque. From the estimated parameters, the motor losses and other motor performance parameters have also been estimated. The proposed method is capable of estimating the variation of parameters from their reference values with change of load. Fig 4.6 depicts the variation of motor equivalent circuit parameters and inertia from their reference values whereas, Fig. 4.7 portrays the variation of losses with load variation respectively.

It may be observed from Fig. 4.6 that, the stator and rotor resistances increase with load whereas magnetizing reactance, core loss resistance and leakage reactance decrease with it. This is due to fact that, the temperature of the machine is higher for higher load, so the stator and rotor losses increase with load and resistances are also higher.

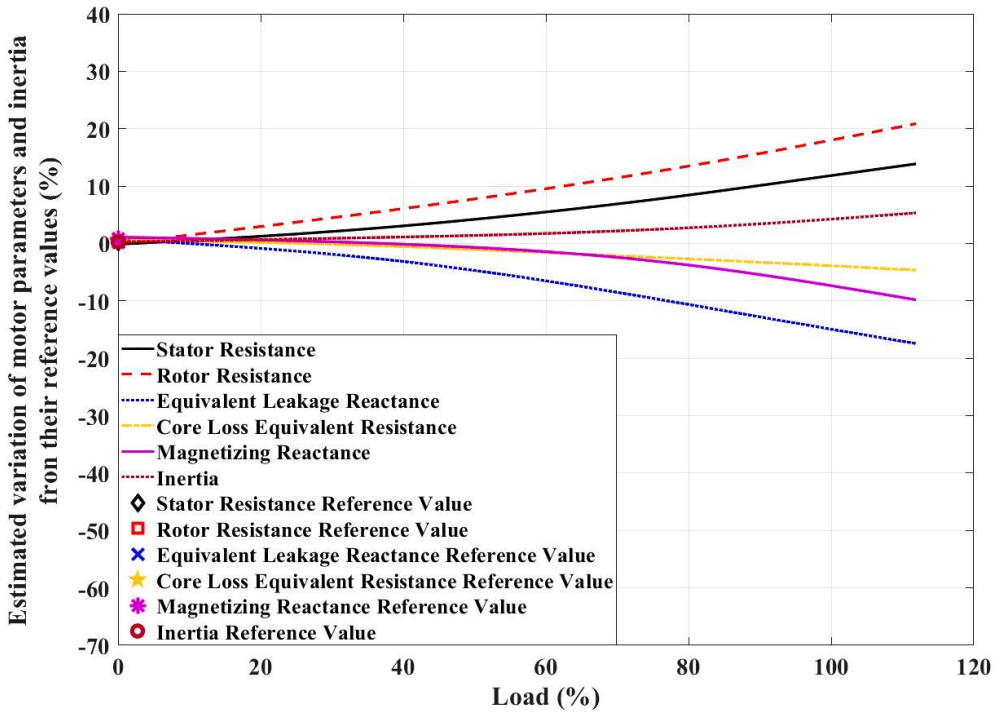

Fig. 4.6. Estimated variation of motor equivalent circuit parameters and inertia from their reference values with load under thermal equilibrium.

Both magnetizing reactance and leakage reactance decreases with increase in load owing to lower magnetization at higher temperature. Eddy current loss component decreases with temperature rise due to an increase in lamination resistance and decrease in flux density. This leads to small decrement of overall core loss with load (as shown in Fig. 4.7) which results change in core loss resistance (presented in Fig. 4.6).

In Fig 4.7, the estimated losses have been depicted and compared with the measured value. Total loss of the machine has been measured from input and output power. Stator copper loss, rotor copper loss and core loss have been segregated from total measured loss using mathematical calculation [87]. It may also be observed from Fig. 4.7 that, the estimated total loss is close enough to the measured loss which validates that the proposed scheme is capable of estimating the power losses accurately.

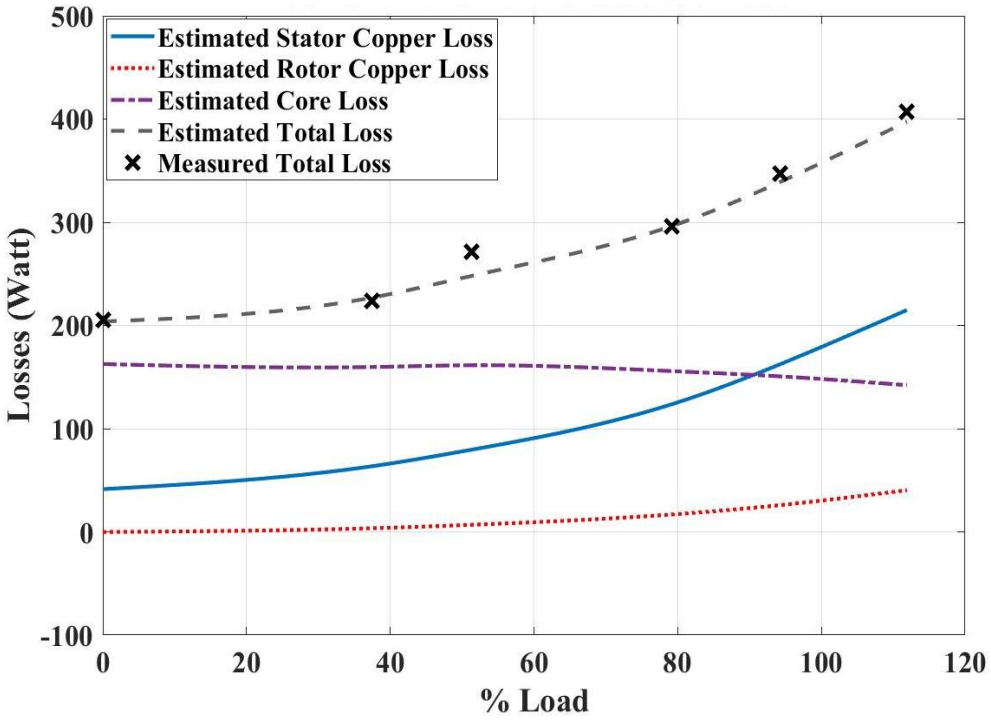

Fig. 4.7. Variation of motor losses with load under thermal equilibrium.

Transient stator currents (in ampere) of the three phases have been estimated using equation (4.9) and compared with the corresponding measured values from 0.0 to 0.5 seconds at full load condition. The comparison is presented in Fig. 4.8. It is observed from Fig. 4.8 that, the estimated stator transient currents are close to the corresponding measured values thus validating the proposed technique.

Fig 4.9 compares the measured and predicted motor performance (phase current, power factor, speed, output power, and load torque) with variation of motor loading. The performance parameters have been represented as a percentage of their corresponding rated value obtained from the nameplate. It can be observed from Fig. 4.9 that, the estimated values of performance parameters show a good agreement with the corresponding measured values thus confirm the precision of the proposed scheme.

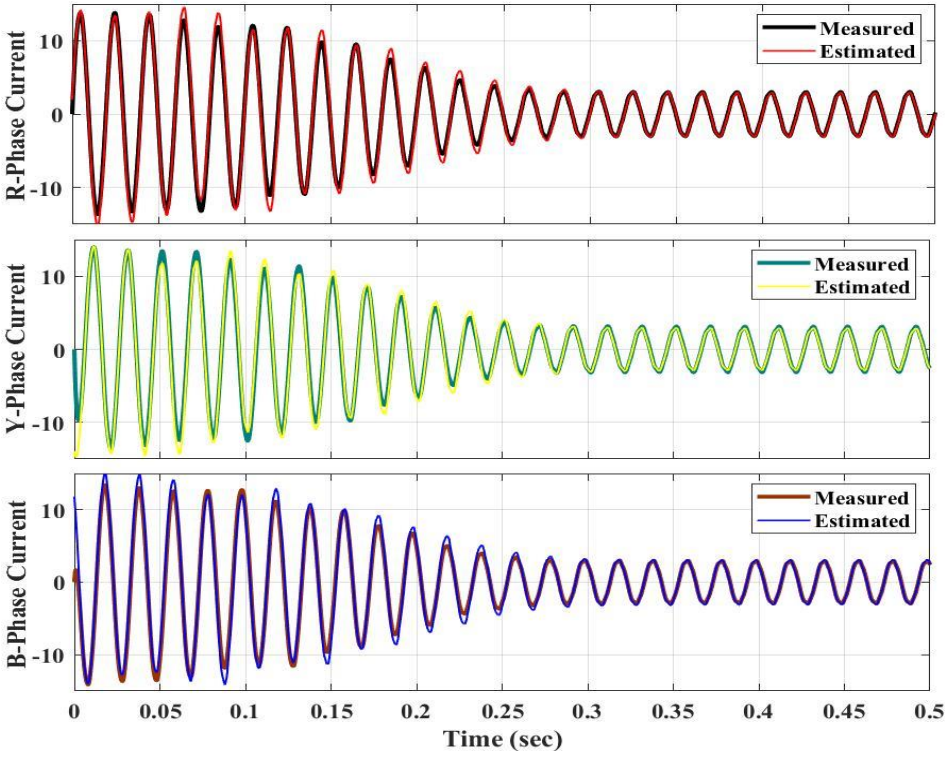

Fig. 4.8. Comparison of measured and simulated stator currents considering time frame from 0.0 to 0.5 sec.

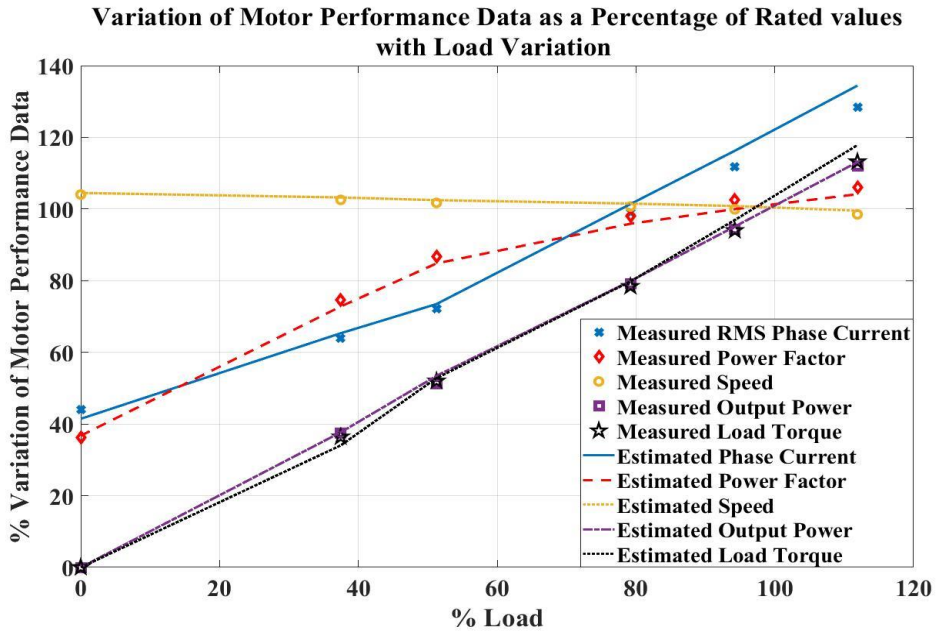

Fig. 4.9. Variation of motor performance parameters with load represented as percentage of rated value.

4.4.2 Error analysis

The values of motor equivalent circuit parameters vary with change in operating conditions. Increase in temperature during runtime, aging, rewinding even stressful ambient condition can alter the parameter values, Therefore, comparison of absolute parameter values is an inadequate indicator of accuracy of any proposed scheme. Hence, machine performance has been considered here as the précised indicator of reliability. The steady-state performance indicating quantities such as starting torque, maximum torque and starting current has been analysed here and the estimation error has been evaluated using the equations (4.10) – (4.12).

$$\varepsilon T_{st} = \sqrt{\frac{1}{n}\sum_{i=1}^{n}\left(T_{st\_calc_i} - T_{st\_est_i}\right)^2} \tag{4.10}$$

$$\varepsilon T_{max} = \sqrt{\frac{1}{n}\sum_{i=1}^{n}\left(T_{max\_calc_i} - T_{max\_est_i}\right)^2} \tag{4.11}$$

$$\varepsilon I_{st} = \sqrt{\frac{1}{n}\sum_{i=1}^{n}\left(I_{st\_calc_i} - I_{st\_est_i}\right)^2} \tag{4.12}$$

Here, 'εT_{st}' 'εT_{max}' and 'εI_{st}' implies the RMS deviation in starting torque, maximum torque and starting current respectively. Suffix '$calc$' stands for calculated value from measured data whereas, suffix 'est'represents the estimated values from the proposed model.

Fig 4.10 represents the estimation error of the above-mentioned performance indicators at different load condition under thermal equilibrium state. The figure indicates that the estimation error is negligible, suggesting that the proposed model can effectively track the actual motor performance with precision.

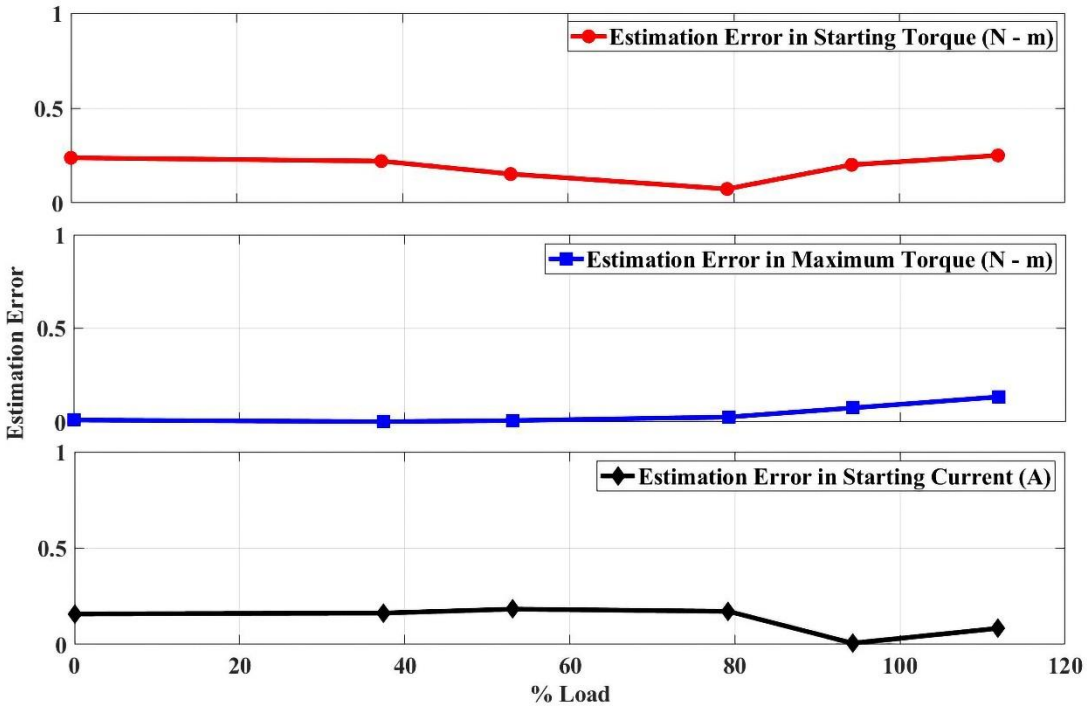

Fig. 4.10. Estimation error of starting torque, maximum torque and starting current considering transient measurement from 0.0 to 0.5 sec.

4.4.2.1 Influence of boundary values and swarm size on estimation

In section 4.4.1, the parameter estimation was done based on the boundary conditions and variables of PSO given in Table 4.2 and 4.3 with a population size of 50. It is evident from Fig 4.7, Fig 4.8 and Fig. 4.9 that, with the estimated parameters, the predicted performance from the motor model is close enough to the actual one which proves the accuracy of the proposed estimation technique. However, to prove the robustness of the proposed scheme, influence of the variation of boundary values and swarm size have been studied. Table 4.4 represents three new sets of boundary conditions and swarm size considered for the validation purpose. In set I, search area as well as the population size was shrunk whereas, in set II they were expanded. In set III, search boundary was expanded and population size

was reduced. These three variations provide all the circumstances under which the model should be tested to establish its robustness.

Table 4.4. New sets of search area and variables of PSO considered for validation of the proposed scheme

Performance Parameters	Set I		Set II		Set III	
	Lower Bound	Upper Bound	Lower Bound	Upper Bound	Lower Bound	Upper Bound
R_s(in Ω)	1.0	25.0	0.00	100.0	0.00	100.0
R_r'(in Ω)	1.0	25.0	0.00	100.0	0.00	100.0
X_{eq}(in Ω)	1.0	25.0	0.00	100.0	0.00	100.0
R_c(in Ω)	100.0	1000.0	10.0	50000.0	10.0	50000.0
X_m(in Ω)	1.0	500.0	0.00	1000.0	0.00	1000.0
Population Size	25		100		25	
Max. Iteration	600		600		600	
Max. Iter. Stalling	100		100		100	
Function Tolerance	1e-6		1e-6		1e-6	

Fig 4.11 illustrates a strong correlation between the estimated three-phase currents (considering sets I, II, and III) and the measured three-phase currents (in ampere). This signifies that the proposed estimation technique exhibits strong resilience to significant diversity in boundary conditions as

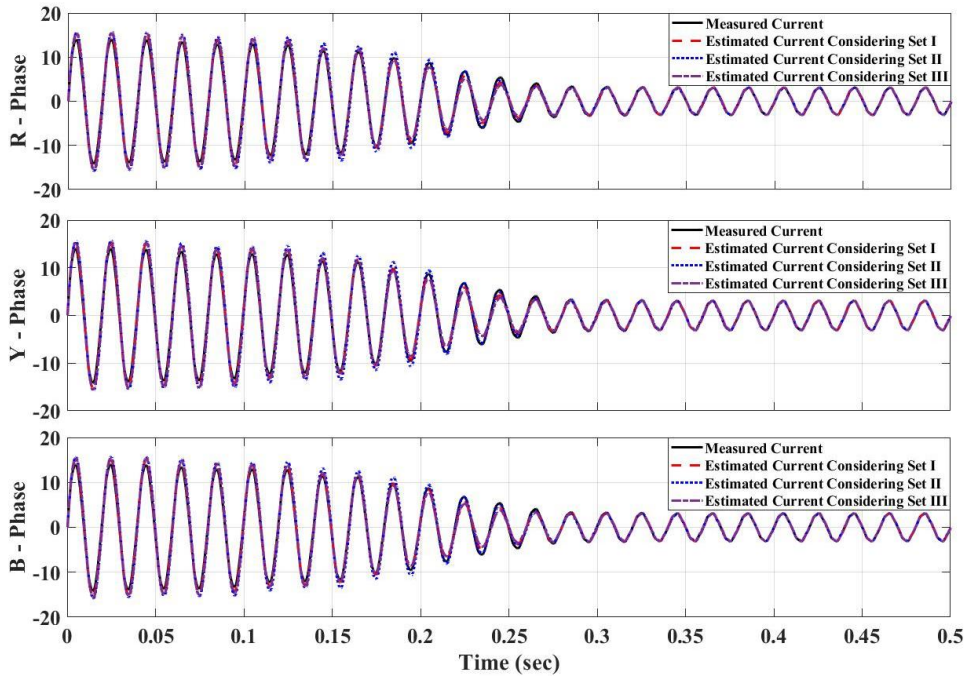

Fig. 4.11. Comparison of measured current waveforms with current waveforms predicted from different search space and population size.

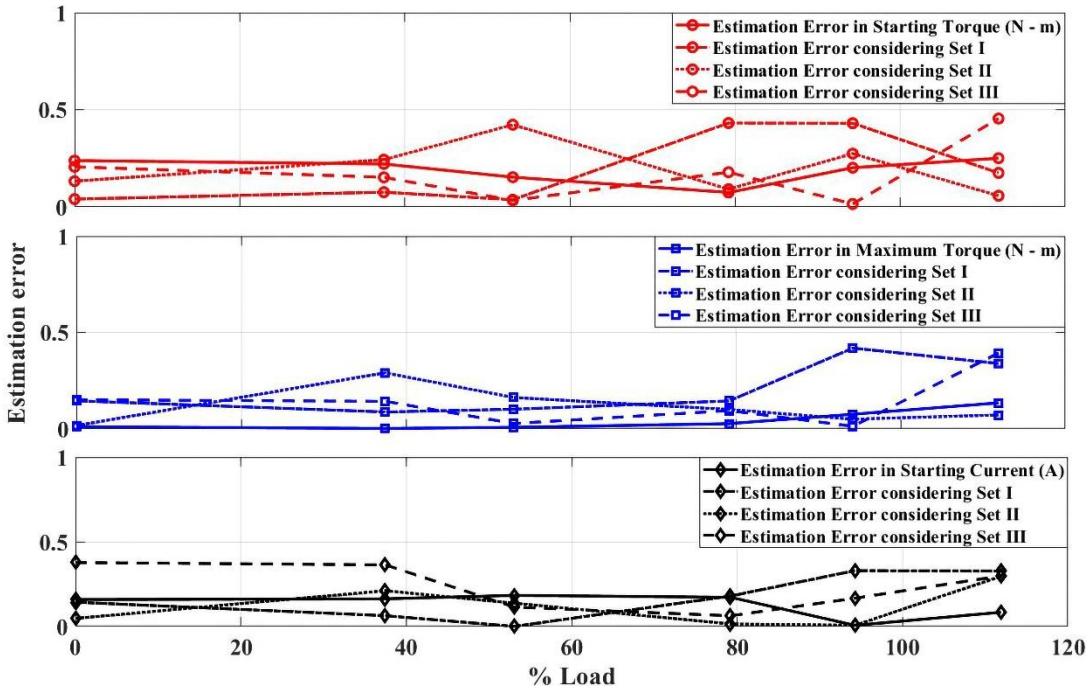

Fig. 4.12. Estimation error of starting torque, maximum torque and starting current for different sets of search space and population.

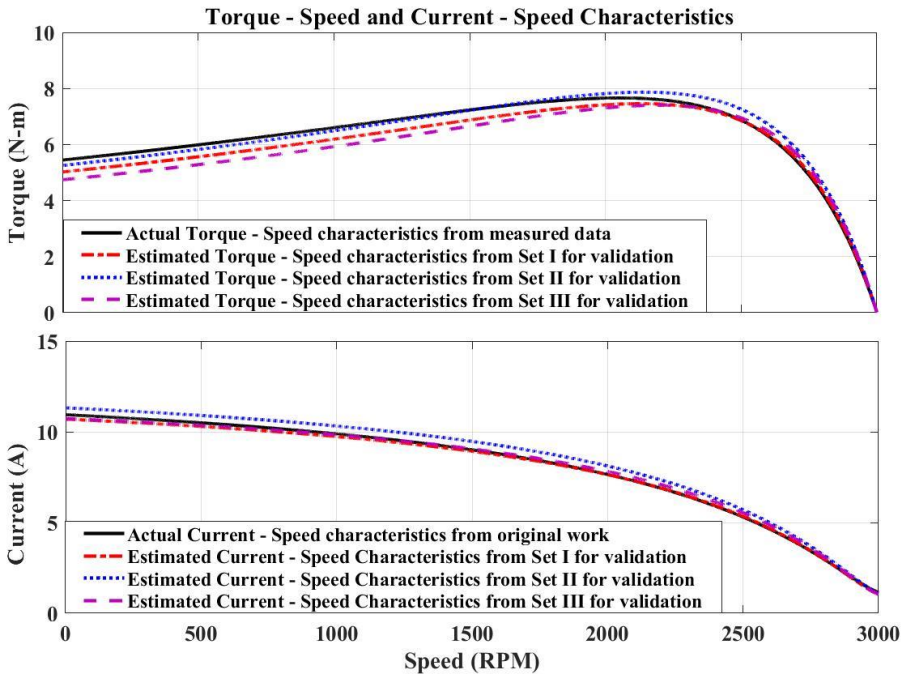

Fig. 4.13. Influence of boundary values and population size on predicted Torque – Speed and Torque – Current characteristics.

well as swarm size. Fig 4.12 shows that even with a large variation in swarm size and boundary conditions, the estimation errors are within limit. Fig 4.13 shows torque - speed and current – speed characteristics obtained with different boundary values and population size. From the above observations it can be concluded that the proposed scheme is robust and can be used for general purpose without any special consideration. The convergence capability of the proposed technique with large search area and any population size makes the scheme highly adoptable for parameter estimation.

4.4.2.2 Influence of time frame on estimation

The selection of time frame plays an important role in any estimation process. As motor parameters are being estimated from measured data, wrong data window selection may lead the system to converge to some

erroneous results. That's why it is necessary to investigate the algorithm for different time frame. It should be kept in mind that the complete transient portion should be included for accurate estimation. However, a larger data size increases the computational burden as well as time and memory requirement. So, the actual work has been carried out considering the time frame of 0.0 – 0.5 seconds and validated using data for 0.0 – 1.0 second span to ensure the minimum influence of data size on accuracy of the system. Fig 4.14 signifies that with the time frame of 0.0 – 1.0 seconds, the estimated stator current (in ampere) is close enough to the measured values. So, it can be concluded that the proposed system is capable of estimating the stator current for all three phases accurately.

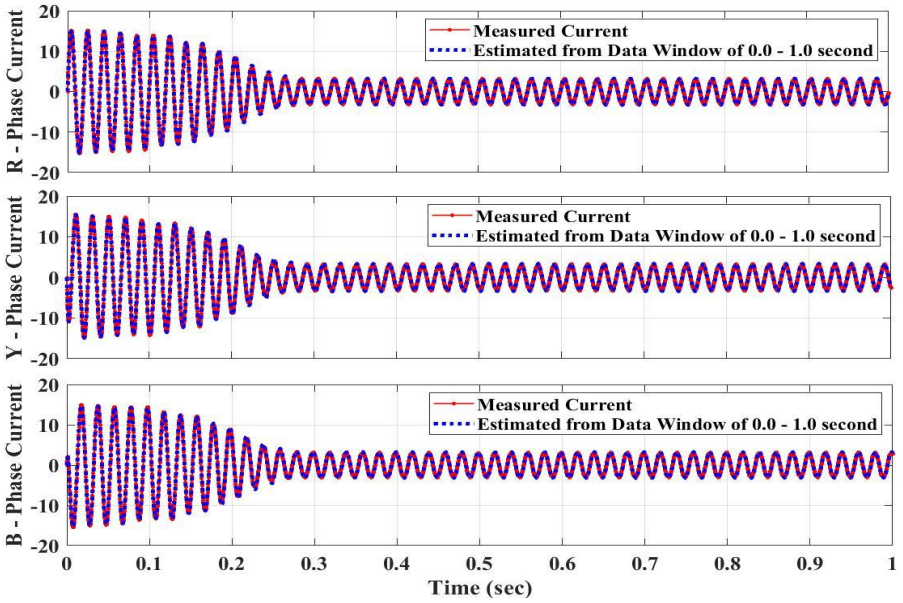

Fig. 4.14. Comparison of measured and simulated stator currents considering data window from 0.0 to 1.0 sec.

However, the other motor performance indicating variables (starting torque, maximum torque and starting current) should also be analysed under this condition and compared with the actual one so that the accuracy and robustness of the proposed system can be justified. The estimation errors of starting torque, maximum torque and starting current under new

time frame have been determined using equation (4.10) – (4.12) and compared with the estimation errors under old time stretch (0 to 0.5s) for different loading of the induction motor. The error comparisons at old (0 to 0.5s) and new time (0 to 1s) stretch have been represented in Fig 4.15. It may be observed from Fig 4.15 that estimation error for starting torque, maximum torque and starting current is negligible.

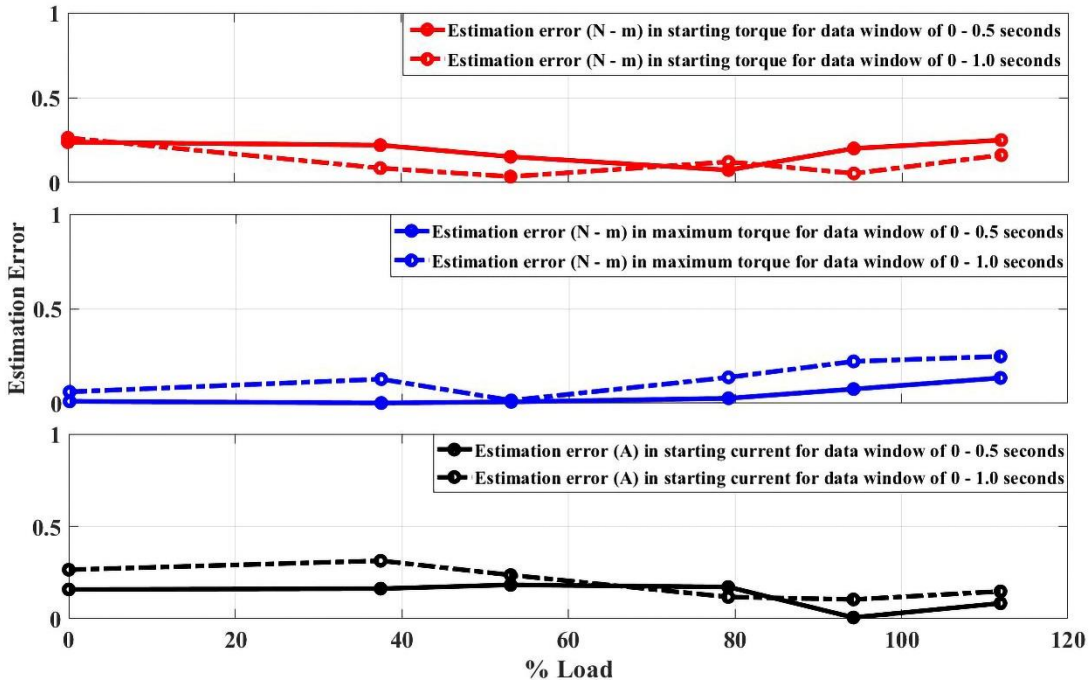

Fig. 4.15. Estimation error of starting torque, maximum torque and starting current for different time frame.

Fig 4.16 portrays the comparison of torque – speed and current – speed characteristics of the experimental induction motor obtained under the two different time frames (0 to 0.5s and 0 to 1s) which reveals no significant change in the torque – speed and current – speed characteristics. These studies illustrate the immunity of the proposed system against the variation in selection of data window. Thus, it can be concluded that, in spite of considerable variations in boundary condition, population size or time

frame selection, the proposed scheme encounters negligible amount of error in estimation.

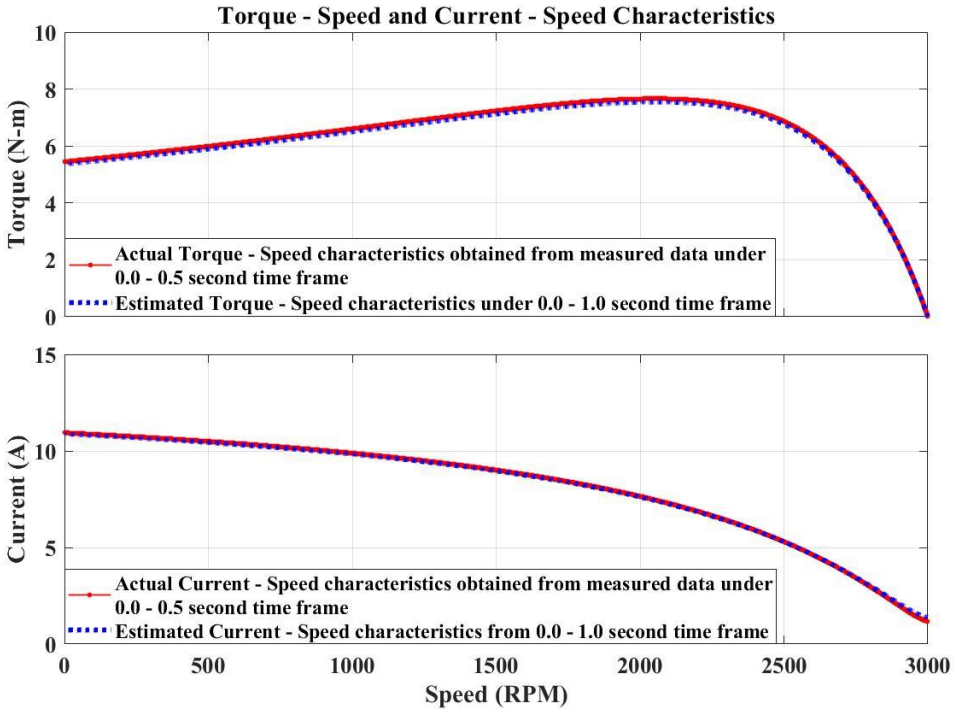

Fig. 4.16. Influence of time frame on predicted Torque – Speed and Torque – Current characteristics.

4.5 Advantage of transient model over steady state model

The transient data contains lot of information regarding the characteristics and performance of induction motor. It has been observed that, a lot of additional measurements such as input power, output power, input power factor, no load current and speed are required for accurate estimation of motor parameters and losses from steady state data. Moreover, steady state data do not contain any information about the machine inertia which can only be acquired from the transient measurement.

It is a known fact from machine design experience that, two different induction motors with same rating, designed with same current density,

flux density and turns ratio can have different slot dimension, different number of stator and rotor slots or different winding arrangements leading a dissimilar set of parameter values. Therefore, it's very difficult to estimate the machine parameters as well as losses properly from steady state measurement only, as the scheme might have a chance to converge to some different set of parameter values which produce the same steady state measurements. However, it has been observed that, if the machine parameters are different from the actual one, then they produce different transient response which is illustrated in Fig 4.17. Here the parameters estimated from steady state measurement, produces similar steady state current (in ampere) whereas, the transient part differs from the measured value and hence, the estimation become erroneous.

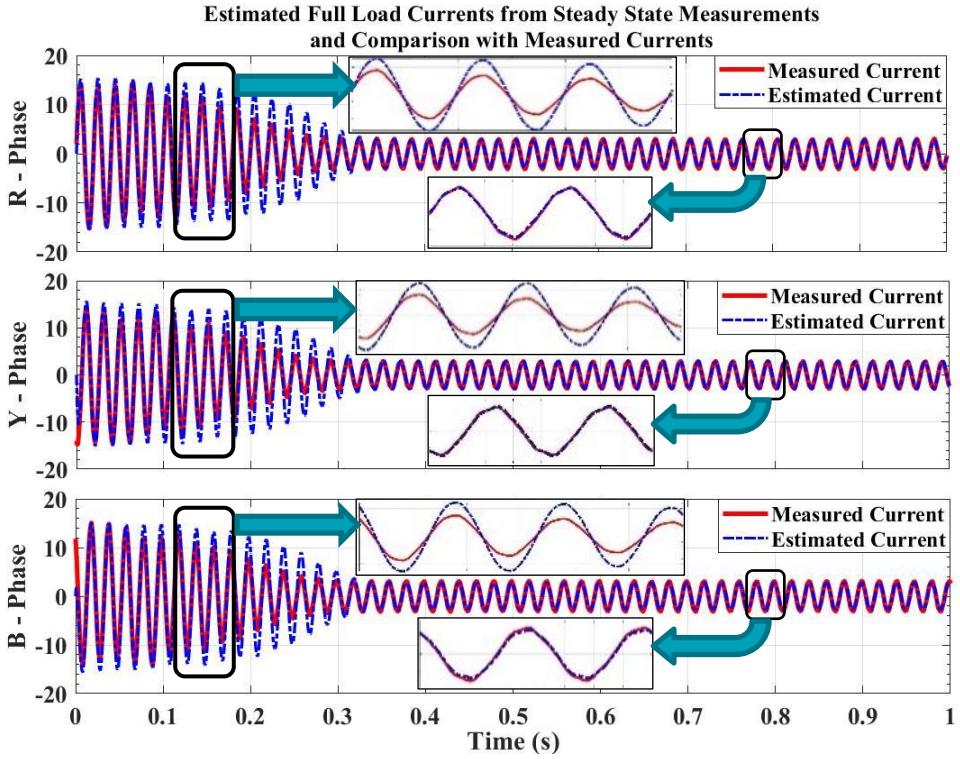

Fig. 4.17. Disparity of full load measured stator currents and stator currents simulated based on the parameter estimation from steady state (0.5 to 1.0 sec) measurements.

Comparison of Fig 4.8, Fig 4.11, Fig 4.14 and Fig 4.17, concludes that estimation involving transient measurement, irrespective of consideration of timeframe, boundary condition or population size, provides improved model responses hence produce more accurate results.

4.6 Conclusion

The work presents a simple and accurate method for estimating the induction machine equivalent circuit parameters using Particle Swarm Optimization technique. Based on the analysis, following observations can be made

- The stator transient current evaluated from the estimated parameters closely resembles the measured values.
- The estimated values do not vary with the population size, boundary condition and different time frame consideration.
- The estimated performance parameters (phase current, power factor, speed and output power) are close to the corresponding measured values for different load.
- The estimated total loss shows a good agreement with the measured values for different loads.

Thus, the proposed technique is effective to estimate the equivalent circuit parameters of induction motor and can be effectively used for monitoring the performance of induction machines used in industries which is important from fiscal point of view. Furthermore, the proposed technique can be extended by modifying the scheme for inverter fed induction machines. As the proposed scheme can estimate the losses accurately,

hence, the estimated losses can be fed into a thermal model to estimate the temperature of different parts of the motor under varying load condition.

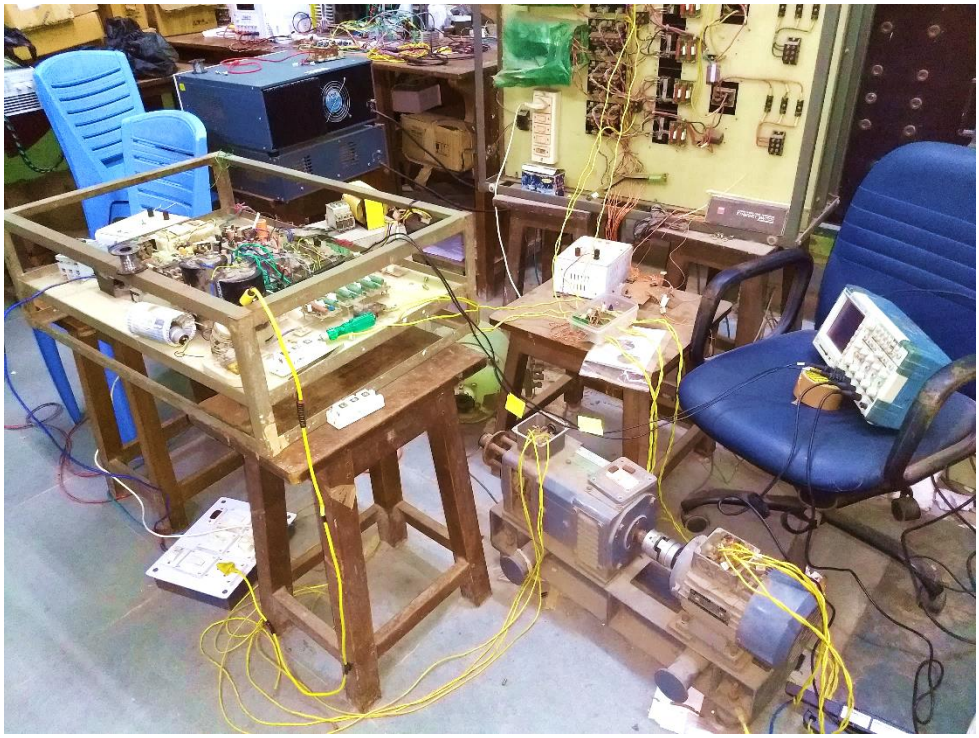

CHAPTER 5

Estimation of Inverter Fed Three Phase Induction Motor Performance at Reduced Flux Condition

This study investigates the performance characteristics of an inverter fed three-phase induction motor operating particularly under reduced flux conditions. Inverter-fed motors are integral components in various industrial applications and are subject to diverse operating conditions. For example,industrial machines often run at partial torque or no-load condition.Under this circumstances, for efficiency improve of the machine, general practice is to run the motor with flux weakening. Understanding the motor's behavior under reduced flux conditions is crucial for optimizing energy efficiency and extending the motor's operational lifespan. This research aims to unveil insights into the dynamic response, efficiency, and operational limits of the inverter-fed three-phase induction motor in scenarios where flux levels are intentionally reduced. The outcomes of this study hold significant implications for the development of advanced health monitoring strategies and reliable motor operation in real-world applications.

5.1 Introduction

Inverter fed induction motors are commonly used machines in industry because of its improved dynamic response as well as precise speed control. Due to ease of voltage and frequency control, Pulse Width Modulated (PWM) Inverter supply is advantageous over the commercial sinusoidal supply. Voltage and frequency control improves the machine dynamics resulting in good speed response even in low-speed operation of induction motor. Sinusoidal supply produces pure sinusoidal flux in induction motors. From the insulation point of view, $\frac{dV}{dt}$ is small enough to withstand. $\frac{dV}{dt}$ is very high in inverter fed machines. As, in inverter fed machines, during each switching, peak dc voltage is applied to the stator windings. This high $\frac{dV}{dt}$ imposes high stress on the winding insulation, increasing risk of insulation failure. Therefore, health monitoring of inverter fed induction motors is of immense importance.

This investigation is particularly focused on understanding the behavior of an inverter-fed three-phase induction motor under reduced flux conditions. This is crucial for optimizing energy efficiency and extending the motor's operational lifespan. In industrial settings, machines often operate at partial torque or no-load conditions. To enhance efficiency in such situations, field weakening is commonly employed. The outcomes of this study can significantly enhance health monitoring strategies, ensuring reliable motor operation in practical applications. By thoroughly understanding the motor's behavior under reduced flux conditions, the research provides valuable insights for developing advanced health monitoring systems, ensuring optimal performance in diverse operational scenarios.

5.2 Objective of the work

When the motor is running at partial torque or no-load condition, core loss becomes predominant. Hence, to improve the efficiency of the machine the machine is run at reduced voltage condition reducing the flux. To correctly predict behavior of the induction motor fed from PWM supply, running under reduced flux condition, a technique of parameter and loss estimation has been proposed. The Particle Swarm Optimization has been used to correctly estimate the parameters and losses of a three phase, 50 Hz, star connected induction motor (0.75 kW, 380 V (line-line)) from voltage and current measurement. 'Particle swarm optimization' has been used as the estimation tool because of its simplicity, faster convergence capability and accuracy [91], [89]. The estimated parameters, losses and the performance characteristics of the induction motor have been compared with the measured one.

5.3 Formation of objective function

Here, the objective function is formulated referring the same procedure as given in chapter 4. The mathematical expression is given as:

$$O = \min\left[\text{sum}\left(\frac{I_{ph}-I_{ph_{est}}}{I_{ph}}\right)^2\right] \tag{5.1}$$

5.4 Experimental setup and procedures

Fig. 5.1 represents the complete laboratory setup used for performing the experiment. The experiment has been performed a three-phase induction motor (specification given in table 5.1) coupled with a dc generator with specification 0.75kW, 1500 rpm, 200V, 5.0A. The induction motor was supplied from a PWM inverter at fixed

fundamental frequency. A Tektronix TPS 2014 four channel digital storage oscilloscope has been used for the transient voltage and current measurement. The separately excited dc generator, coupled with the experimental machine, has been used for loading purpose.

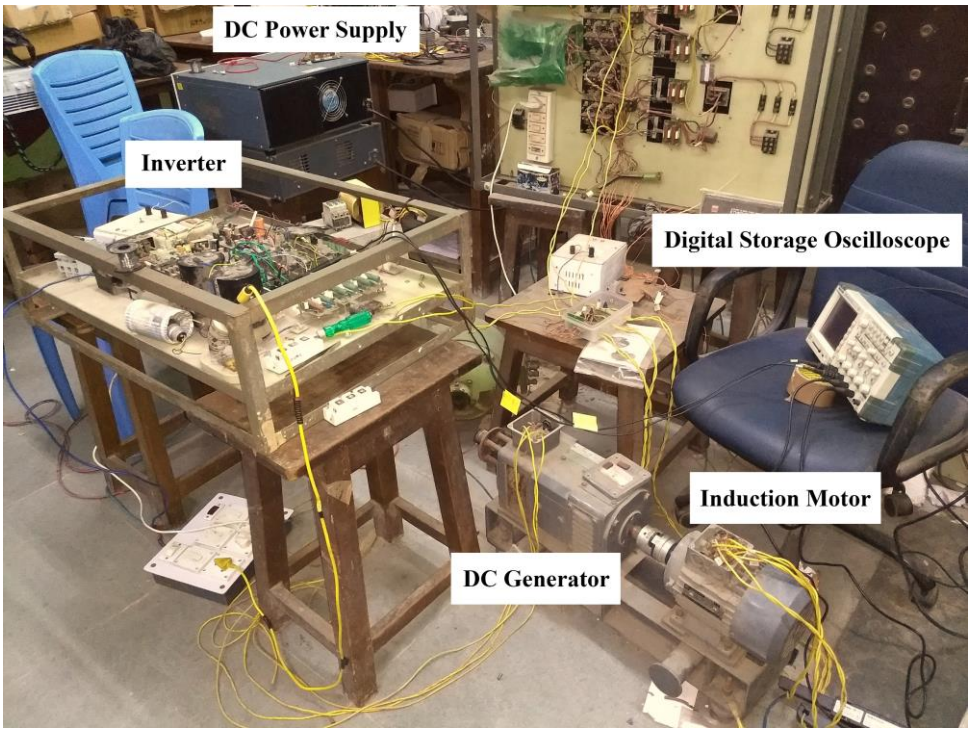

Fig. 5.1. Complete experimental setup of induction motor used in laboratory.

Transient voltage and current data have been recorded with the oscilloscope under no load condition. The recorded transient voltage was fed into the induction motor dynamic model and the phase currents were estimated. Using particle swarm optimization, the estimated phase currents have been compared with the recorded currents, considering the objective function given in equation (5.1).

On the other hand, the machine was also feed from a normal three phase sinusoidal commercial supply and the parameters and losses have been estimated. This experiment provides a comparative study about the change in machine parameters and losses under different types of input

conditions. The fundamental component of the PWM voltage was selected to have the same r.m.s. voltage and same frequency as the commercial sinusoidal supply.

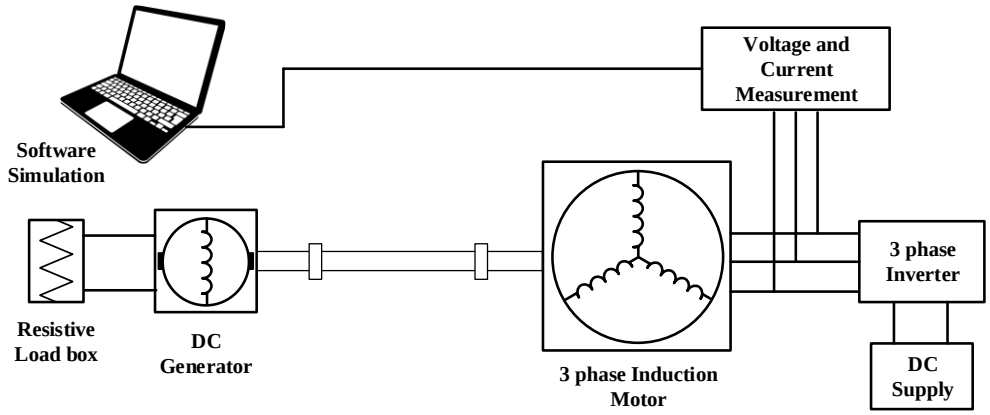

Fig. 5.2. Schematic diagram of the proposed parameter estimation process.

Table 5.1. Motor nameplate data

Machine Nameplate Data	***Values***
Voltage (V)	380/220
Power (kW)	0.75
Current (A)	2.2/3.8
Connection	Y/Δ
Speed (RPM)	1390

The validation of the estimated results has been done by performing dc resistance test, no-load test and blocked rotor test on the experimental machine. The estimated parameters have been compared with the experimentally obtained parameters and the comparative study has been presented in the section 5.5.

5.5 Results and Analysis

5.5.1 Result analysis

Table 5.2 represents the comparative study of the experimentally obtained and estimated equivalent circuit parameters and inertia under both sinusoidal and PWM inverter input. From Table 5.2, it could have been concluded that estimated parameters for both sinusoidal as well as PWM supply are within the acceptable limit of accuracy.

Table 5.2 Comparison of experimentally obtained and estimated equivalent circuit parameters under different input condition

Parameters	Parameters obtained from dc resistance, no load and blocked rotor test	Estimated parameters when supply is sinusoidal	Estimated parameters when supply is PWM inverter fed	% Estimation error for sinusoidal supply	% Estimation error for Inverter-fed supply
R_s (in Ω)	11	10.90	12.03	-0.91	9.36
R_r' (in Ω)	7.53	7.76	8.84	3.05	17.40
X_{eq} (in Ω)	22.37	23.02	22.03	2.91	-1.52
X_m (in Ω)	126.6	130.5	121.44	3.08	-4.08
J (in kg-m^2)	0.0059 (from datasheet)	0.0055	0.0055	-6.78	-6.78

Performance characteristics obtained by using estimated parameters was far better than that derived by using experimentally obtained parameters. This phenomenon is illustrated in Fig. 5.3.

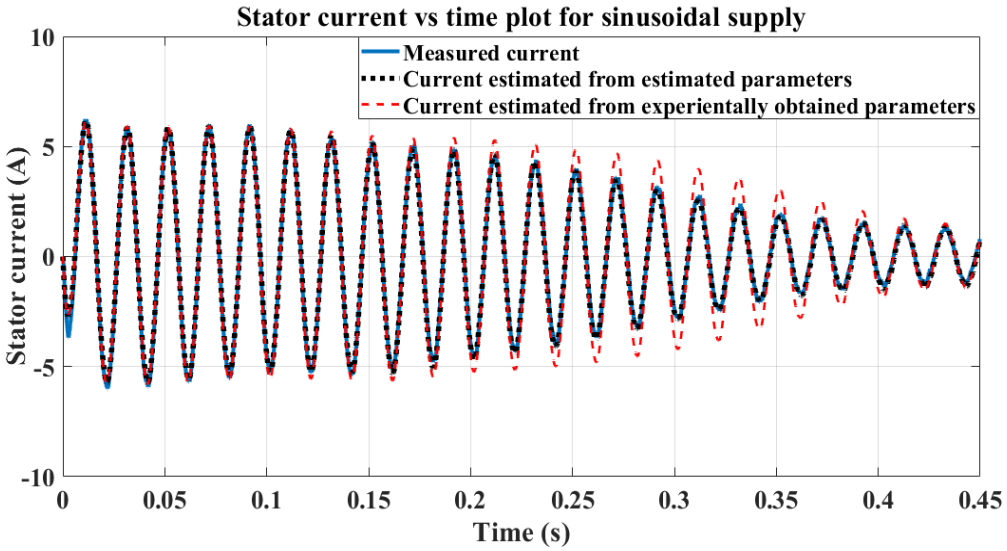

(a)

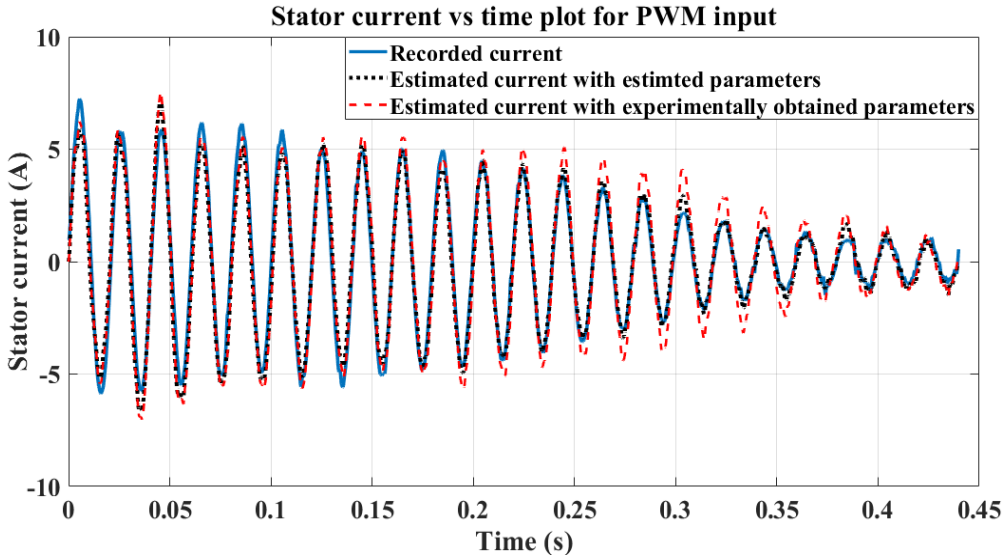

(b)

Fig. 5.3. Estimated and measured stator currents for (a): sinusoidal input. (b): PWM input.

Fig. 5.4 (a) – (e) shows the oscilloscope responses obtained for sinusoidal supply at transient state.

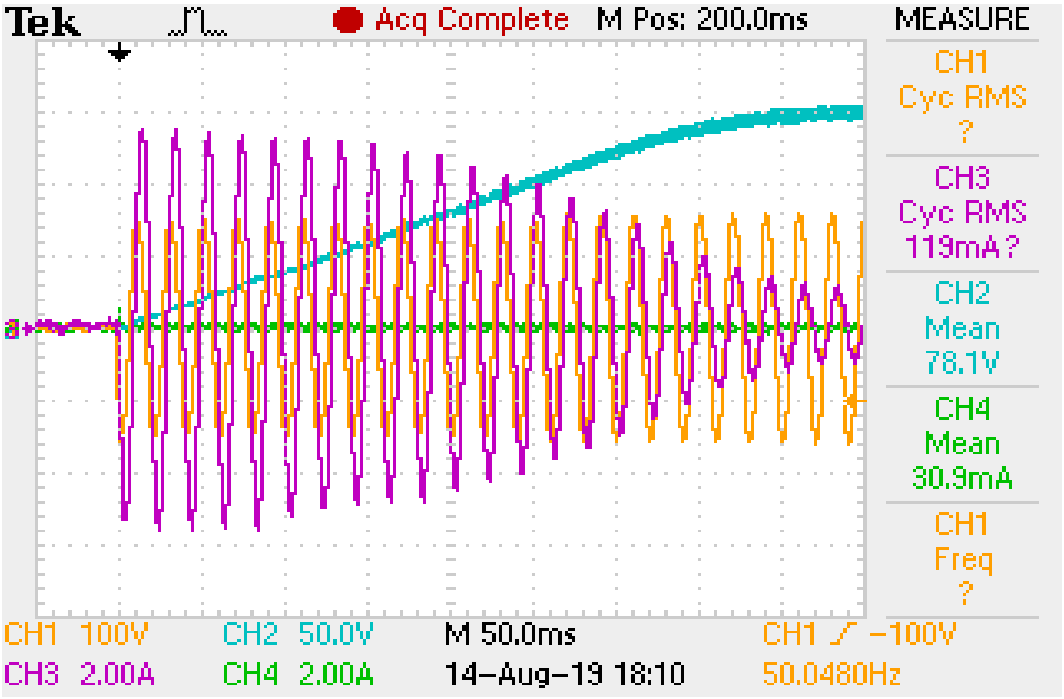

5.4 (a) Screenshot of the oscilloscope

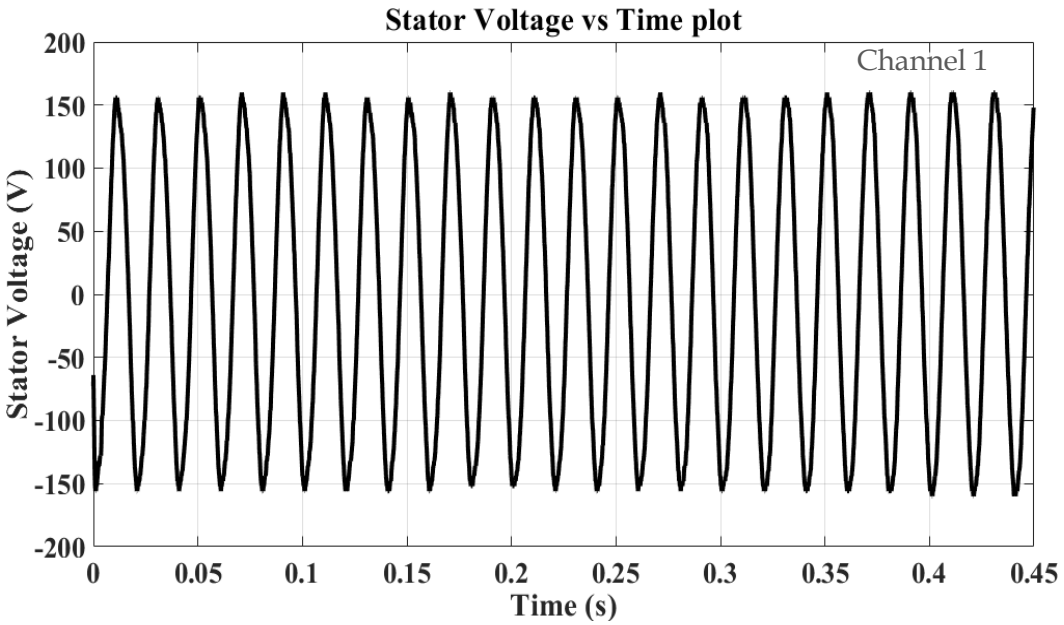

5.4 (b) Sinusoidal supply voltage waveform

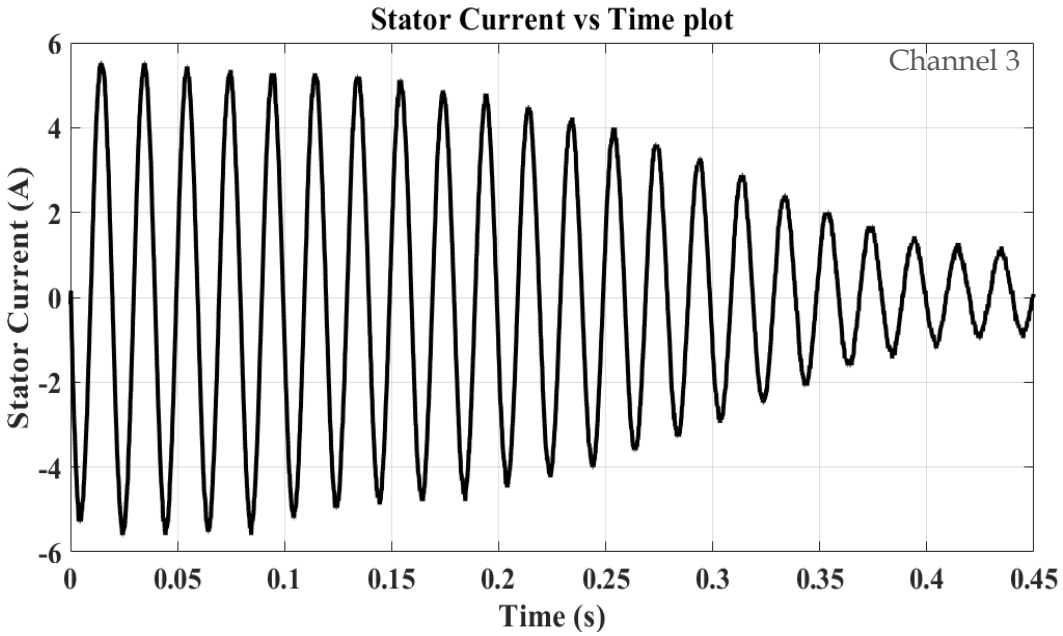

5.4 (c) Starting transient of input current under sinusoidal supply

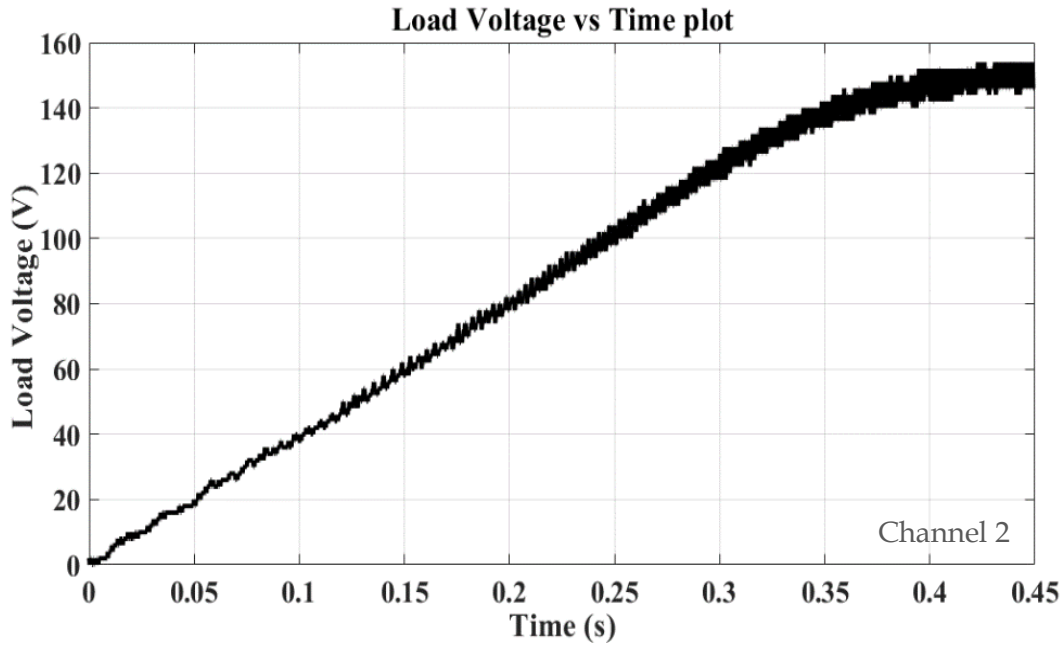

5.4 (d) Generated DC voltage at load side

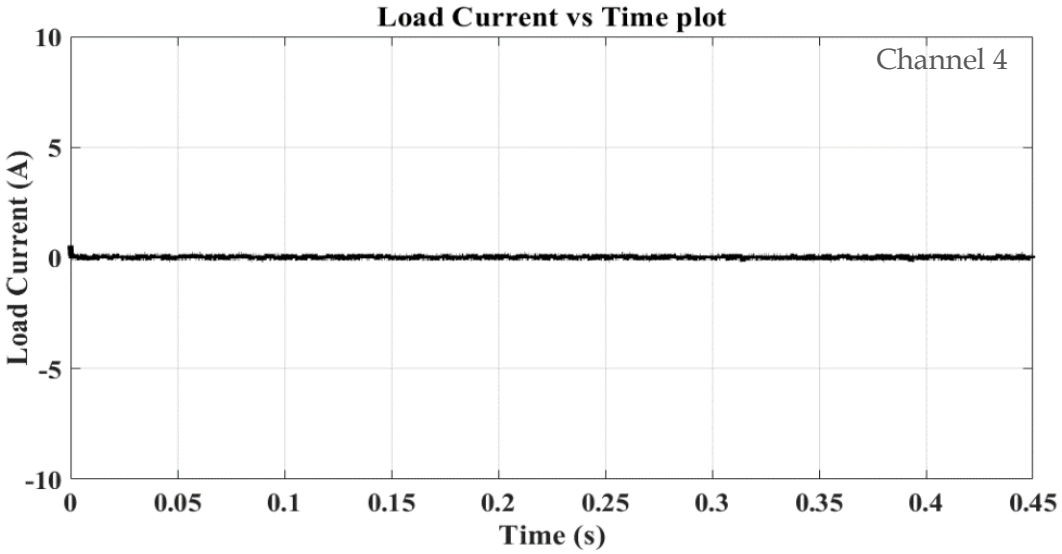

5.4 (e) Load current (DC) profile

Fig. 5.4 (a) – 5.4 (e). Transient oscilloscope response for sinusoidal input

Fig. 5.5 (a) – (e) represents the steady state oscilloscope response for sinusoidal supply.

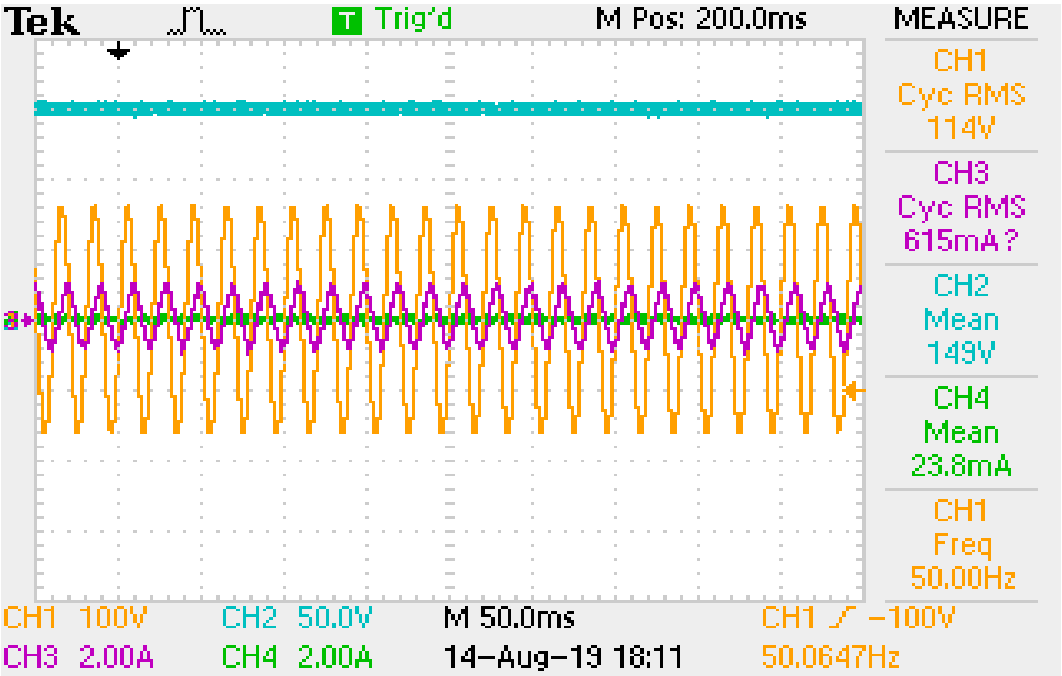

5.5 (a) Oscilloscope Screenshot

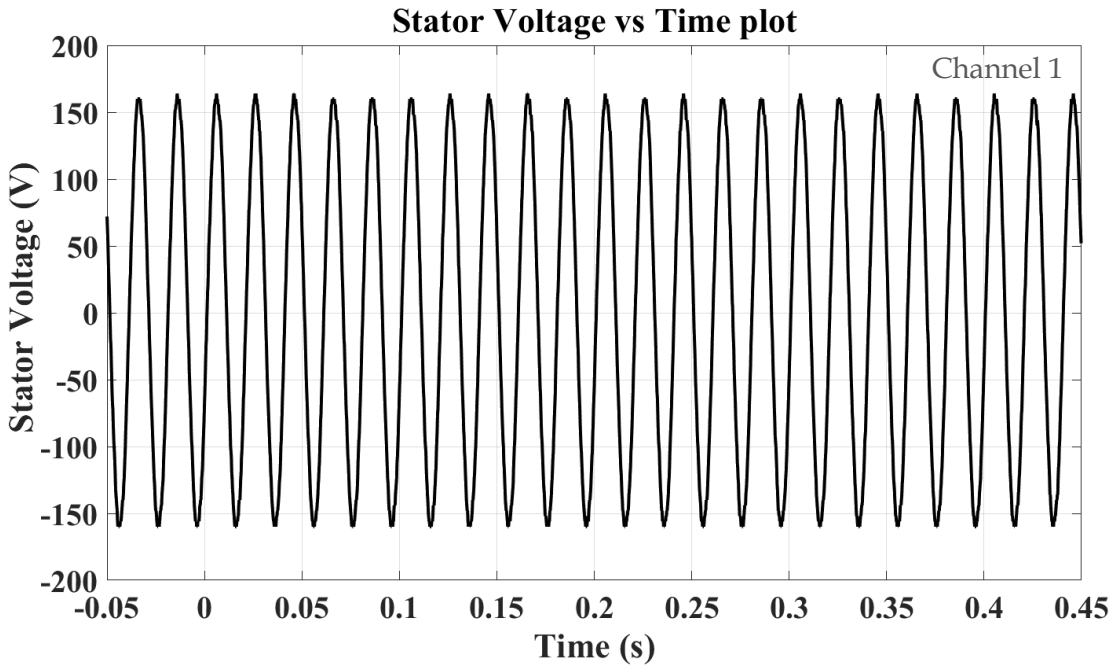

5.5 (b) Sinusoidal supply voltage waveform

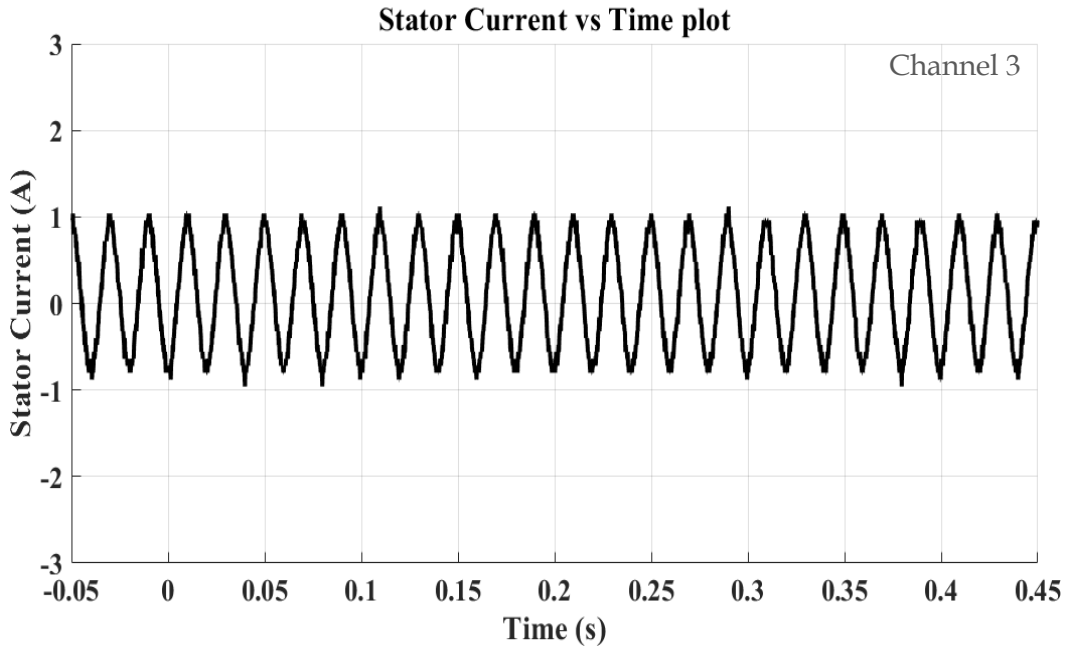

5.5 (c) Input motor current waveform under steady state

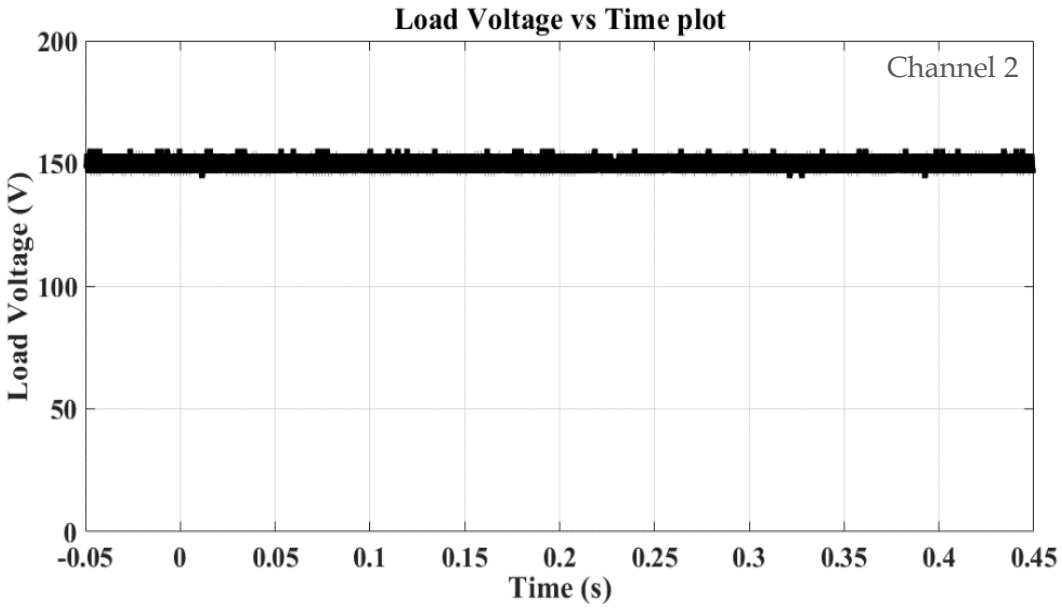

5.5 (d) Generated load side DC voltage at steady state

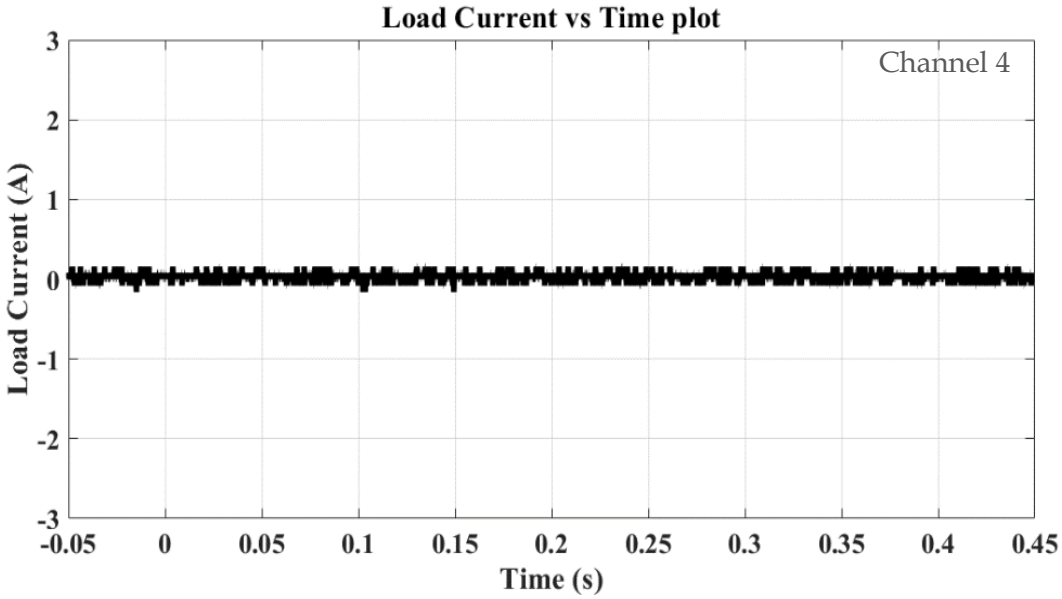

5.5 (e) DC load current profile

Fig. 5.5 (a) – 5.5 (e). Steady state oscilloscope response for sinusoidal input

Figure 5.6 (a) – (e) illustrates the oscilloscope responses during the transient state under PWM supply conditions.

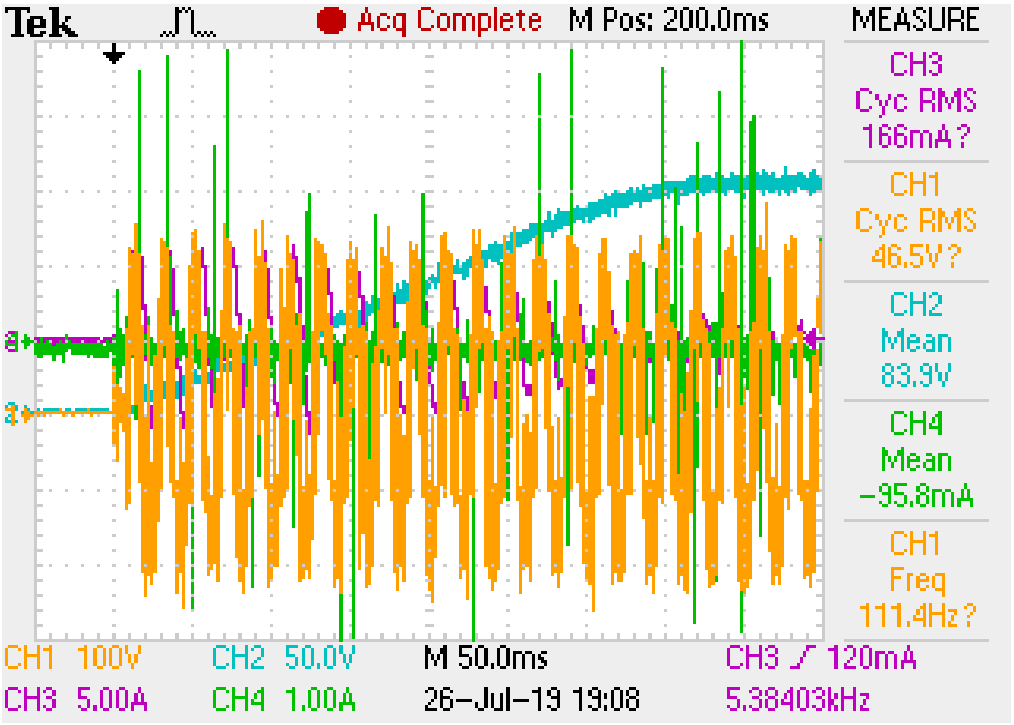

5.6 (a) Oscilloscope screenshot

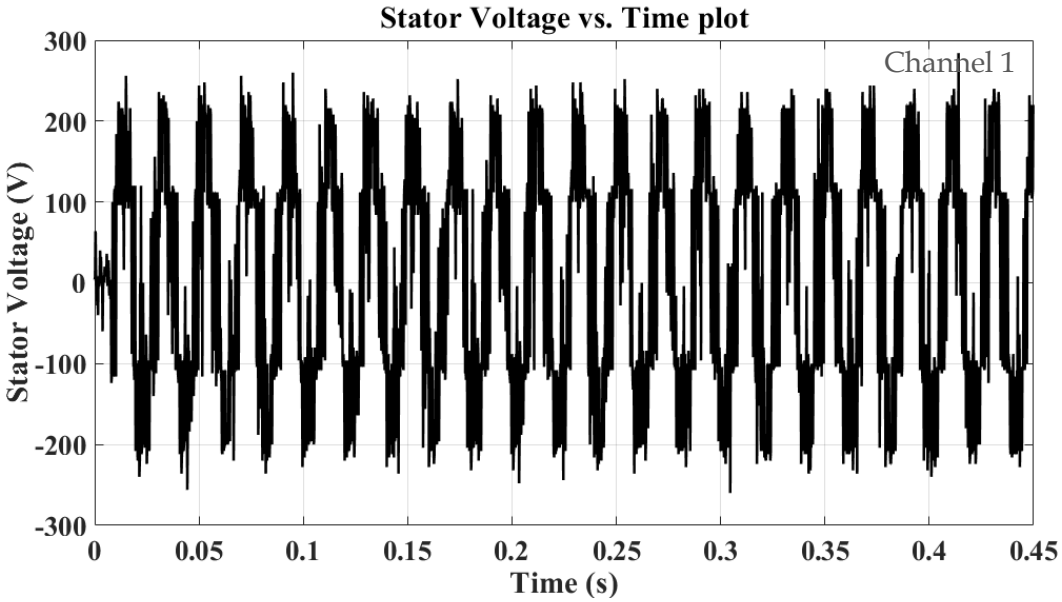

5.6 (b) Supply PWM voltage waveform

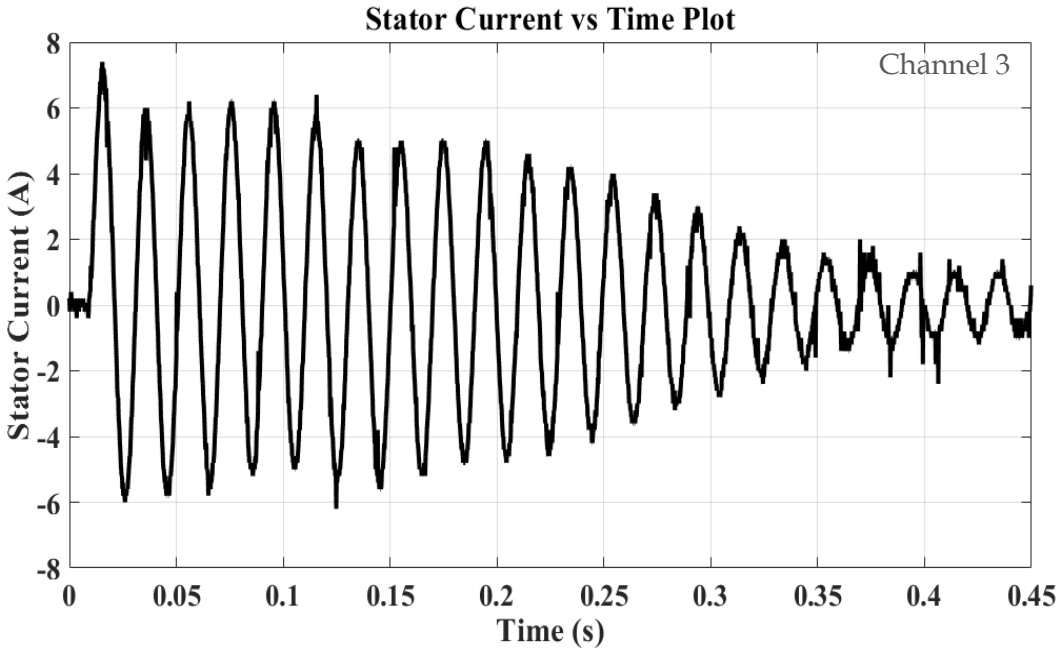

5.6 (c) Starting transient of input current under PWM supply

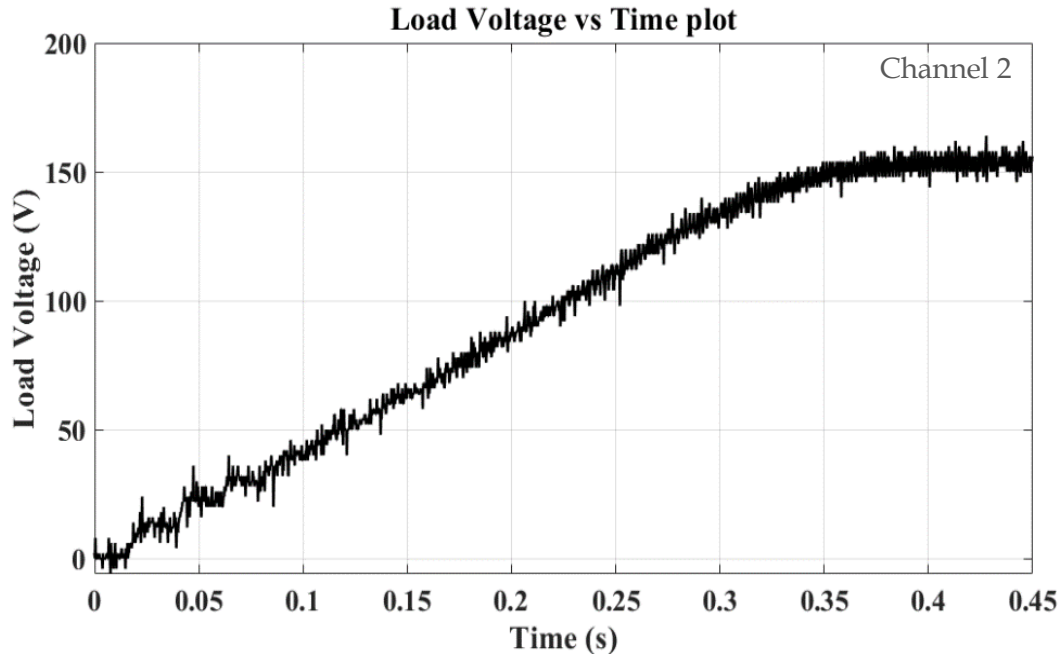

5.6 (d) DC voltage generated at load side during starting

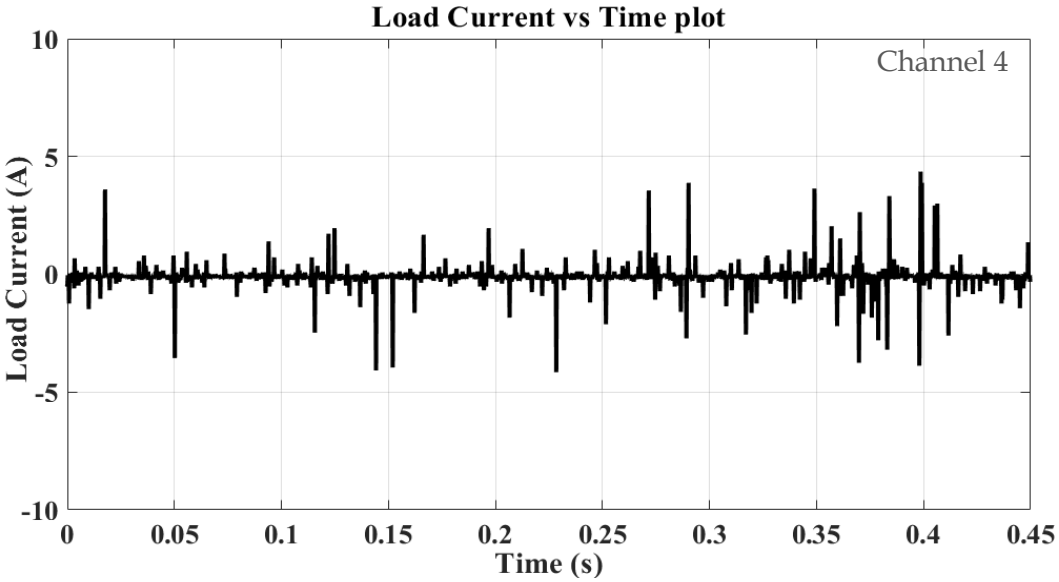

5.6 (e) DC load current

Fig. 5.6 (a) – 5.6 (e). Oscilloscope response for PWM input at transient condition.

Figure 5.7 (a) – (e) depicts the steady state oscilloscope's responses with PWM supply.

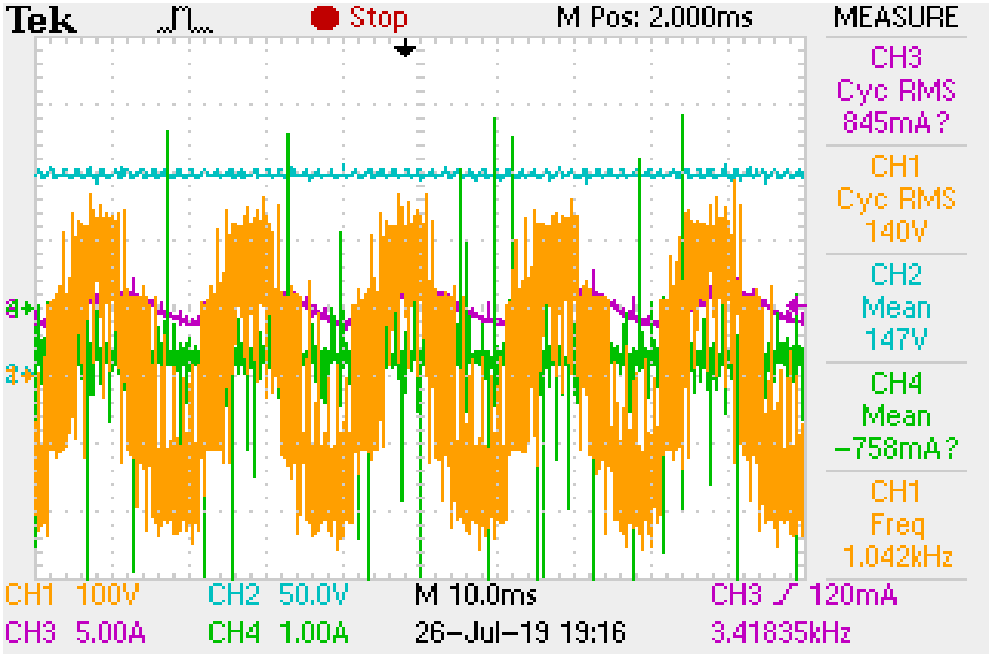

5.7 (a) Oscilloscope screenshot

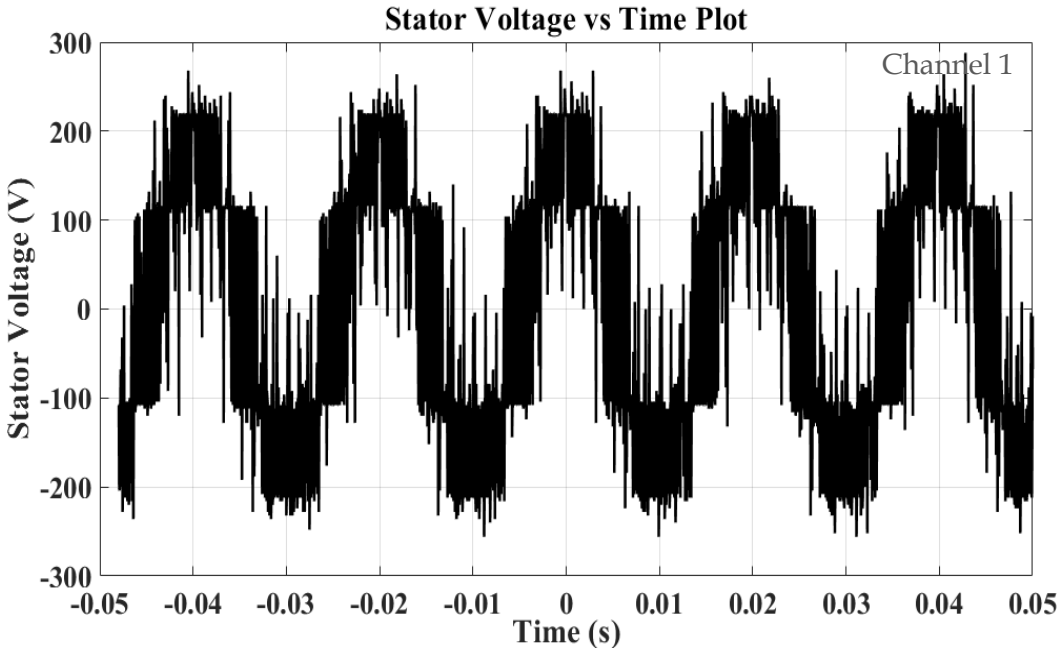

5.7 (b) Input steady state voltage waveform with PWM supply

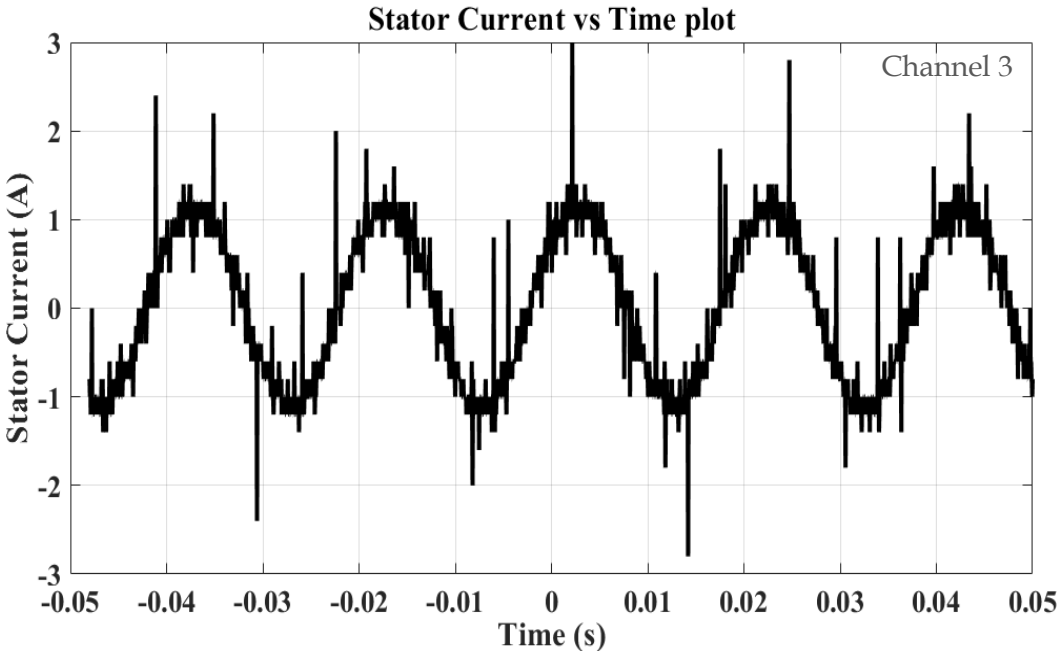

5.7 (c) Input steady state current waveform with PWM supply

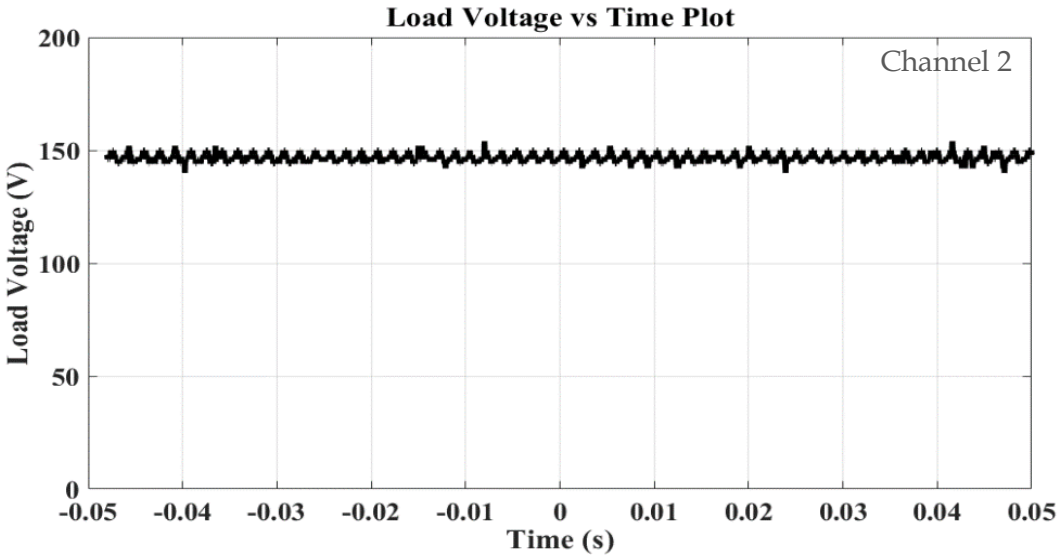

5.7 (d) DC load voltage at steady state under PWM supply

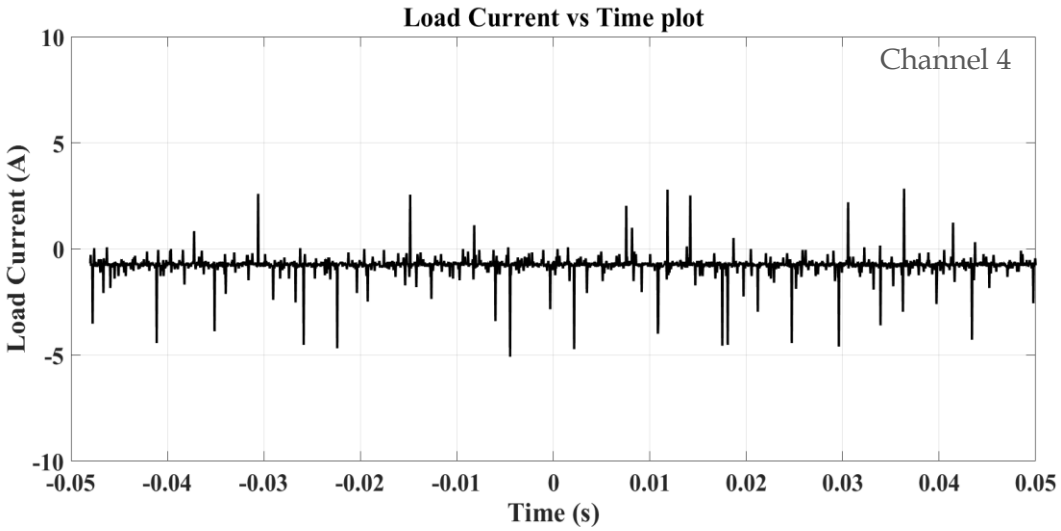

5.7 (e) Steady state DC load current under PWM supply

Fig. 5.7 (a) – 5.7 (e). Steady State Oscilloscope response for PWM input

In Fig. 5.4 (a), Fig. 5.5 (a), Fig 5.6 (a) and Fig 5.7 (a), channel 1 and channel 3 of the oscilloscope shows the induction motor input voltage and current respectively, whereas, channel 2 and channel 4 shows the generated dc output voltage and current.

From Fig. 5.6 and Fig 5.7 it has been observed that PWM input introduces torque ripples because of its high switching frequency which indicates the presence of harmonics in the system. Table 5.3 and 5.4 represents the comparison of estimated speed and losses for both sinusoidal and PWM inverter supply with the measured one.

Table 5.3 Comparison of experimentally obtained and estimated motor performance indicator under different input condition

For Sinusoidal Supply	Measured	Estimated from sinusoidal supply	% error
Speed (in rpm)	1491	1490	0.0670
Total Loss (in Watt)	69.82	72.2432	-3.466

For PWM Supply	Measured	Estimated from PWM supply	% error
Speed (in rpm)	1491	1491.4	-0.0268
Total Loss (in Watt)	91.37	94.5313	-3.46

Table 5.4 Separation of losses

Type of supply	Estimated Losses				Total Measured Loss
	Stater copper loss	Rotor copper loss	Core loss	Total loss	
Sinusoidal Supply	22.4693	0.2349	49.5390	72.2432	69.82
PWM Supply	22.7542	4.1556	67.6215	94.5313	91.37

5.5.2 Performance characteristics

Fig 5.8 shows the estimated performance characteristics of the experimental induction motor for sinusoidal and PWM supply. During experiment, r.m.s. value of the fundamental component as well as the fundamental frequency of the PWM were same as that of the commercial sinusoidal supply voltage. Fig. 5.8(a) represents the speed response of

the machine with time, whereas Fig. 5.8(b) represents the torque response. Fig. 5.8(c) represents the torque-speed characteristics of the experimental motor.

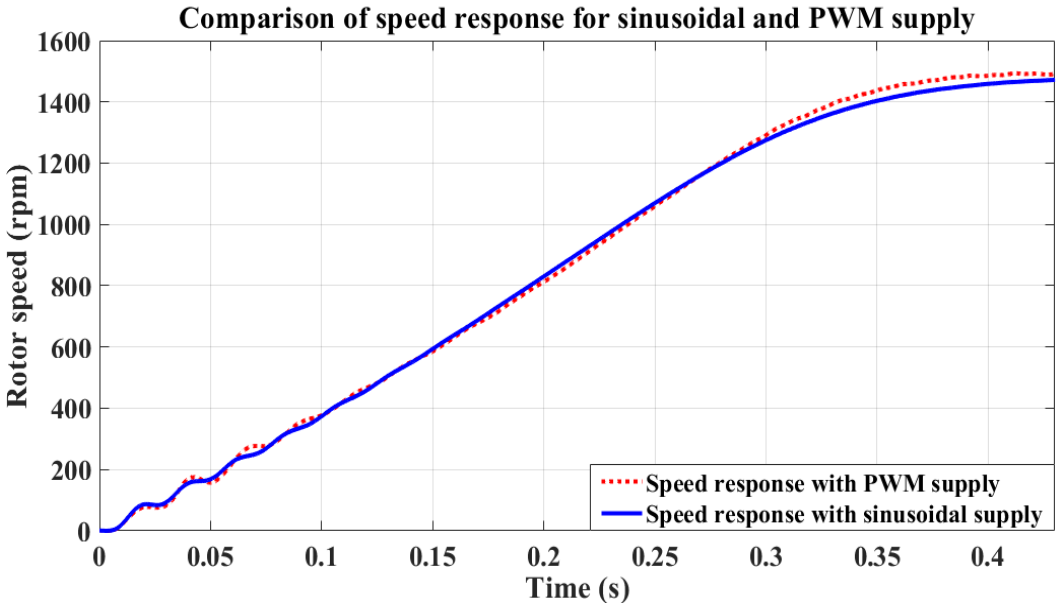

(a)

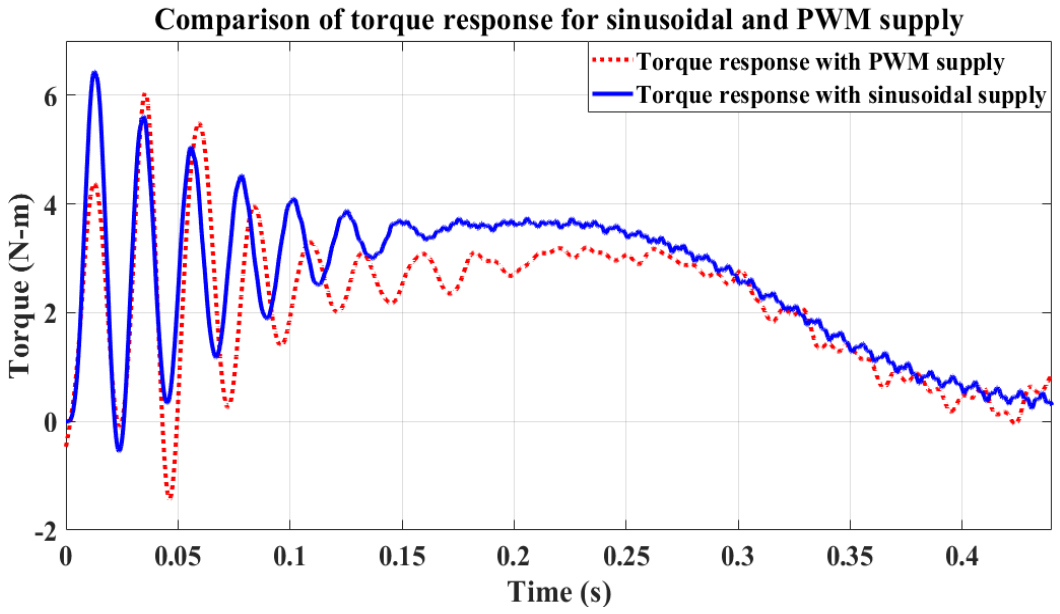

(b)

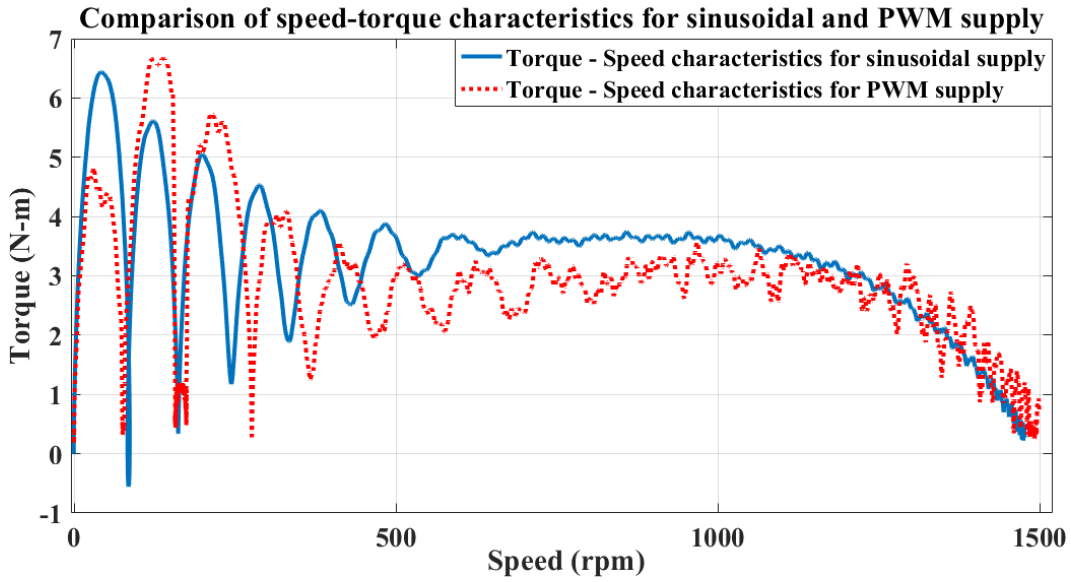

(c)

Fig. 5.8. Comparison of experimental (a) speed response, (b) torque response and (c) Torque – Speed characteristics for sinusoidal and PWM supply.

5.6 Conclusion

A scheme has been proposed that can estimate the equivalent circuit parameters, losses and inertia of the induction motor operating under reduced flux conditions, from its performance data, using Particle Swarm Optimization. A lot of work has been reported till date on parameter estimation of three phase induction motors. But most of them consider the situation when the machine runs at rated voltage. However, in practice, situations may arise when torque requirement is less than the rated torque. To make the machine energy efficient, the machine is run at a lower voltage to reduce the flux. For continuous health monitoring of the machine, it is very important to accurately estimate the equivalent circuit parameters, losses and machine inertia even under reduced flux condition. From the estimated parameters and losses, a thermal model can be built for temperature estimation of

different parts of the motor. This thermal model can provide continuous monitoring of the machine and protect it from incipient faults. Thus, the proposed scheme is feasible for extension to a temperature based continuous health monitoring scheme for induction motors. This scheme provides a cost-effective solution without compromising on the reliability or effectiveness of the system.

CHAPTER 6

Development of a Temperature Estimation Scheme for Induction Motor from Estimated Parameters and Losses

This study addresses a critical aspect of induction motor health monitoring by proposing a novel temperature estimation scheme. Temperature monitoring is crucial for preventing overheating, optimizing performance, and ensuring the reliability of industrial systems. Focused on utilizing estimated losses, this work seeks to develop an accurate and practical method for assessing the temperature profile within an induction motor. By integrating advanced estimation techniques, this scheme aims to provide real-time insights into the motor's thermal behavior, contributing to the advancement of predictive maintenance strategies. The outcomes of this research have the potential to enhance the operational efficiency and longevity of induction motors.

6.1 Introduction

The "Thermal model" is an equivalent circuit, designed to emulate the temperature distribution within an induction motor, which can provide a comprehensive analysis of heat flow through the system. This model serves as a pivotal element in temperature-based predictive condition monitoring schemes for induction motors, offering valuable insights into the thermal dynamics of the machine. The components of this thermal model include:

I) Thermal Resistance:

This component characterizes the heat transfer capacity between two adjacent machine parts. It quantifies the ability of the motor to dissipate heat and provides a crucial parameter for understanding thermal conductivity within the system.

II) Thermal Capacitance:

Thermal capacitance represents the heat retention capacity of specific machine parts. It accounts for the ability of components to store and release thermal energy, enabling the modeling of transient temperature changes and thermal inertia within the motor.

III) Heat Source:

The heat source (equivalent to current source in electrical circuit) in the thermal model signifies various motor losses within the machine, which produce the heat. This component encapsulates factors such as resistive losses, core losses, and other sources contributing to the overall heat generation within the motor.

Collectively, this thermal model creates an interconnected network of thermal resistances, thermal capacitances, and heat sources, mirroring the

intricate interplay of heat dynamics in the induction motor. By representing the temperature-related aspects of the motor in an electrical circuit, this model enables a detailed analysis of how heat propagates through different components during operation.

In the broader context, the thermal model plays an elemental role in the development and implementation of predictive condition monitoring strategies. By providing a quantitative approach for assessing temperature changes within the motor, it empowers operators and maintenance professionals to anticipate potential issues, optimize motor performance, and proactively address thermal concerns, thereby enhancing the overall reliability and longevity of induction motors in diverse industrial applications.

6.2 Objective of the work

The primary objective of this work is to design, develop, and validate a cost-effective, simple and robust temperature estimation scheme, tailored for induction motors. Induction motors are integral components in numerous industrial applications, and their reliable performance is dependent upon maintaining optimal operating temperatures. The proposed scheme aims to address critical aspect of temperature estimation of induction motor by focusing on the utilization of estimated losses in conjunction with advanced modeling techniques. The parameter and loss estimation scheme has already been developed and validated on different machine under various operating condition. It has been discussed in detail in chapter 2 to chapter 5. A temperature estimation algorithm has to be designed that estimate the temperature of the motor utilizing estimated losses. This algorithm has to take into account the dynamic nature of motor operation, effect of load variations, duty cycles, and other operational factors. The scheme exploits

the acquired performance data of the induction motor to provide real-time temperature profiles. The developed thermal model for temperature prediction, integrated with the parameter and loss estimation scheme has been described in this chapter.

The developed temperature estimation scheme was validated to ensure its accuracy and reliability. Experimental data, collected from induction motors was used to validate the model predictions. This validation process aims to demonstrate the scheme's effectiveness in capturing the intricate thermal dynamics of induction motors.

A successful temperature estimation scheme empowers operators and maintenance professionals to preemptively address potential issues, prevent overheating-related failures, and optimize the performance and longevity of induction motors. The outcomes of this work hold significant implications for industries, offering a valuable tool for enhancing operational efficiency, reducing downtime, and facilitating proactive maintenance strategies.

6.3 Development of thermal model

Thermal model is basically an equivalent circuit representing heat flow throughout the machine. It comprises of thermal resistances, thermal capacitances and heat sources. Thermal model calculates the heat flow and predicts the temperature at different nodes of the circuit.

To understand the development of the thermal model from the point of view of the induction motor, let us have a look at the geometry of the induction motor, depicted in Fig 6.1. (a).

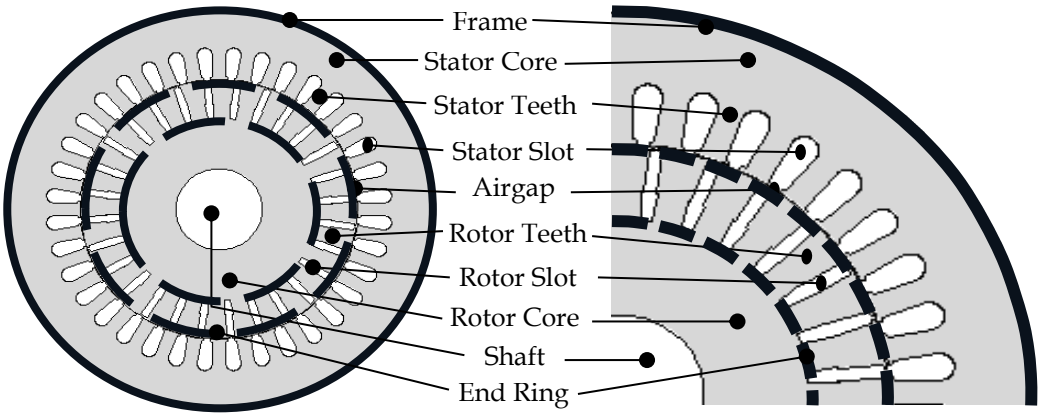

Fig. 6.1. (a). Representation of cross-sectional geometry of stator and rotor lamination of induction motor.

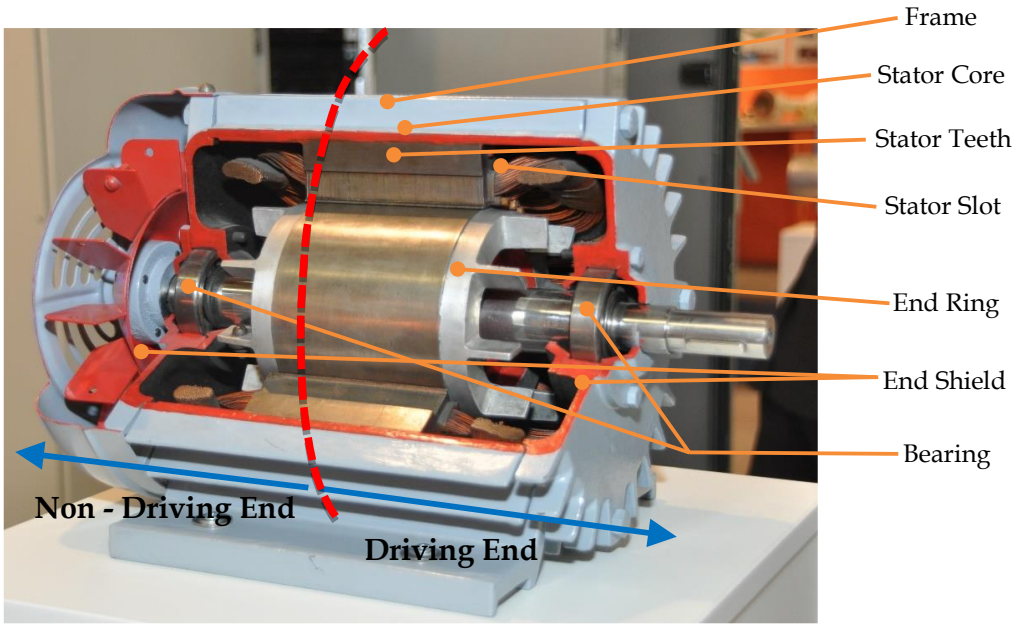

Fig. 6.1. (b). Cut-sectional view of a TEFC induction motor.

Fig 6.1. (b) represents a cut model of a totally enclosed fan cooled (TEFC) squirrel cage, three phase induction motor. In this figure, the induction motor is divided into two sections.

- Driving end
- Non-driving end

Driving end is the section with drive shaft extension. Whereas, the fan is mounted on the non-driving end. Due to the placement of the fan at non-driving end, cooling effect is slightly better on that side than driving end. Hence, under running condition, generally there is a temperature difference at these two sides of the machine under thermal equilibrium.

From the motor geometry, depicted in Fig 6.1. (a) and 6.1. (b), it is evident that for a lumped parameter thermal model, following objects and parts of the machine are essential to be considered as nodes in a thermal network.

1. Ambient

<u>At driving end</u>

2. Frame
3. Stator Core
4. Stator Slot
5. Stator Teeth
6. Air Gap
7. Rotor Slot
8. Rotor Teeth
9. Rotor Core
10. Shaft
11. End Shield

<u>At non – driving end</u>

12. Frame

13. Stator Core
14. Stator Slot
15. Stator Teeth
16. Air Gap
17. Rotor Slot
18. Rotor Teeth
19. Rotor Core
20. Shaft
21. End Shield

From the motor geometry, a thermal model was developed for the TEFC induction motor and depicted in Fig. 6.2. Here, every node is connected to an adjacent node by thermal resistance. Every node is equipped with a thermal capacitance and a heat source. Heat sources signify different losses of the machine which are the main producer of heat. If some parts of the machine do not have any significant loss (e.g., rotor core), heat generated on that node will be considered as 'zero'.

For the development of the thermal model, following assumptions have been considered.

Assumptions:

1. Uniformity of temperature within the elements and on the surface.
2. Uniformity of heat generated in the active elements.
3. Uniformity of physical properties within each element.

4. Heat transfer is only in the axial and radial directions since circumferential temperature variation is negligible.
5. Heat flow in the radial and axial planes are independent of each other.
6. The mean temperature in either direction is same.
7. Radiation heat transfer is neglected.

Fig 6.2 represents the schematic diagram of the developed thermal model.

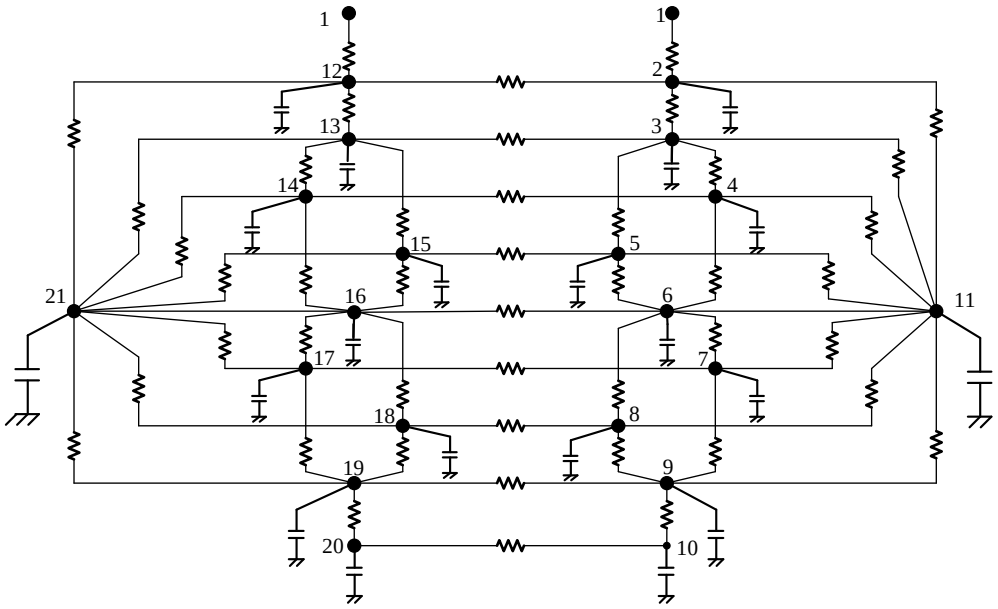

Fig. 6.2. Schematic representation of the developed thermal model.

Heat transfer in a motor mainly occurs in two methods.

1) Conduction

2) Convection

Convection heat transfer occurs in those parts of the machine where the fluid (air) is involved e.g., heat transfer through the air gap (between node 4 and 6, node 5 and 6, node 7 and 6, node 8 and 6 for driving end whereas, between node 14 and 16, node 15 and 16, node 17 and 16, node 18 and 16 for non-driving end) and heat transfer from surface to ambient (between

node 1 and 2, node 1 and 12). Conduction heat transfer occurs through the solid metallic parts of the machine e.g., heat transfer between stator core and teeth (between node 3 and 5, node 13 and 15), rotor core and teeth (between node 8 and 9, node 18 and 19) or rotor core and shaft (between node 9 and 10, node 19 and 20) etc.

6.3.1 Thermal resistance

6.3.1.1 Thermal resistance for conduction

For conduction heat transfer, thermal resistance can be formulated as:

$$R_{cond} = \frac{1}{k} \times \frac{Length\ of\ heat\ flow\ path}{Area\ of\ heat\ transfer} \tag{6.1}$$

Where, R_{cond} = Thermal resistance

k = Thermal conductivity of the material

6.3.1.2 Thermal resistance for convection

Whereas, for convection heat transfer, thermal resistance can be formulated as:

$$R_{conv} = \frac{1}{h \cdot A_c} \tag{6.2}$$

Where, h = Convection heat transfer co-efficient that depends upon the nature of air flow and temperature of the surface.

A_c = Area of convective heat transfer.

$h \approx 5 - 25\ W/m^2$℃ for the free convection in air and.

$h \approx 10 - 500\ W/m^2$℃ for the forced convection in air.

At the air gap the stator and rotor act as two concentric cylinders rotating relative to each other. Therefore, for heat transfer through air-gap, the film

coefficient, h, need to be considered and it can be defined in terms of a dimension less Nusselt number, N_u, the air gap length l_g and the thermal conductivity of air K_{air} as the following equation:

$$h = N_u \times \frac{K_{air}}{l_g} \tag{6.3}$$

Taylor gives the value of the Nusselt number for the convective heat transfer between two smooth cylinders rotating with respect to one another. In an actual machine, however, there will be greater heat transfer across the air gap than that is obtained for the smooth cylindrical surfaces, because of the additional fluid disturbances caused by the teeth and the slots. The Nusselt number (N_u) for the small air-gap machines are obtained from the modified expressions as suggested by Taylor, can be expressed as:

$$N_u = 2.2 \; for \; N_{Ta} < 41$$

$$N_u = 0.23(N_{Ta})^{0.63}(N_{Pr})^{0.27} \; for \; 41 \leq N_{Ta} \leq 100 \tag{6.4}$$

The dimensionless Taylor number N_{Ta} and Prandtl number N_{Pr} are defined in terms of the air gap dimensions and fluid constants. The fluid constant values, which are temperature dependent, are taken at the expected full-load air gap temperature. The critical value 41 of the Taylor number refers to a change from laminar flow, which usually occurs in a small air-gap machine, to the turbulent flow in large air-gap machine. When the machine is stationary, the heat flow is assumed to be by conduction only, which represents a Nusselt number of 2.0.

6.3.1.3 Thermal contact resistance

As different parts of the machine are built with different materials, therefore, when heat get transfer form one part of the machine to another, there should be a thermal contact resistance in between two adjacent parts, which can be formulated as:

$$R_{tc} = 1/(h_{tc}.A) \tag{6.5}$$

Where, R_{tc} = Thermal contact resistance

A = Area of contact

h_{tc} = Contact coefficient

The thermal contact resistance is important to take into account. This resistance is offered to the heat flow at the interface between the two parts of the machine, such as, outer diameter of the stator stamping and the frame. As expected, the metallic contact-resistance depends on the metals involved, the surface roughness, the contact pressure, the material occupying the void spaces and the temperature difference. The value of h_{tc} may be taken as $10^3\ W/m^2°C$ [92] in the present case.

6.3.2 Thermal capacitance

On the other hand, thermal capacitance (C_{th}) of a node completely depends upon the property as well as dimension of the material and can be represented as:

$$C_{th} = \rho \cdot C_p.V \tag{6.6}$$

Where, ρ = Density of the material

V = Volume of the material

C_p = Specific heat capacity of the material

Each node in the thermal network, is associated with a heat source, which basically indicate different losses of the machine. For example, node 4 and node 14 represents the stator slot of the machine at driving and non-driving end respectively. Therefore, stator copper loss is the heat source which is associated with these two nodes. Similarly, core loss is associated with node 3, 5, 13 and 15 (stator core and teeth at driving and non-driving end). On the other hand, nodes with no such source of losses, e.g., rotor core, frame, end shield etc., no heat source is associated.

6.3.3 Updating parameters and losses

From the expression for thermal resistance and capacitance, it is evident that thermal resistance and thermal capacitance values depend upon the motor dimension. It is not possible to measure the exact motor dimensions without completely dismantling it. Hence, the dimensions of the machine are considered as that of standard NEMA design of induction motor of similar rating for calculation of thermal resistance and capacitance. The estimated loss data was fed into the developed thermal model to predict the temperature rise at different parts of the machine. However, with change in temperature, winding resistance changes, which alters the losses. This phenomenon was incorporated in the thermal model by updating the winding resistance and loss values with temperature, after specific interval of time. The following relationship was used to describe the temperature dependance of the stator and rotor resistance:

$$R_s{}^{+} = R_s \times \frac{(T_s{}^{+} - T_{0i_{cu}})}{(T_s - T_{0i_{cu}})} \tag{6.7}$$

$$R_r{}'^{+} = R_r{}' \times \frac{(T_r{}^{+} - T_{0i_{al}})}{(T_r - T_{0i_{al}})} \tag{6.8}$$

Where,

$R_s{}^+ = updated\ stator\ resistance$

$R_s = previous\ stator\ resistance$

$R_r{}'^+ = updated\ rotor\ resistance$

$R_r{}' = previous\ rotor\ resistance$

$T_s{}^+ = updated\ temperature\ of\ stator\ winding$

$T_s = previous\ temperature\ of\ stator\ winding$

$T_r{}^+ = updated\ temperature\ of\ rotor\ winding/bar$

$T_r = previous\ temperature\ of\ rotor\ winding$

$T_{0i_{cu}} = inferred\ absolute\ zero\ temperature\ of\ copper\ (-234.5℃)$

$T_{0i_{al}} = inferred\ absolute\ zero\ temperature\ of\ alluminium\ (-236℃)$

Alteration in winding resistance can in turn change the current and hence the losses. Therefore, updated loss can be formulated as:

$$P_{cu_s}{}^+ = (I_s{}^+)^2 \times R_s{}^+ \tag{6.9}$$

$$P_{cu_r}{}^+ = (I_r{}'^+)^2 \times R_r{}'^+ \tag{6.10}$$

These updated losses were fed into the thermal model to improve the temperature estimation. In this manner, a closed loop temperature estimation system was developed. Fig. 6.3 depicts the schematic diagram of the proposed temperature estimation scheme.

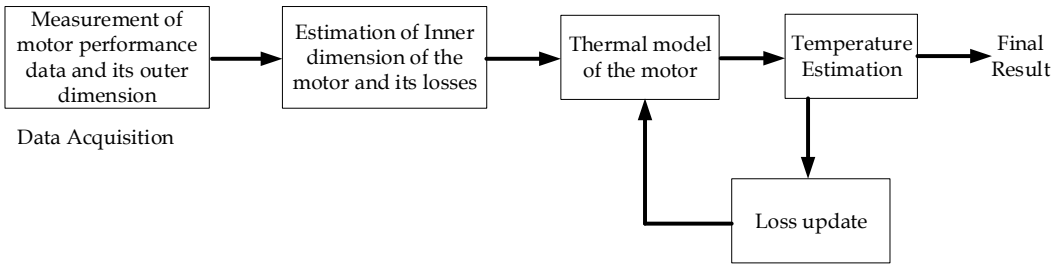

Fig. 6.3. Schematic representation of the proposed temperature estimation scheme.

6.4 Experimental setup and procedures

The experimentation was conducted on a 415 V, 0.75 kW, 50 Hz, three-phase, squirrel cage, totally enclosed fan-cooled (TEFC) induction motor, identical to the one described in Chapter 4. In the preceding chapter, the motor's parameters and losses were precisely estimated and validated. In this context, these established parameters and losses were integrated into the proposed thermal model to predict the temperature distribution across various components of the induction motor, considering equations (6.1) – (6.8). The computed temperatures were then compared against the actual measurements to validate the proposed methodology.

To acquire the temperature data, the motor was allowed to operate continuously with constant load for two hours, to achieve thermal equilibrium. Subsequently, the motor underwent a three-hour cooldown period without any active cooling. This procedure was repeated for six distinct load conditions. Throughout the experimental duration, infrared thermometer was employed to record frame temperatures at both the driving and non-driving ends of the motor at five-minute intervals. Simultaneously, shaft and end shield temperatures were monitored at the driving end only, using the same method, as the non-driving end was equipped with a fan and fan cover.

Stator winding temperatures were recorded at five-minute intervals during the cooling phase only, using a Kelvin double bridge. Measuring winding temperature during the operational phase was unfeasible due to the inability to connect the Kelvin double bridge while the motor was running. The comparison between the measured and estimated temperatures, illustrated in Fig 6.5 – 6.7, establishes the accuracy of the proposed temperature estimation technique. For all other internal parts of the machine, the estimated temperature profiles show the expected characteristics, which is presented in Fig 6.8 – 6.14.

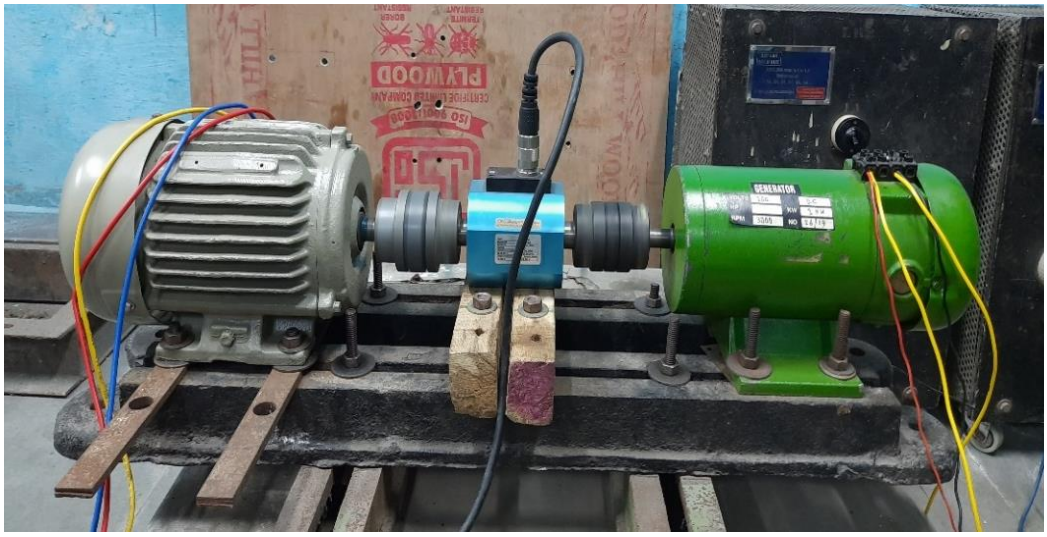

Fig. 6.4. Induction motor under experiment, coupled with DC generator through a torque transducer.

6.5 Results and Analysis

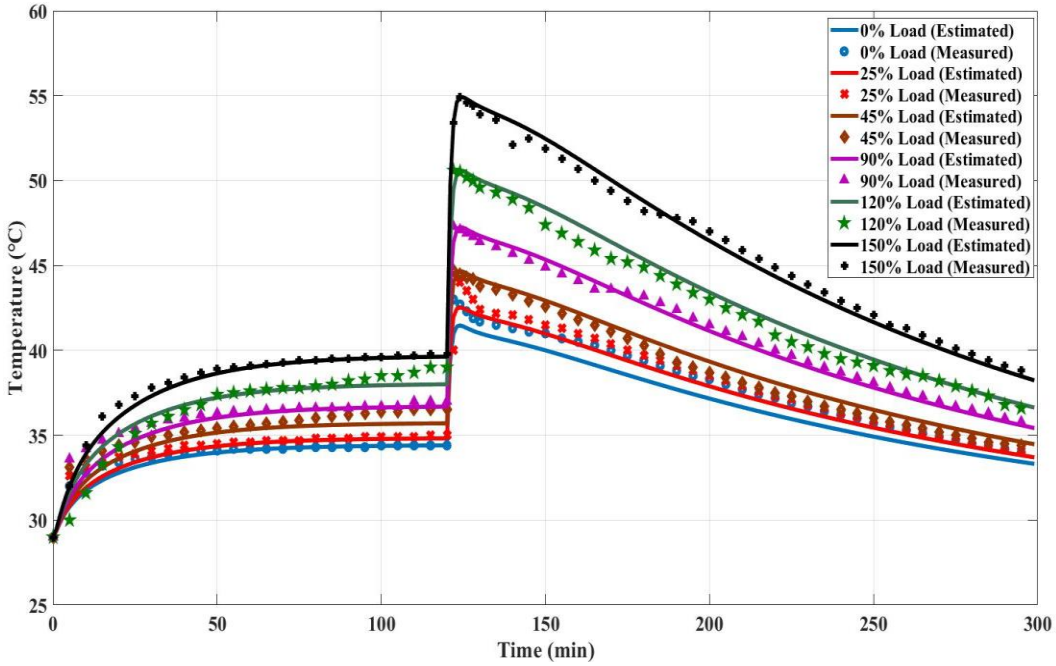

(a)

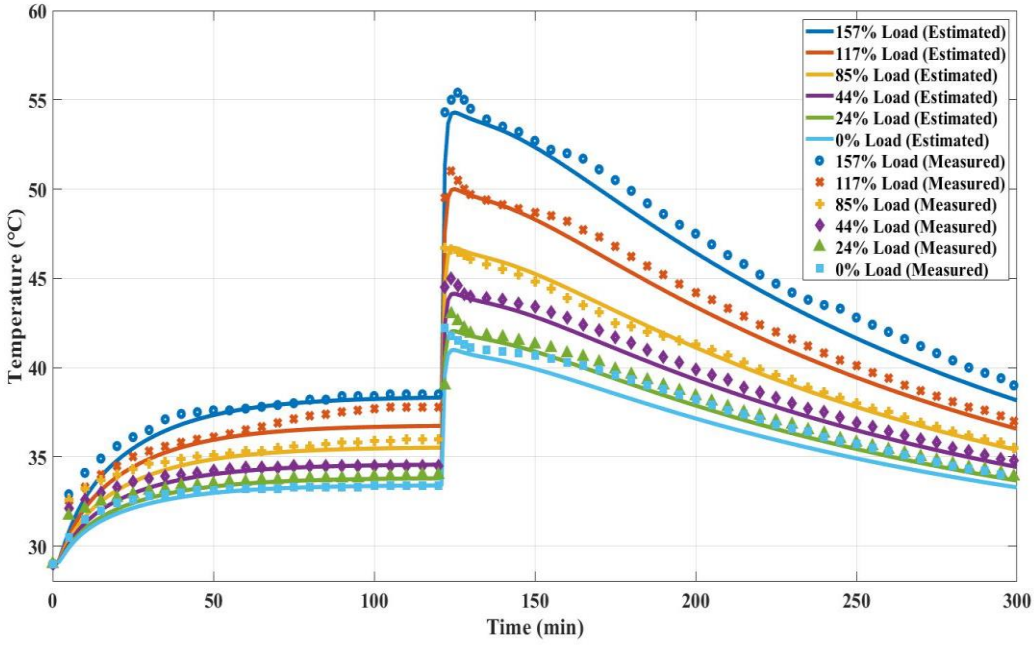

(b)

Fig. 6.5. Comparison of estimated and measured frame temperatures at (a) driving end, (b) non-driving end.

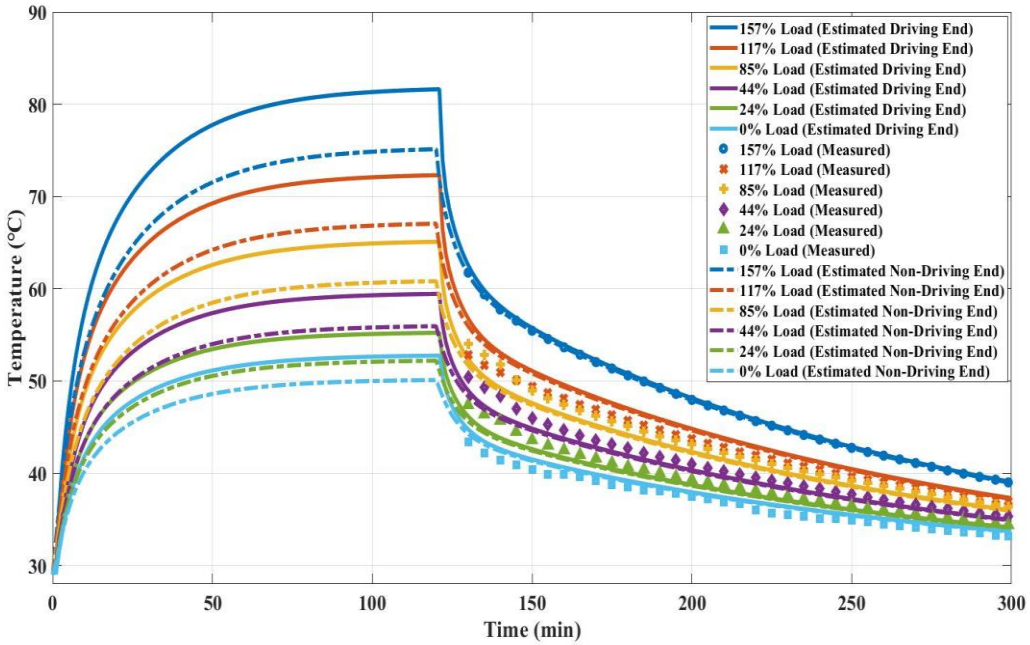

(a)

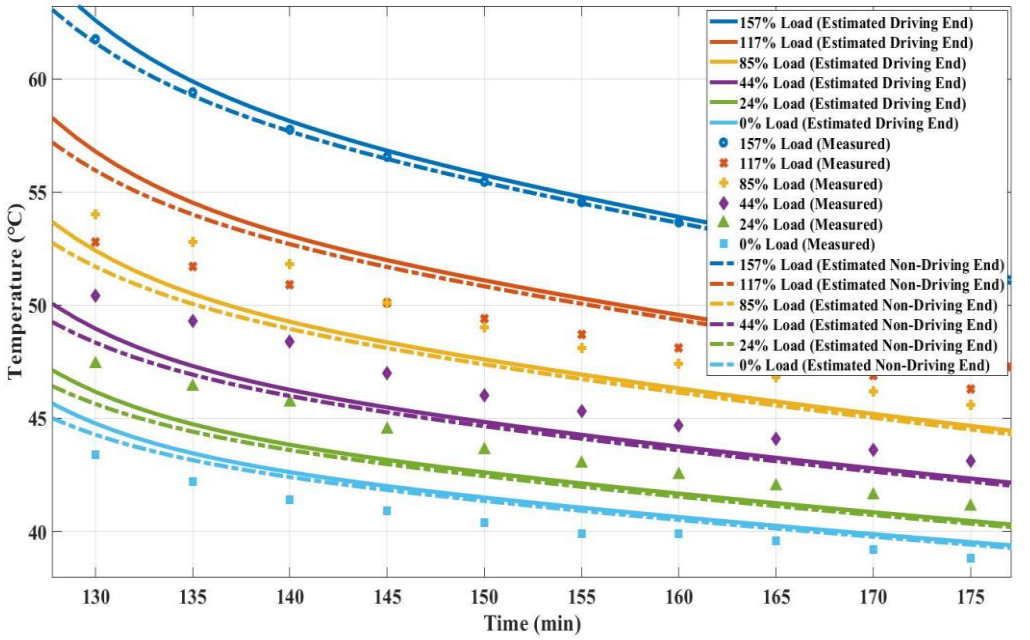

(b)

Fig. 6.6. (a) Estimated stator winding temperature at driving and non-driving end and comparison with measured values, (b) Zoomed in view of stator winding temperature profile during cooling period.

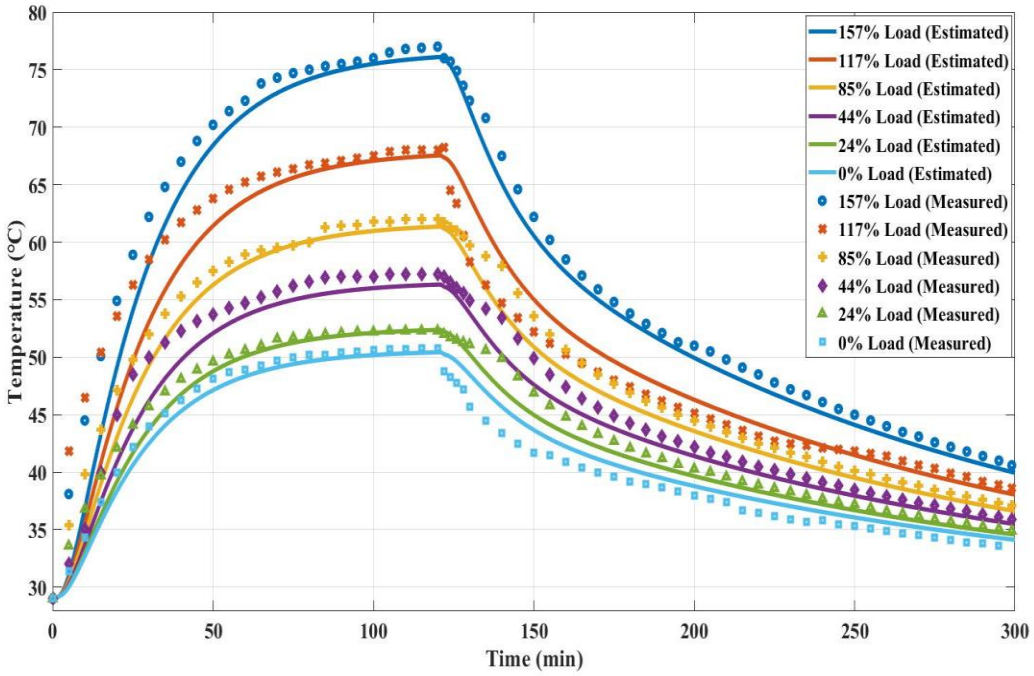

(a)

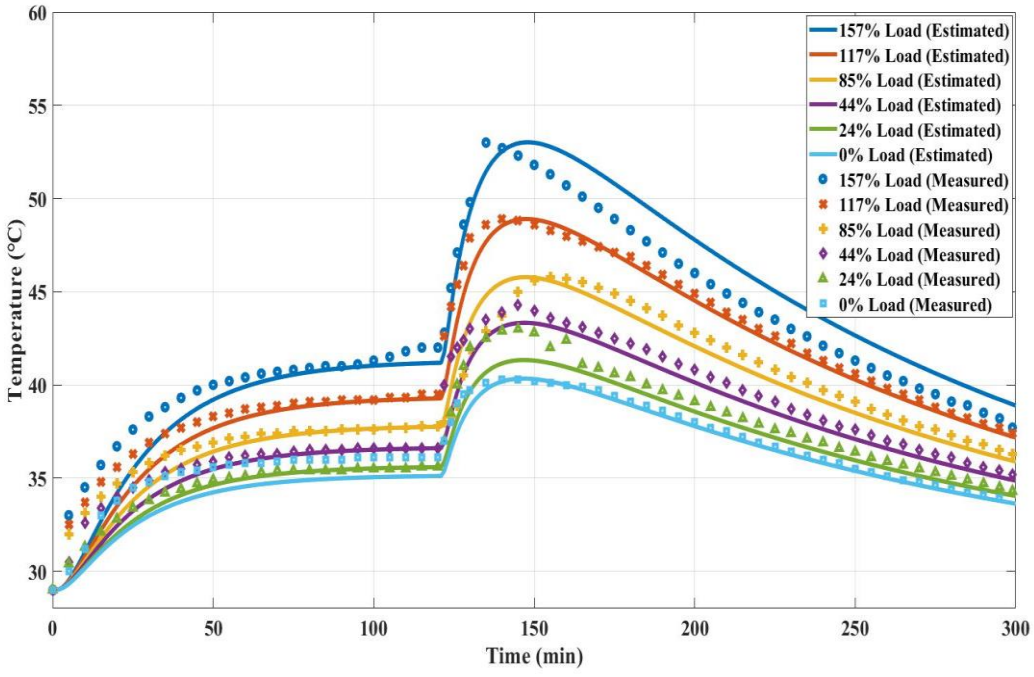

(b)

Fig. 6.7. Comparison of estimated and measured (a) Shaft temperature at driving end, (b) End shield temperature at driving end.

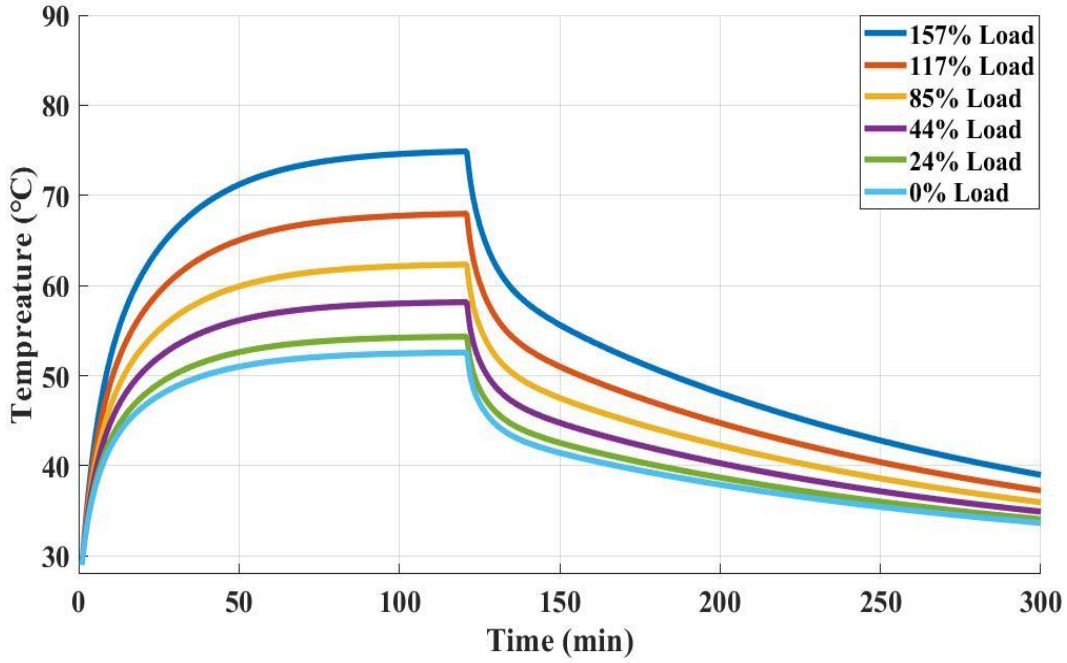

(a)

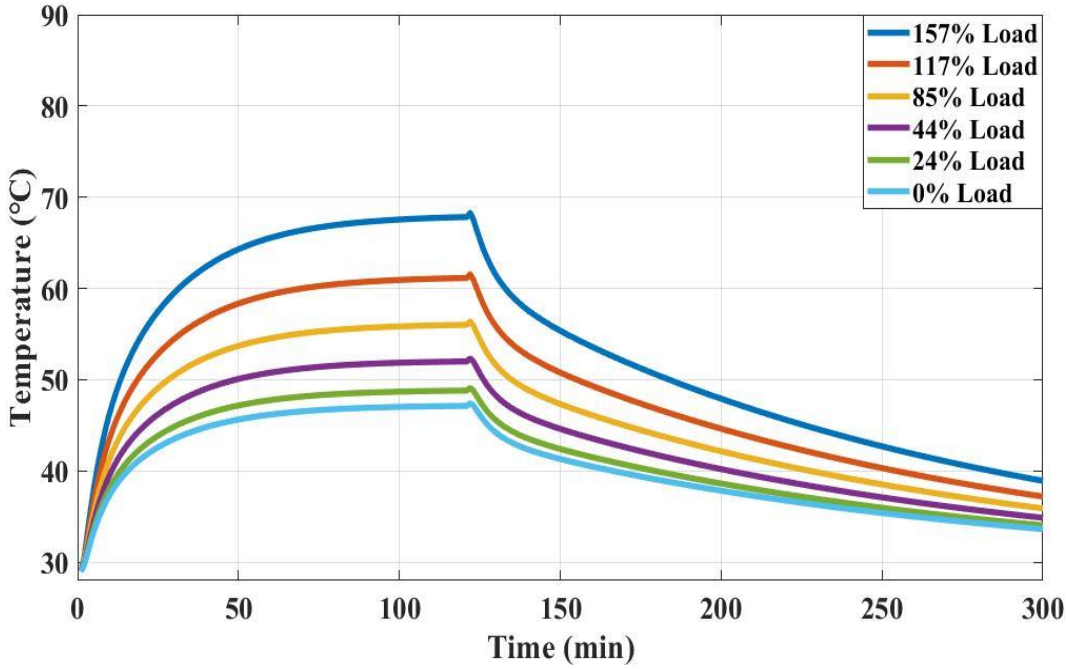

(b)

Fig. 6.8. Estimated stator core temperatures at (a) driving end, (b) non-driving end.

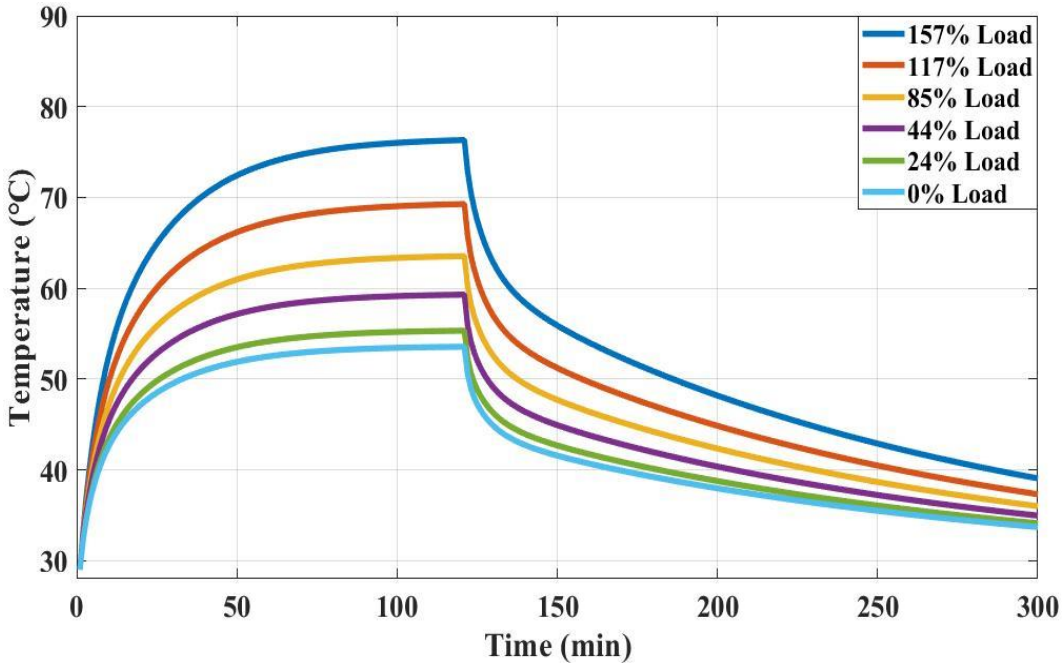

(a)

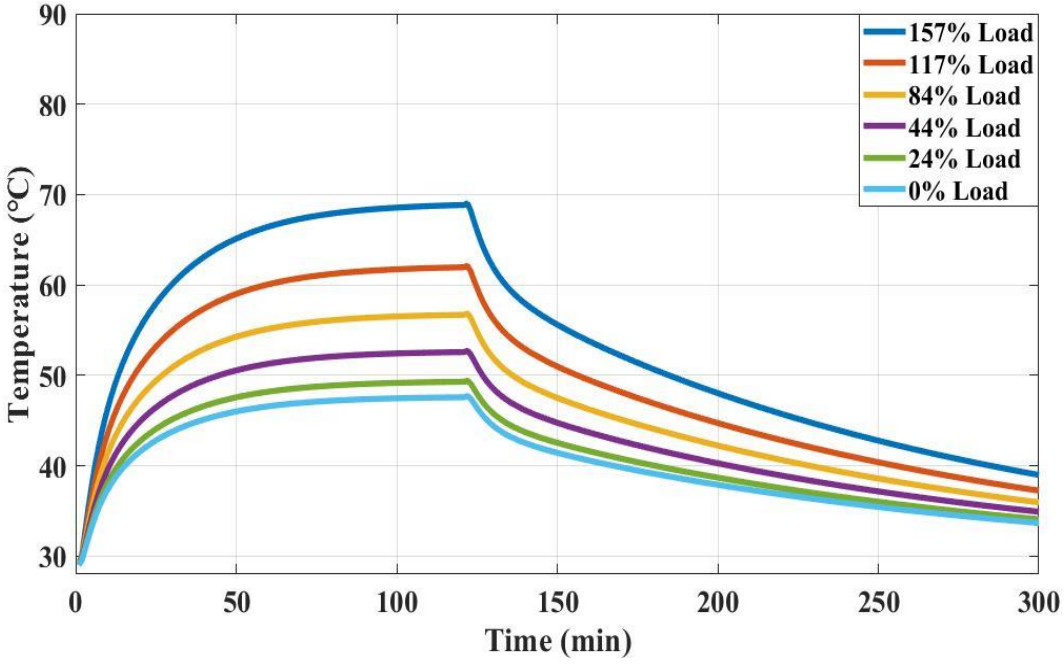

(b)

Fig. 6.9. Estimated stator teeth temperatures at (a) driving end, (b) non-driving end.

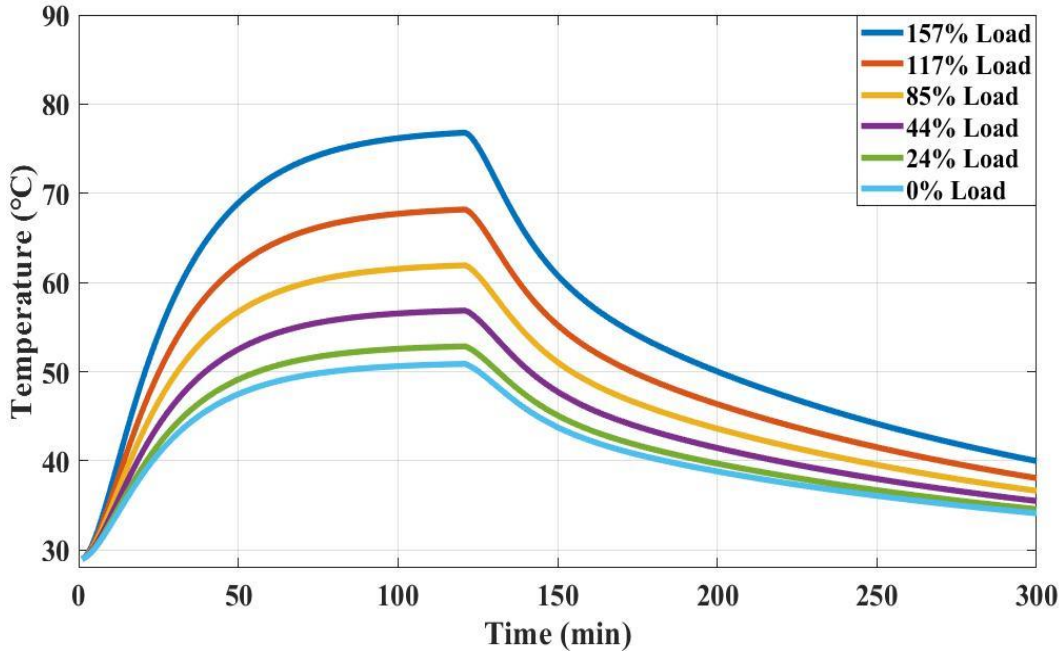

(a)

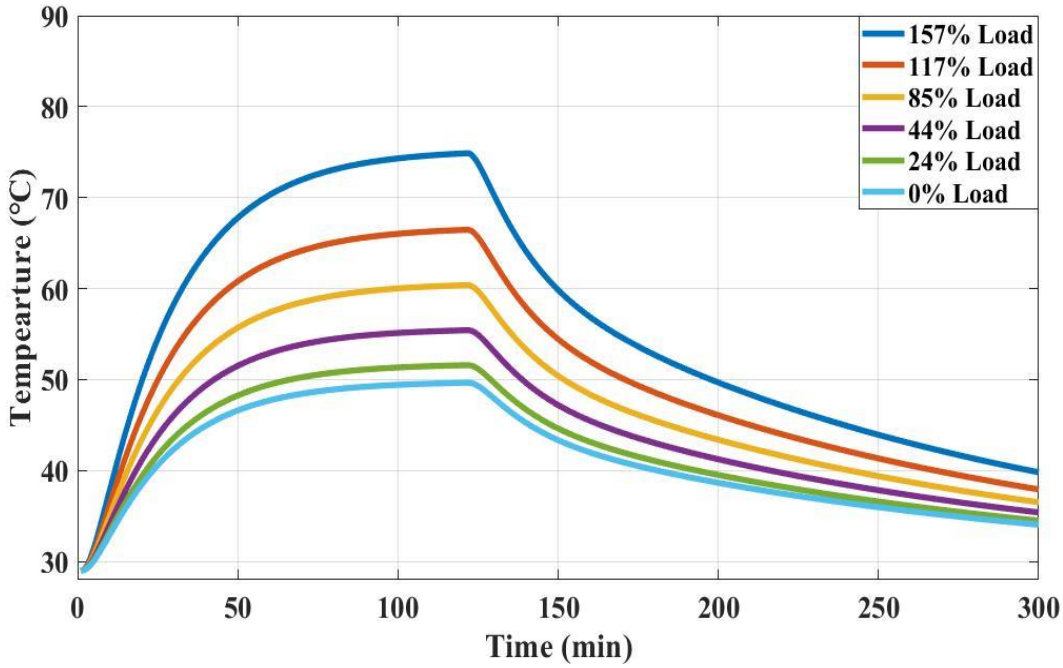

(b)

Fig. 6.10. Estimated rotor teeth temperatures at (a) driving end, (b) non-driving end.

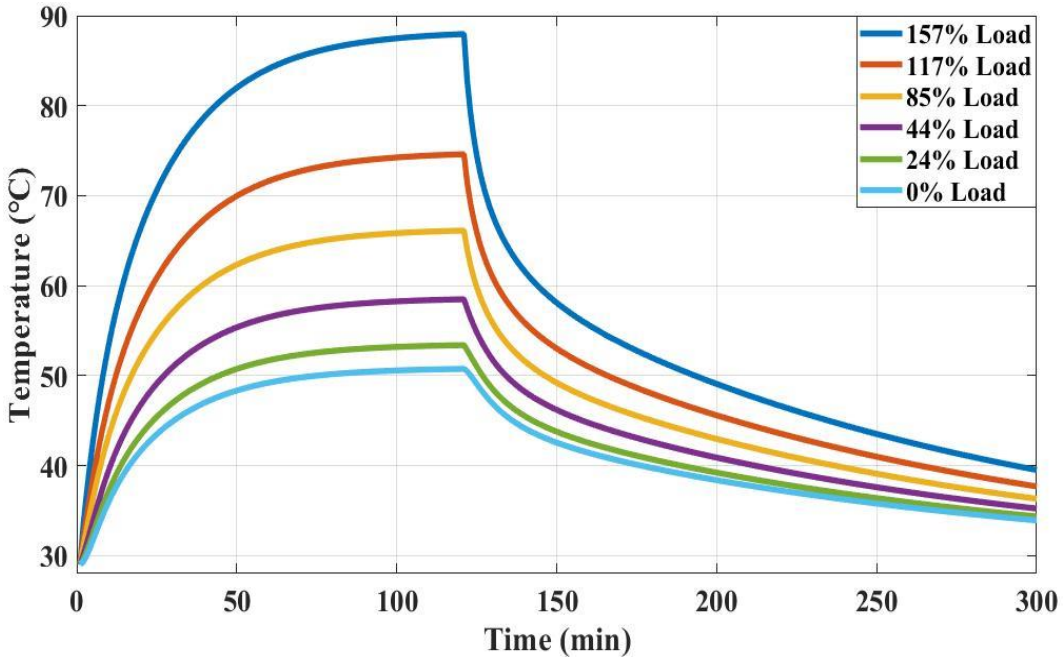

(a)

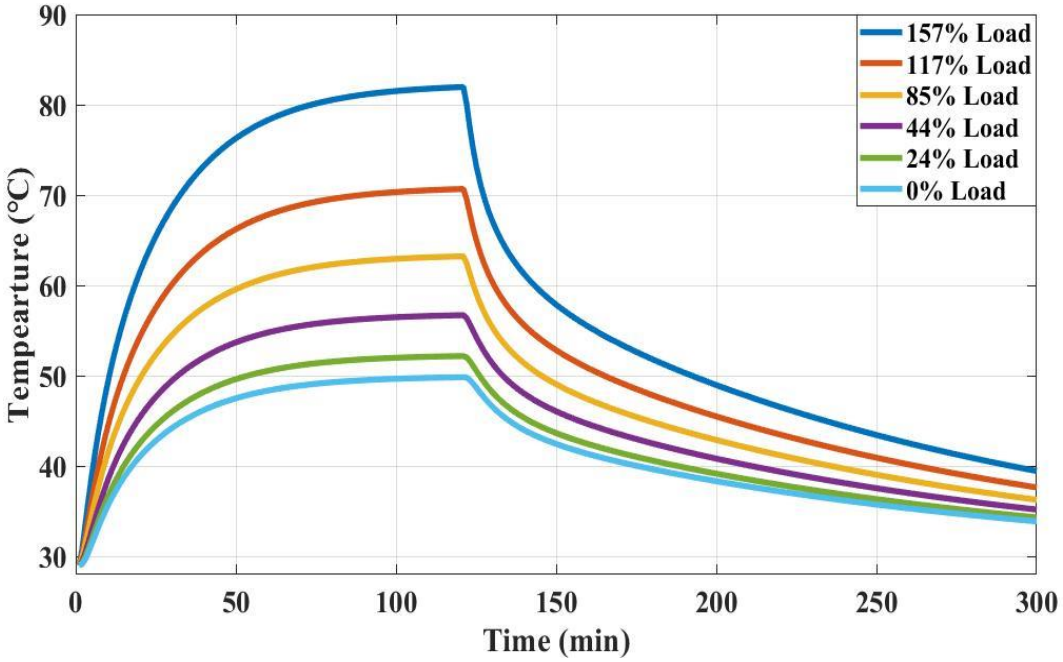

(b)

Fig. 6.11. Estimated rotor slot temperatures at (a) driving end, (b) non-driving end.

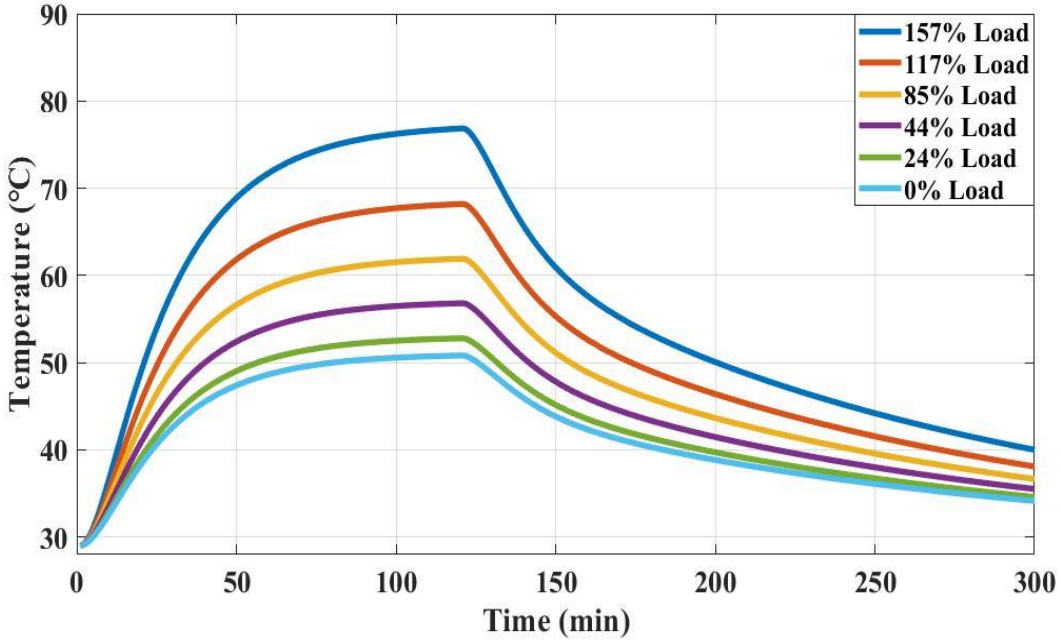

(a)

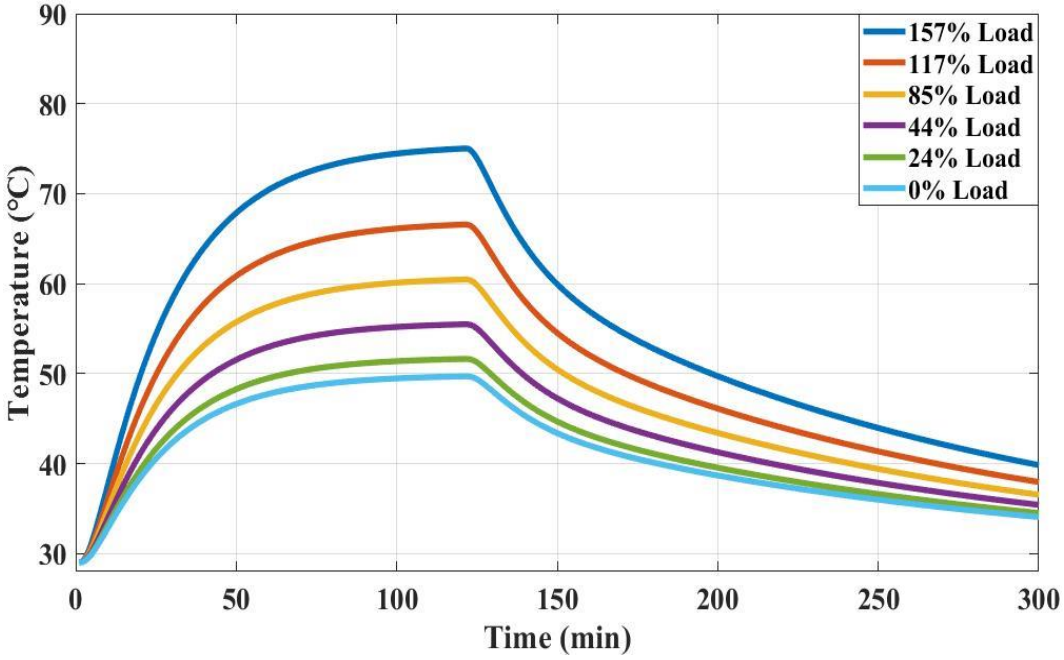

(b)

Fig. 6.12. Estimated rotor core temperatures at (a) driving end, (b) non-driving end.

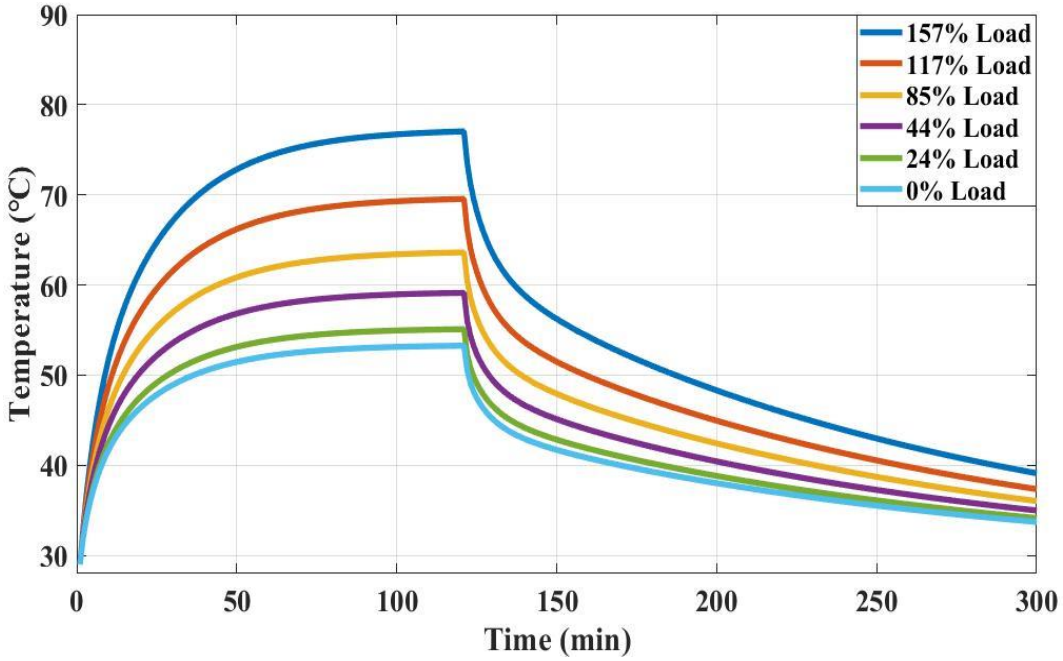

(a)

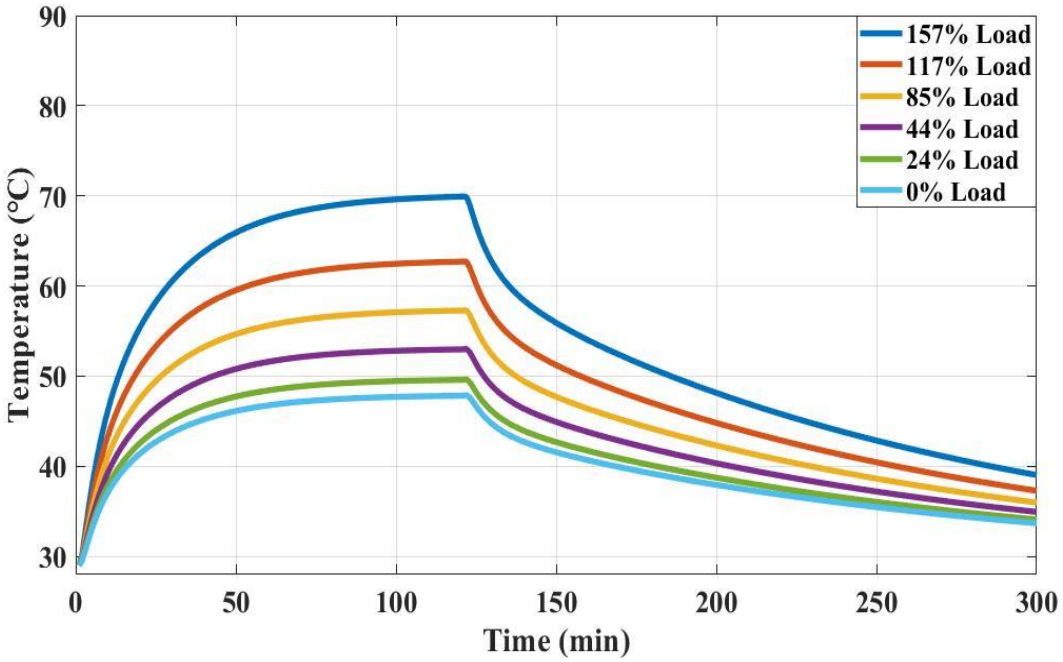

(b)

Fig. 6.13. Estimated airgap temperatures at (a) driving end, (b) non-driving end.

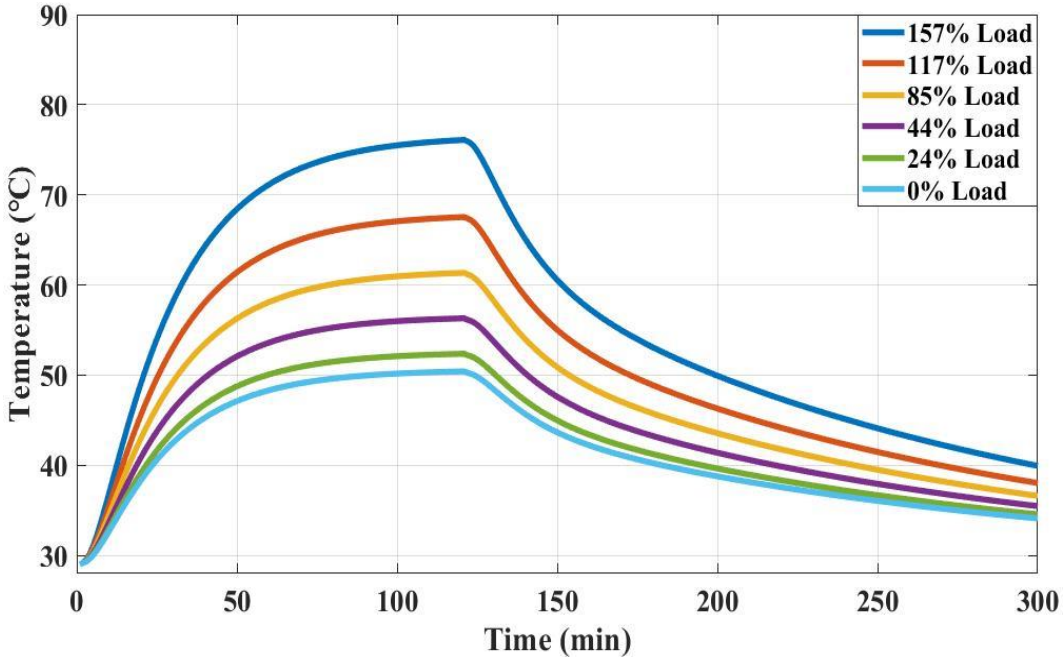

(a)

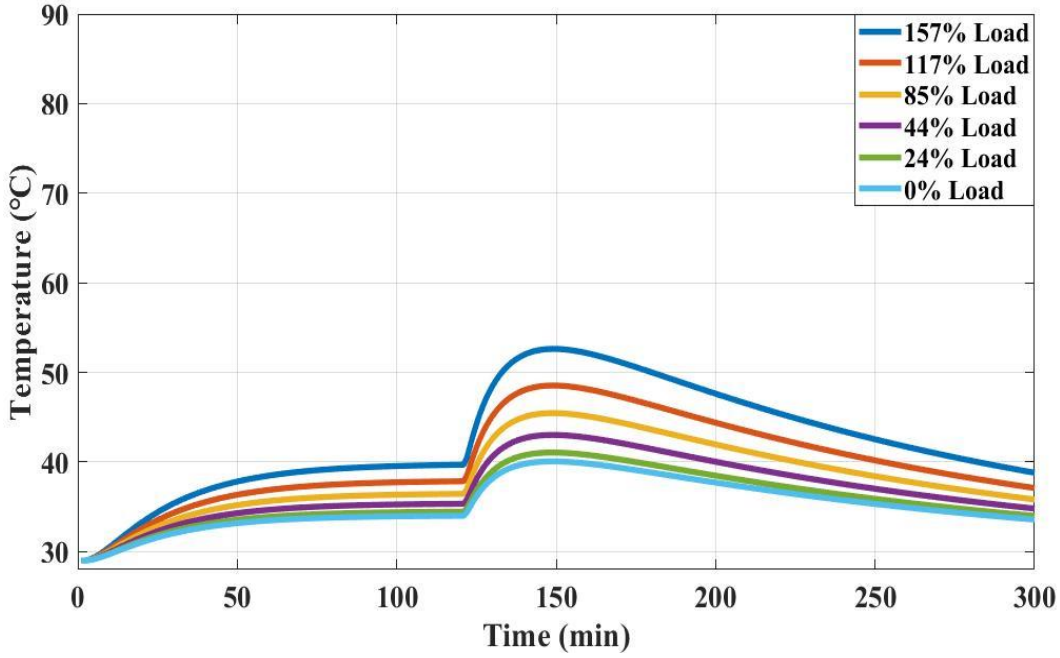

(b)

Fig. 6.14. Estimated (a) shaft temperatures and (b) end-shield temperature at non-driving end.

Fig 6.15 compares the steady state temperature of all nodes at (a) driving and (b) non-driving end. This comparison depicts that the estimated temperature distribution characteristics exhibits the expected nature.

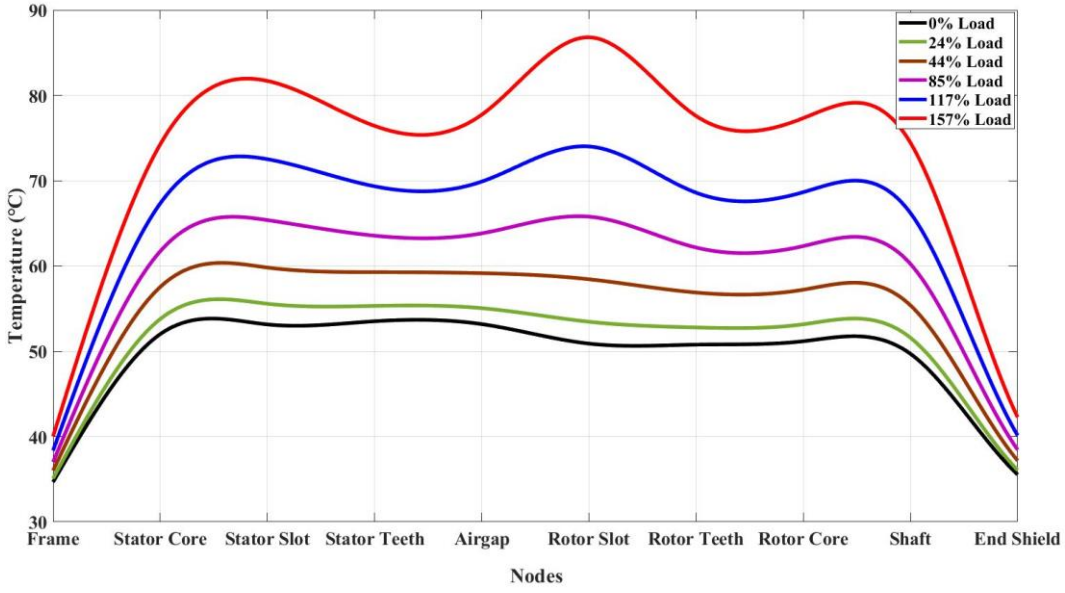

(a)

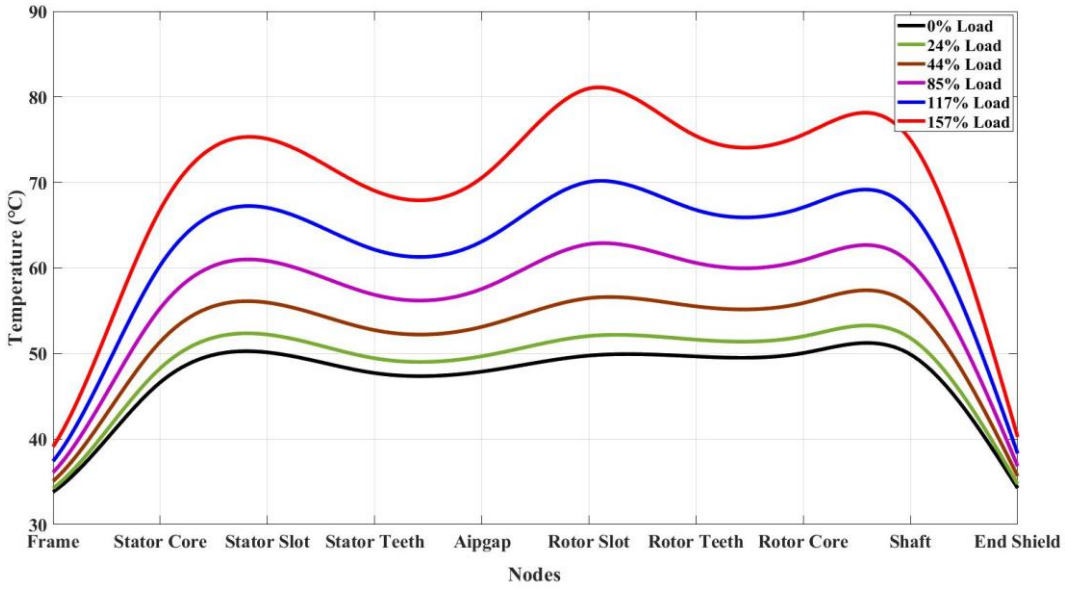

(b)

Fig. 6.15. Estimated temperature distribution characteristics throughout the induction motor at (a) driving end and (b) non-driving end.

6.6 Conclusion

A novel technique has been proposed which is capable of precisely predicting the temperature profile with time at different parts of induction motor under variable load condition, as well as, the temperature distribution throughout the machine. The advantages and the future scope of the proposed technique is discussed hereafter.

The proposed scheme can estimate the temperature of different parts of the induction motor from estimated equivalent circuit parameters and losses, where the parameters and losses were estimated from voltage and current measurement. Hence, the proposed scheme can practically predict motor temperature from voltage and current measurement. The comparison of estimated temperature with the corresponding measured value concludes that, the proposed scheme is effective in this regard. In the area of continuous health monitoring of induction motor, this scheme may provide a temperature-based condition monitoring of induction motor.

The dimensions of the machine were considered as that of standard NEMA design of induction motor of similar rating for calculation of thermal resistance and capacitance. Therefore, sometimes the estimation results may suffer from accuracy issue if the actual design considerations are other than the standard one. Therefore, only accurate prediction of motor dimensions can lead to precise determination of thermal resistances and capacitances which in turn, can carry out accurate thermal analysis of the machine and estimate temperature at different parts of the motor.

CHAPTER 7

Development of a Temperature Estimation Scheme for Induction Motor from Estimated Parameters and Losses - An Extension

A thermal model for predicting temperature of different parts of the induction utilizing estimated motor parameters and losses has been developed. The developed thermal model relies on the dimensional data of the motor, which is neighter readily available, nor provided by the manufacturer.

This chapter specifically explores the critical domain of estimating inner dimensions of an induction motor. The principal objective is to develop an innovative temperature estimation scheme that integrates estimated parameters and losses with the predicted inner motor dimensions, directing to provide an inclusive temperature based condition monitoring technique.

7.1 Introduction

Thermal model of an induction motor is an equivalent circuit which represents the temperature distribution and provides the heat flow analysis throughout the motor. As discussed in chapter 6, a thermal model comprises of mainly three components. I) thermal resistance, II) thermal capacitance and III) heat source. Thermal resistance represents the heat transfer capacity between two adjacent parts of the machine, whereas, thermal capacitance represents the heat retention capacity of a particular part. Under running condition, different losses that occur at different parts of the machine, generate heat and rise the motor temperature. The heat sources in a thermal model signify different motor losses and represent the sources of heat in the machine. In this work, the main objective is to develop an accurate thermal model for TEFC (Totally Enclosed Fan Cooled) induction motor which can predict the machine temperature accurately and serves as the key component of a temperature based predictive condition monitoring scheme for TEFC induction motor.

The accuracy of a thermal model depends upon the accurate calculation of thermal resistances, thermal capacitances and motor losses. Now, thermal resistance and capacitance of any part of the machine, depends upon the properties of the material, geometry and dimension of that motor parts. This has already been discussed in detail in previous chapter section 6.3. Therefore, to develop an accurate thermal model, precise knowledge of motor dimension is required. However, the detailed dimensional data of motor is not readily available. Motor dimensions can be obtained by taking physical measurement. However, measuring the inner dimension of the machine (e.g., slot dimension, teeth dimension, core dimension etc.) are very difficult without completely removing the windings from slot. After

complete winding removal and recording of the necessary data, the machine needs to be rewound. Now, rewinding mostly alter the motor properties which is not acceptable. Hence in this work, for precise determination of thermal resistances and capacitances, an estimation scheme, to predict motor inner dimensions from motor performance data and motor size, has been established. This predicted motor dimensions, along with the estimated losses, when fed into the thermal model, provides temperature at different parts of the machine.

7.2 Objective of the work

The primary objective of this work is to extend the previously established temperature estimation scheme by integrating it with the newly proposed inner dimension estimation technique for induction motors. To accurately predict the temperature distribution across different components of the induction motor, which can estimate the temperature of different parts of the machine, evaluating thermal resistances and capacitances for each node within the motor, is necessary.

The challenge lies in the assessment of thermal resistances and capacitances, as it is dependent upon the motor's dimensions, which are often unavailable or difficult to measure. Therefore, an estimation scheme becomes essential to predict the inner dimensions of the motor. This estimation scheme is designed to rely on the motor's performance characteristics and frame size.

This proposed extended scheme compares the estimated motor performance indicators with corresponding measured values obtained using machine design equations. From this comparison, the proposed technique identifies the design parameters that align optimally with the actual performance of the motor.

7.3 Estimation of motor inner dimensions from motor outer dimension and performance data

Motor performance is highly dependent on motor design and its dimensional data. However, in this competitive market, manufacturers go for the compact design of the machine in order to reduce material cost of the machine. Accommodation of higher performance in standard frame size requires a lot of research on machine design which involves financial and intellectual properties. Therefore, internal design data of induction motor is not available in any public domain. As the dimensional data is not publicly available information, it is difficult to get them for an existing motor. However, induction motor dimensional data are essential for developing the thermal model. Therefore, it is difficult to develop the proposed thermal model on an existing motor.

The only option remains to get an overview about the inner dimensions of an existing motor is to develop some mathematical equations, from which, the inner dimension of a three-phase induction motor can be predicted based on its performance and frame size. In this work, a set of mathematical equations has been established, using which, motor inner dimensions can be predicted without completely dismantling the machine.

Motor data available from nameplate:

V_{line} = Line voltage,

P_{out} = Output power of the machine,

eff = Motor efficiency,

pf = Motor power factor

Motor data available from physical measurement:

D = Stator bore diameter,

L = Length of the stator,

D_{out} = Outer diameter of stator,

D_r = Outer diameter of rotor,

D_{sh} = Shaft diameter,

S_s = No. of stator slot = No. of stator teeth,

S_r = No. of rotor slot = No. of rotor teeth,

L_b = Length of rotor bar,

D_{er} = Diameter of end ring,

W_{er} = Width of end ring,

Motor dimension to be estimated:

w_{st} = Width of stator teeth,

w_{sst} = Width of stator slot at top,

w_{ssb} = Width of stator slot at bottom,

d_{st} = Depth of stator teeth,

d_{sc} = Depth of stator core,

w_{rtt} = Width of rotor teeth at top,

w_{rtb} = Width of rotor teeth at bottom,

w_{rs} = Width of rotor slot,

d_{rt} = Depth of rotor teeth,

d_{rc} = Depth of rotor core,

Motor loss components to be estimated:

P_{iron} = Iron loss = $P_{iron_{sc}} + P_{iron_{st}}$, where, $P_{iron_{sc}}$& $P_{iron_{st}}$are the iron losses in stator core and teeth

P_{fw} = Friction and windage loss of the machine,

$P_{cu_{stat}}$ = Stator copper loss of the machine,

$P_{cu_{rot}}$ = Rotor copper loss of the machine,

Variables to be optimized for the estimation:

B_{av} =Average flux density,

$Stator\ current\ density$ = Current density in stator conductors,

B_{st} =Flux density at stator teeth,

B_{sc} =Flux density in stator core,

$specific\ iron\ loss_{st}$ = Specific iron loss at stator teeth,

$specific\ iron\ loss_{sc}$ = Specific iron loss at stator core,

$Rotor\ current\ density$ = Current density in rotor bars,

B_{rtt} =Flux density at rotor teeth at top,

B_{rtb} =Flux density at rotor teeth at bottom,

B_{rc} =Flux density in rotor core,

These motor variables need to be specified within a specific search space for estimation of the inner dimension of the motor. The optimization algorithm (Particle Swarm Optimization) will find a suitable set of these variables within the predefined boundary condition for which, the estimated motor

performance matches the actual performance. Under these circumstances, the estimated dimensions, losses and motor variables can be considered as the actual corresponding values of the machine. The design equations considered for the induction motor are given below.

Design equations of induction motor:

$$\text{Flux per pole:} \quad \emptyset_m = B_{av} \cdot \tau \cdot L \tag{7.1}$$

where, B_{av} = average flux density τ = pole pitch and L = length of the machine.

$$\text{Pole pitch:} \quad \tau = \frac{\pi D}{P} \tag{7.2}$$

where, D = Bore diameter and P = No. of poles. L and D in (6.1) and (6.2) can be obtained by physical measurement after opening the machine.

$$\text{Phase voltage:} \quad E_{ph} = V_{line}/\sqrt{3} \tag{7.3}$$

$$\text{Phase current:} \quad I_{ph} = (P_{out}/eff)/(\sqrt{3} \times V_{line} \times pf) \tag{7.4}$$

where, V_{line} = Line voltage, P_{out} = Output power of the machine, eff = Motor efficiency, pf = motor power factor which can be obtained from the nameplate of the machine.

$$\text{Total no. of stator turns:} \quad T_s = E_{ph}/(4.44 \times \emptyset_m \times f \times K_{ws}) \tag{7.5}$$

$$\text{Conductor per slot:} \quad Z_s = (2 \times 3 \times T_s)/S_s \tag{7.6}$$

where, S_s = Total number of stator slot which can be obtained by physical measurement after opening the end shield of the machine.

Now, area of each conductor:

$$a_{cond} = (I_{ph}/Stator\ current\ density) \tag{7.7}$$

Therefore, total conductor area:

$$A_{cond} = (a_{cond} \times Z_s) \tag{7.8}$$

Therefore, width of each stator teeth

$$w_{st} = (\emptyset_m/(B_{st} \times (S_s/P) \times L_i) \tag{7.9}$$

Where, $B_{st} = flux\ density\ at\ stator\ teeth$ and $L_i = net\ iron\ length$, generally considered as $0.9 \times L$

Now, area of stator core

$$A_{sc} = \left(\frac{\emptyset_m}{2}\right)/(B_{sc}) \tag{7.10}$$

Where, B_{sc} = flux density in stator core

Depth of stator core

$$d_{sc} = A_{sc}/L_i \tag{7.11}$$

Depth of stator teeth

$$d_{st} = \frac{(D_{out}-D)}{2} - d_{sc} \tag{7.12}$$

Where, D_{out} = Outer diameter of the stator and D = Bore diameter

Width of stator slot at top

$$w_{sst} = \pi \times \frac{(D+0.004\times2)}{S_s} - w_{st} \tag{7.13}$$

And, width of stator slot at bottom

$$w_{ssb} = \pi \times \frac{(D+d_{st}\times2)}{S_s} - w_{st} \tag{7.14}$$

Length of mean turn $L_{mt} = 2L + 2.3 \times \frac{\pi D}{P} + 0.24$ (7.15)

Resistance of stator winding $R_s = \rho_{cu} \times \frac{L_{mt} \times T_s}{A_{cond}}$ (7.16)

Where, ρ_{cu} = Resistivity of stator winding (copper).

Stator copper loss $P_{cu_s} = 3 \times {I_{ph}}^2 \times R_s$ (7.17)

Rotor bar current $I_b = \frac{2 \times ph \times T_s \times I_{ph} \times K_{ws}}{S_r} \times pf$ (7.18)

Area of rotor bar $A_b = \frac{I_b}{Rotor\ current\ density}$ (7.19)

Depth of rotor core $d_{rc} = \frac{\emptyset_m/2}{B_{rc} \times L_i}$ (7.20)

Where, B_{rc} = flux density at rotor core

Depth of rotor teeth $d_{rt} = (D_r - 2d_{rc} - D_{sh})/2$ (7.21)

Where, D_{sh} = Shaft diameter which is a measurable quantity

Depth of rotor slot (d_{rs}) = Depth of rotor teeth (d_{rt}) (7.22)

Depth of rotor bar $d_{rb} = d_{rs} - (2 \times 0.00015 + 0.002)$ (7.23)

Width of rotor bar $w_{rb} = A_b/d_{rb}$ (7.24)

Width of rotor slot $w_{rs} = w_{rb} + 2 \times 0.00015$ (7.25)

Where, Insulation thickness is considered as $0.00015\ m$ and Depth of lip and wedge is considered as $0.002\ m$.

Width of rotor teeth at bottom

$$w_{rtb} = \emptyset_m/(B_{rtb} \times (S_r/P) \times L_i) \quad (7.26)$$

Where, B_{rtb} = Flux density at the bottom of the rotor teeth

And, width of rotor teeth at top

$$w_{rtt} = w_{rtb} + (2 \times \pi \times d_{rt})/S_r \quad (7.27)$$

Resistance of rotor bar $R_b = \rho_{al} \times L_b/A_b$ (7.28)

Where, ρ_{al} = Resistivity of rotor bar (aluminum) and L_b = Length of rotor bar which can be measured after opening the machine.

Copper loss in rotor bar $P_{cu_b} = S_r \times {I_b}^2 \times R_b$ (7.29)

End ring current $I_{be} = \frac{S_r \times I_b}{\pi \times P}$ (7.30)

Area of end ring $A_{er} = \frac{I_{be}}{Rotor\ current\ density}$ (7.31)

Resistance of end ring $R_{er} = \rho_{al} \times \frac{\pi \times D_{er}}{A_{er}}$ (7.32)

Copper loss in end ring $P_{cu_{er}} = 2 \times {I_{be}}^2 \times R_{be}$ (7.33)

Total rotor copper loss $P_{cu_r} = P_{cu_b} + P_{cu_{er}}$ (7.34)

Weight of stator teeth

$$WT_{st} = L_i \times d_{st} \times w_{st} \times S_s \times \rho_{iron} \quad (7.35)$$

Where, ρ_{iron} = Density of iron.

Iron loss in stator teeth

$$P_{iron_{st}} = WT_{st} \times specific\ iron\ loss_{st} \quad (7.36)$$

Mean diameter of stator core

$$D_{mean} = \frac{D_{out} + (D_{out} - 2 \times d_{sc})}{2} \quad (7.37)$$

Weight of stator core

$$WT_{sc} = \pi \times D_{mean} \times L_i \times d_{sc} \times \rho_{iron} \quad (7.38)$$

Iron loss in stator core

$$P_{iron_{sc}} = WT_{sc} \times specific\ iron\ loss_{sc} \quad (7.39)$$

Total iron loss in stator core and teeth

$$P_{iron} = P_{iron_{sc}} + P_{iron_{st}} \quad (7.40)$$

Friction and windage loss $P_{fw} = \frac{4}{100} \times P_{out}$ (7.41)

Here, as per the rating of the machine, friction and windage loss is considered as 4% of the output power.

Total constant loss $P_{const} = P_{iron} + P_{fw}$ (7.42)

Total motor loss $P_{total} = P_{const} + P_{cu_s} + P_{cu_r}$ (7.43)

Input power $P_{in} = P_{out} + P_{total}$ (7.44)

Efficiency $\eta = \frac{P_{out}}{P_{in}}$ (7.45)

Power factor $\cos\phi = \frac{(P_{in}/3)}{E_{ph} \times I_{ph}}$ (7.46)

From the above-mentioned equations, stator coper loss (P_{cu_s}), rotor coper loss (P_{cu_r}), iron loss (P_{iron}), friction and windage loss (P_{fw}), motor efficiency (η) and motor power factor (pf) have been estimated. The estimated quantities have been compared with the corresponding measured values by particle swarm optimization (PSO) algorithm using the following objective function:

$$0 = \left(\frac{\left(P_{cu_{s_{mes}}} - P_{cu_{s_{est}}}\right)}{P_{cu_{s_{mes}}}}\right)^2 + \left(\frac{\left(P_{cu_{r_{mes}}} - P_{cu_{r_{est}}}\right)}{P_{cu_{r_{mes}}}}\right)^2 + \left(\frac{\left(P_{iron_{mes}} - P_{iron_{est}}\right)}{P_{iron_{mes}}}\right)^2 + \left(\frac{\left(P_{fw_{mes}} - P_{fw_{est}}\right)}{P_{fw_{mes}}}\right)^2 + \left(\frac{(\eta_{mes} - \eta_{est})}{\eta_{mes}}\right)^2 + \left(\frac{(pf_{mes} - pf_{est})}{pf_{mes}}\right)^2 \quad (7.47)$$

PSO minimizes the objective function value to reduce the error between the measured and estimated quantities. Here the minimization of square error technique has been adopted to eliminate negative error problem.

7.4 Experimental setup and procedures

The measurements have been carried out on a 415 V, 1.1 kW, 4 pole, 50 Hz 3 phase induction motor. Fig. 7.1 depicts the induction motors on which the experiment and measurements have been carried out. Table 7.1 and 7.2 represents the nameplate data and dimension of the machine respectively.

Fig. 7.1. Induction motor under experiment, with rotor pulled out.

Table 7.1 Nameplate data of the experimental machine

Nameplate Data	**Values**
Voltage	415±10 V
Current	2.8 A
Output power	1.1 kW / 1.5 HP
Full load speed	1400 RPM
Connection	Y
Full load efficiency	81.4 %
Full load power factor	0.74

Table 7.2 Measured machine dimensions

Motor dimension	**Values (in meter)**
Stator bore diameter (D)	0.08
Length of the stator (L)	0.102
Outer diameter of stator (D_{out})	0.131
Outer diameter of rotor (D_r)	0.0795
Shaft diameter (D_{sh})	0.02405
No. of stator slot = No. of stator teeth (S_s)	24
No. of rotor slot = No. of rotor teeth (S_r)	22
Length of rotor bar (L_b)	0.1027
Mean diameter of end ring (D_{er})	0.0683
Width of end ring (W_{er})	0.016

Using these measurements, the inner dimensions of the induction motor is predicted by solving the mathematical equations discussed in section 6.3, using particle swarm optimization (PSO) algorithm as the optimization tool. The results have been tabulated and analysed in section 7.5.

7.5 Estimation results and analysis

In this section, estimated motor dimension and losses will be displayed and compared with the measured values.

Table 7.3 Estimated inner dimension of the induction motor

Motor inner dimensions	Estimated Values (in meter)
Width of stator teeth (w_{st})	0.0040
Width of stator slot at top (w_{sst})	0.0075
Width of stator slot at bottom (w_{ssb})	0.0099
Depth of stator teeth (d_{st})	0.0131
Depth of stator core (d_{sc})	0.0124
Width of rotor teeth at top (w_{rtt})	0.0082
Width of rotor teeth at bottom (w_{rtb})	0.0038
Width of rotor slot (w_{rs})	0.0026
Depth of rotor teeth (d_{rt})	0.0153
Depth of rotor core (d_{rc})	0.0124

Table 7.4 Estimated values of the variables that has been optimized to estimate the inner dimension of the induction motor

Variables to be optimized	Estimated values
Average flux density (B_{av})	0.4774 Wb/m^2
Current density in stator conductors ($Statorcurrentdensity$)	4.0064 A/mm^2
flux density at stator teeth (B_{st})	1.3891 Wb/m^2
flux density in stator core (B_{sc})	1.3419 Wb/m^2
Specific iron loss at stator teeth ($specificironloss_{st}$)	12.9062 $Watt/kg$
Specific iron loss at stator core ($specificironloss_{sc}$)	4.6034 $Watt/kg$
Current density in rotor bars ($Rotorcurrentdensity$)	6.0732 A/mm^2
flux density at rotor teeth at bottom (B_{rtb})	1.5893 Wb/m^2
flux density in rotor core (B_{rc})	1.3419 Wb/m^2

Table 7.3 and Table 7.4 represent the estimated values of motor inner dimensions and estimated motor variables. These estimated motor dimensions and motor variables were verified by comparing the motor losses and performance. Table 7.5 represent the estimated motor losses under full load condition. Estimated losses were compared with the measured full load losses and the comparison found the estimation error within acceptable limit. Table 7.6 represents the comparison of the estimated values of some of the motor performance indicators with their test values. This comparison also proves the accuracy of the estimation.

Table 7.5 Estimated losses of the induction motor under full load condition and their comparison with the measured values

Losses	**Estimated values (in Watt)**	**Measured values (in Watt)**	**% Error**
Iron loss (P_{iron})	97.1378	98.3064	1.188732
Friction and windage loss (P_{fw})	11	11	0
Stator copper loss ($P_{cu_{stat}}$)	118.3536	122.9075	3.705144
Rotor copper loss ($P_{cu_{rot}}$)	86.4687	85.0357	-1.68517

Table 7.6 Comparison of estimated motor performance indicators with corresponding values obtained from test under rated condition

Motor performance indicators	**Estimated values**	**Test values**	**% Error**
Stator resistance (R_s)	7.3348 Ω	7.2 Ω	-1.87
Rotor resistance (R_r)	5.3587 Ω	5.5 Ω	2.57
Magnetizing current (I_m)	1.2202 A	1.22 A	-0.016
Power factor (pf)	0.7737	0.74	-4.55
Efficiency (η)	0.7785	0.79	1.456
Speed	1402 RPM	1400 RPM	-0.143

Now, from the estimated motor dimensions, if the thermal resistances and capacitances are precisely calculated and losses are fed into the appropriate nodes of a thermal model, the temperature at different parts of the machine can be predicted. For this purpose, an accurate thermal model needs to be developed, which is discussed in section 7.6.

7.6 Temperature estimation and validation of the proposed scheme

This section describes the temperature profiles for different parts of the machine under full load condition. Motor temperature was estimated using the thermal model proposed in section 6.3. The proposed scheme was validated by comparing the estimated temperature with the measured value. In this experiment, the motor was allowed to run under full load condition for two hours continuously. This helps the machine to achieve the thermal equilibrium. After two hours, the machine was stopped and allowed to cool down for three hours. During the experiment, the frame temperature at both driving and non-driving end, shaft temperature at driving end and end-shield temperature at driving end was measured at a 5 min interval during the running as well as cooling period using an optical temperature sensor. As the non-driving end of the motor was equipped with the fan and fan cover, hence, the temperature of end shield and shaft at non-driving end could not be recorded. The temperature of stator winding was measured using a kelvin double bridge during cooling period only. The temperature of other inner parts of the machine could not be measured due to lack of available instrumentation. However, the estimated temperature profile of those machine parts shows good correlation with the temperature of the other parts of the machine. Fig 7.2 – 7.11 depict the estimated temperature profile of different parts of the machine and present a comparison with the measured temperature values, if feasible.

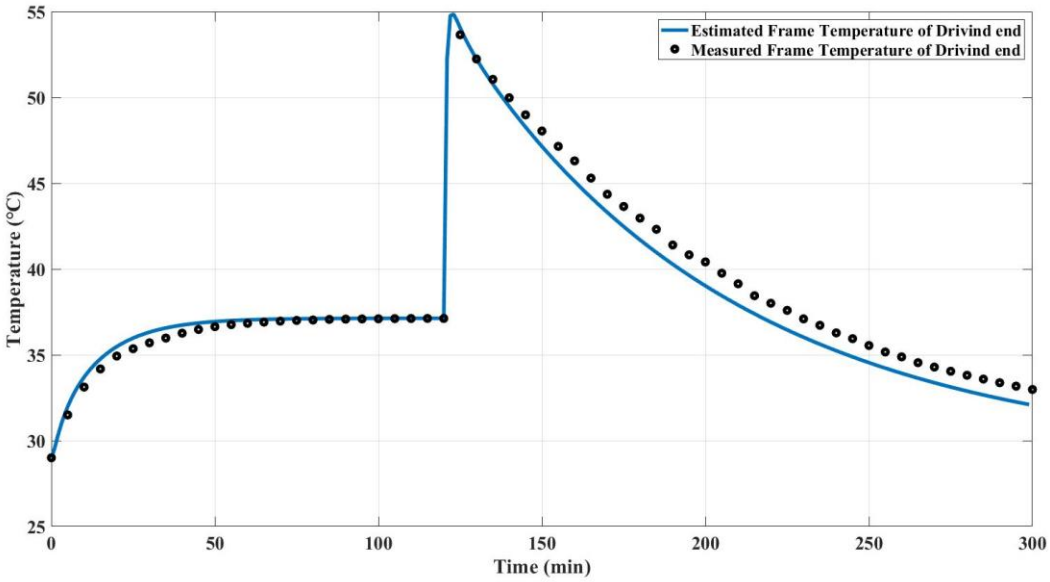

(a)

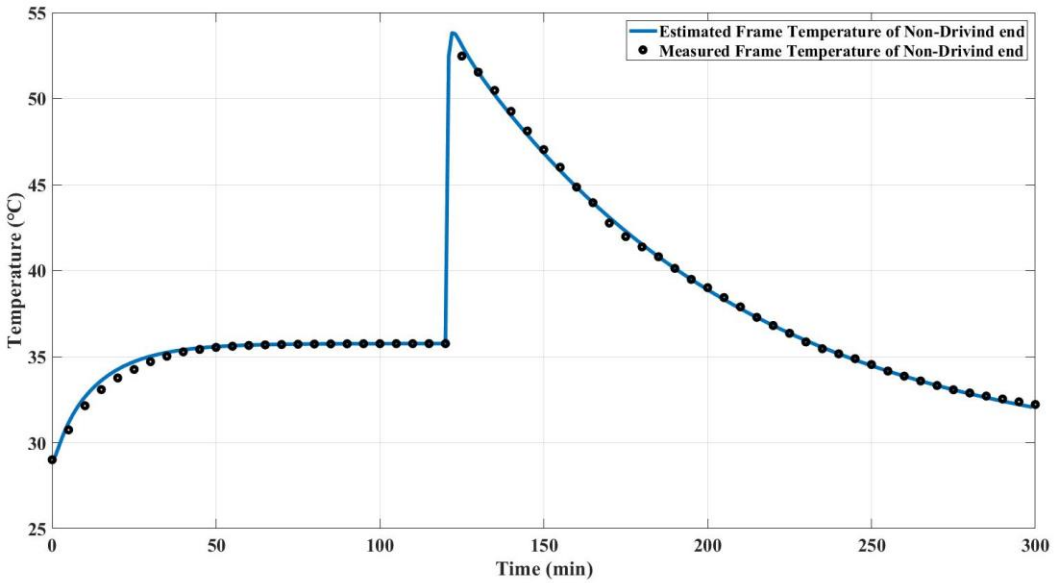

(b)

Fig. 7.2. Comparison of estimated and measured frame temperature at (a) driving end, (b) non-driving end.

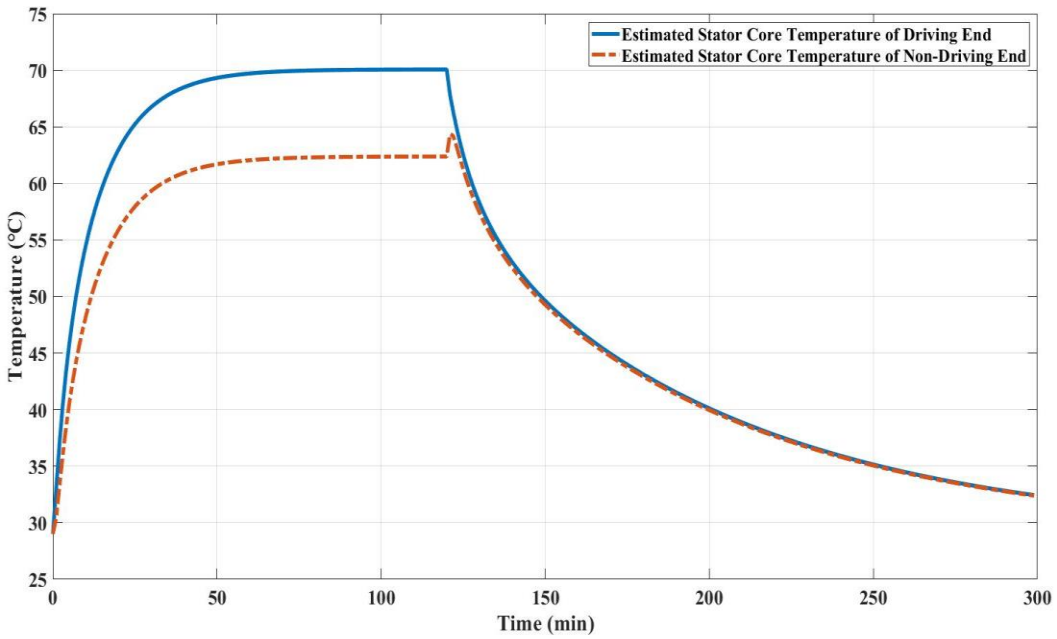

Fig. 7.3. Estimated stator core temperature at driving and non-driving end.

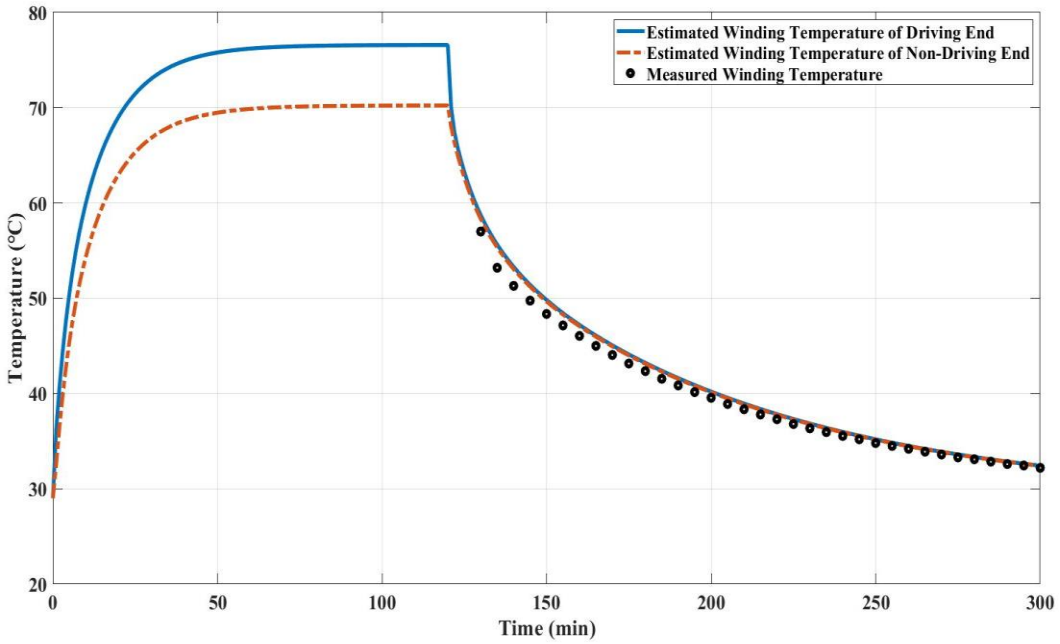

Fig. 7.4. Estimated stator winding temperature at driving and non-driving end and comparison with measured winding temperature during cooling period.

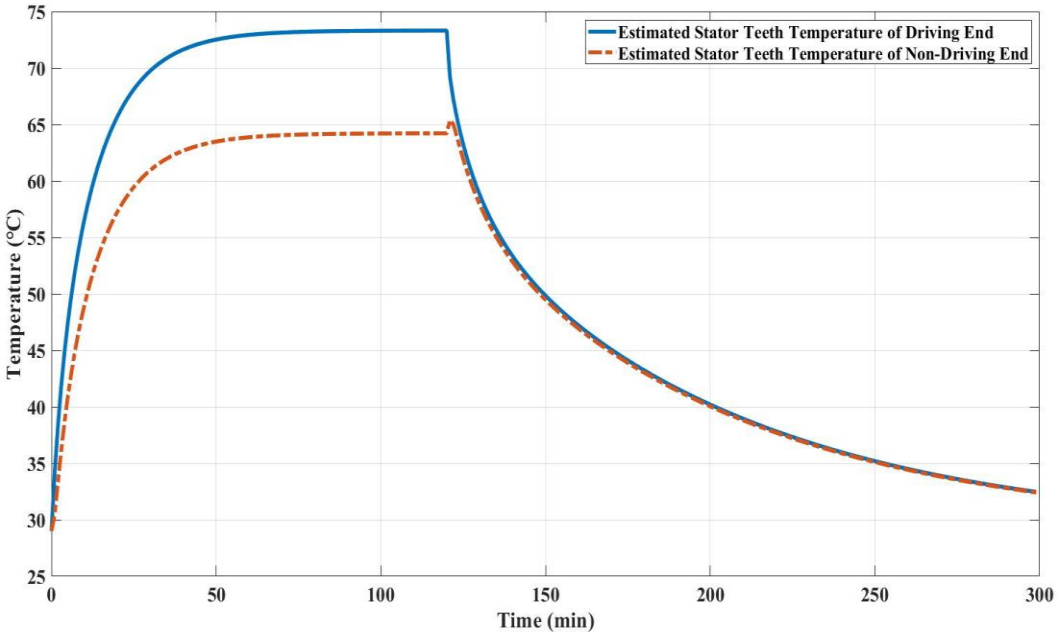

Fig. 7.5. Estimated stator teeth temperature at driving and non-driving end.

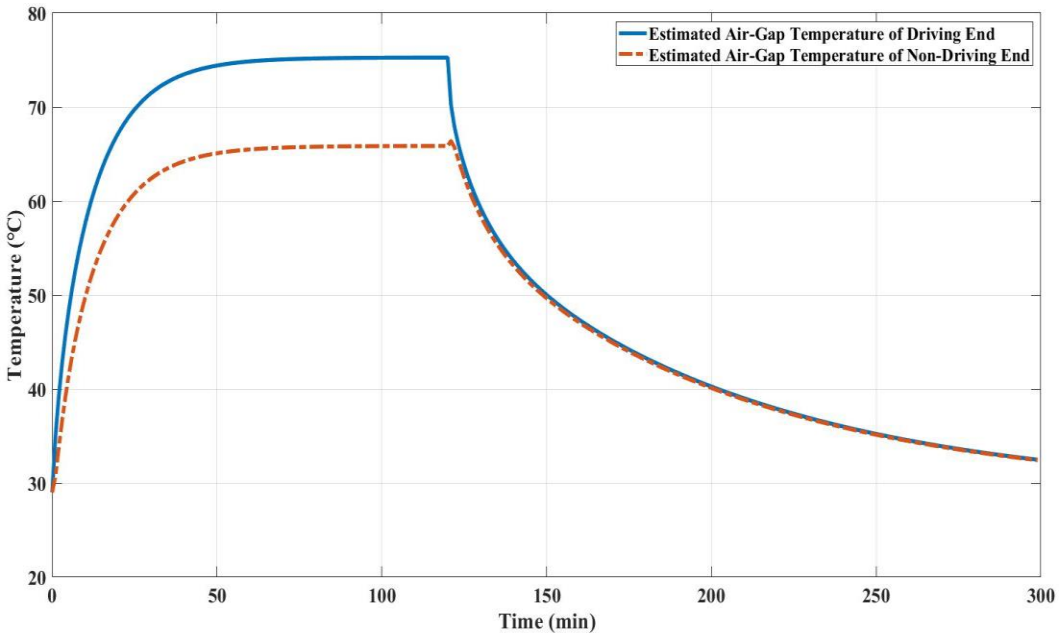

Fig. 7.6. Estimated air-gap temperature at driving and non-driving end.

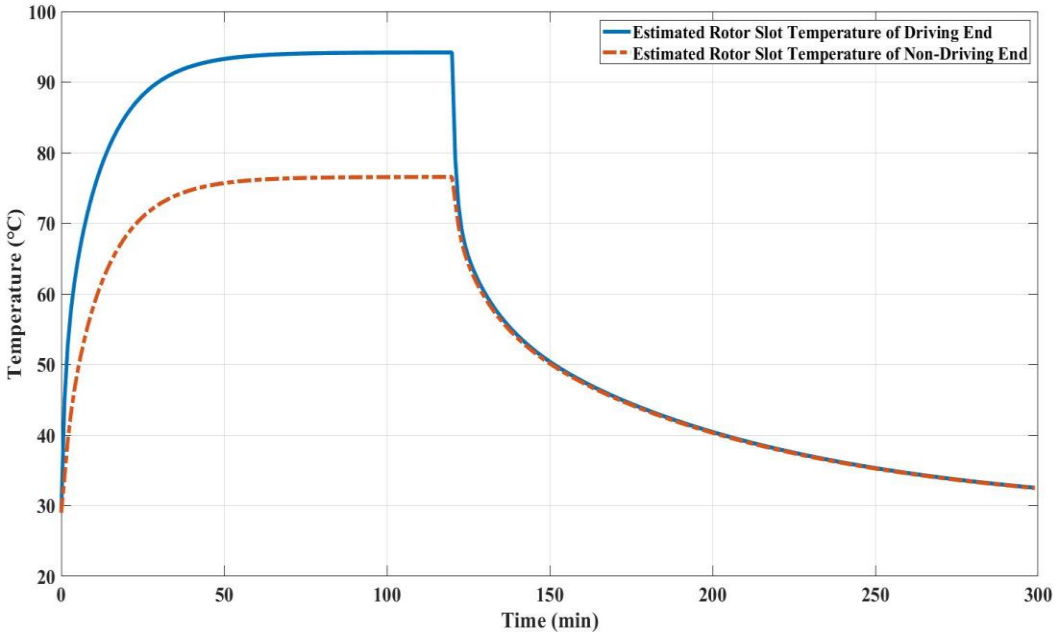

Fig. 7.7. Estimated rotor slot temperature at driving and non-driving end.

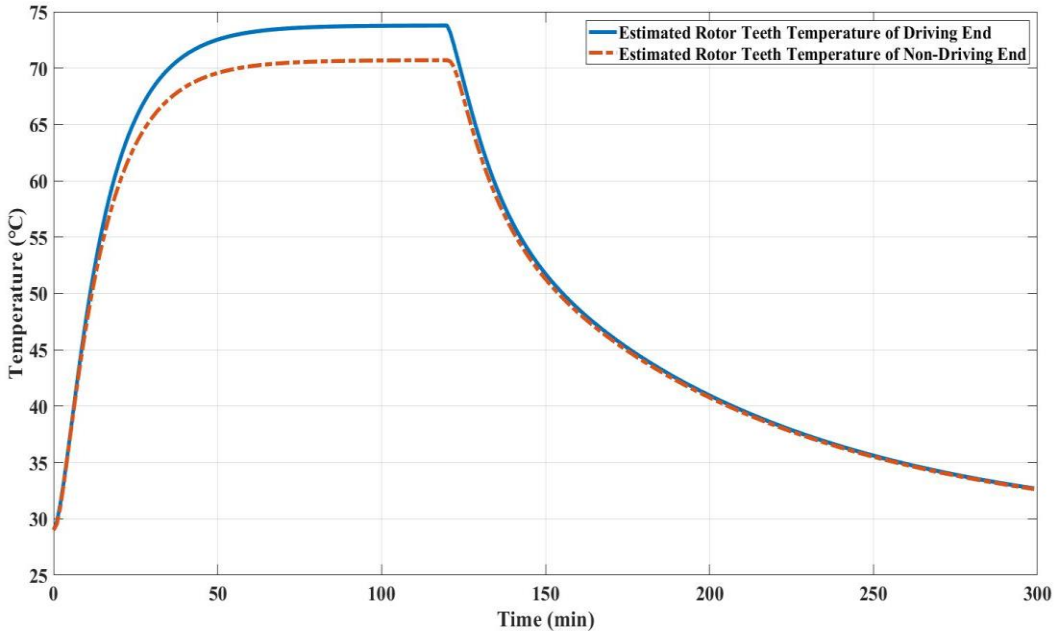

Fig. 7.8. Estimated rotor teeth temperature at driving and non-driving end.

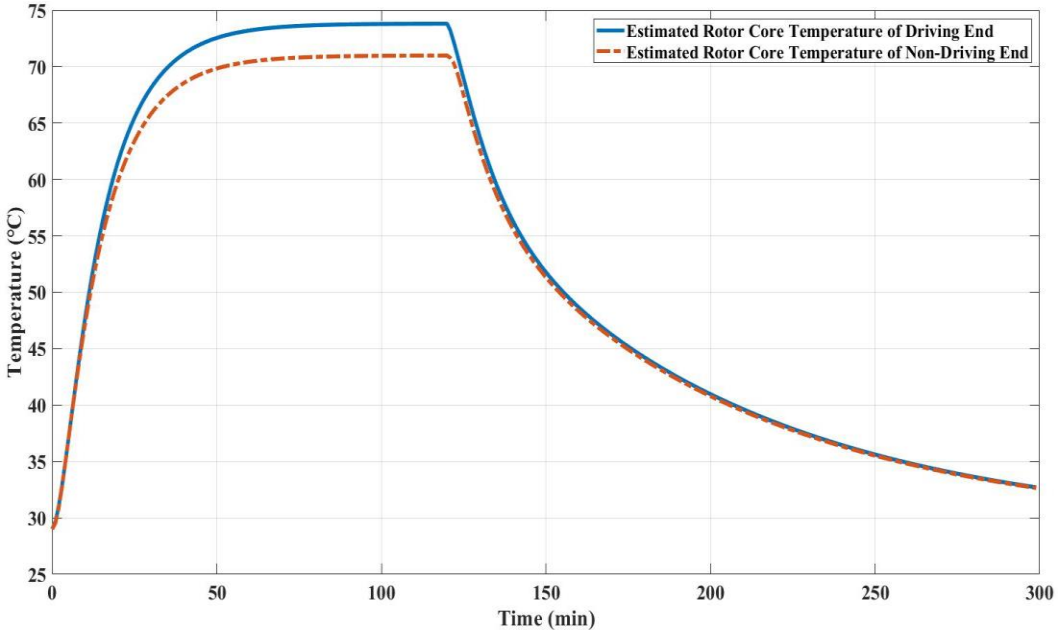

Fig. 7.9. Estimated rotor core temperature at driving and non-driving end.

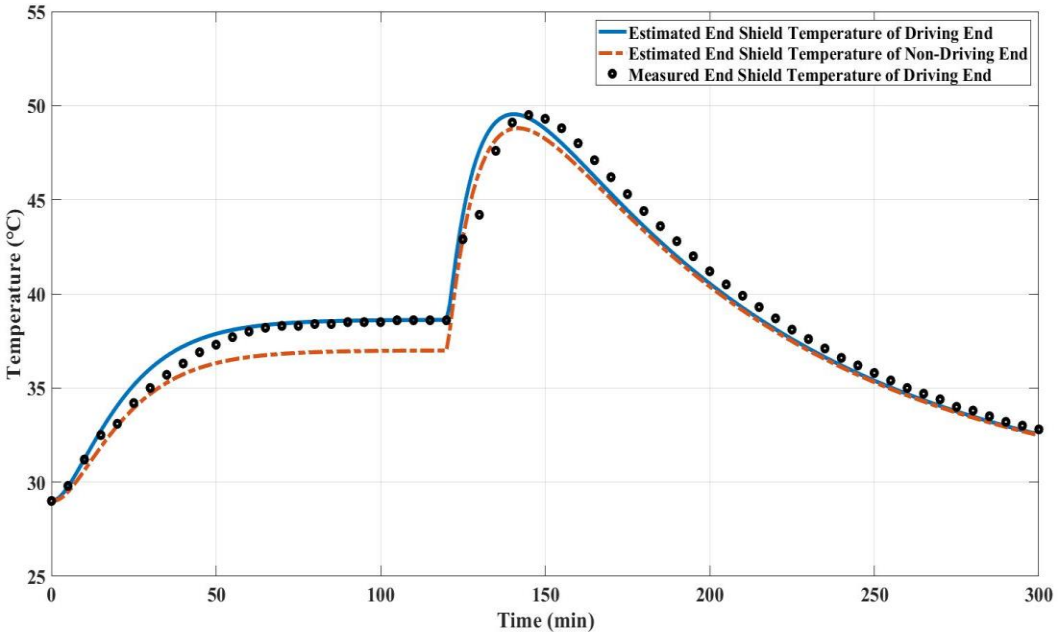

Fig. 7.10. Estimated end shield temperature at driving and non-driving end and comparison with measured value at driving end.

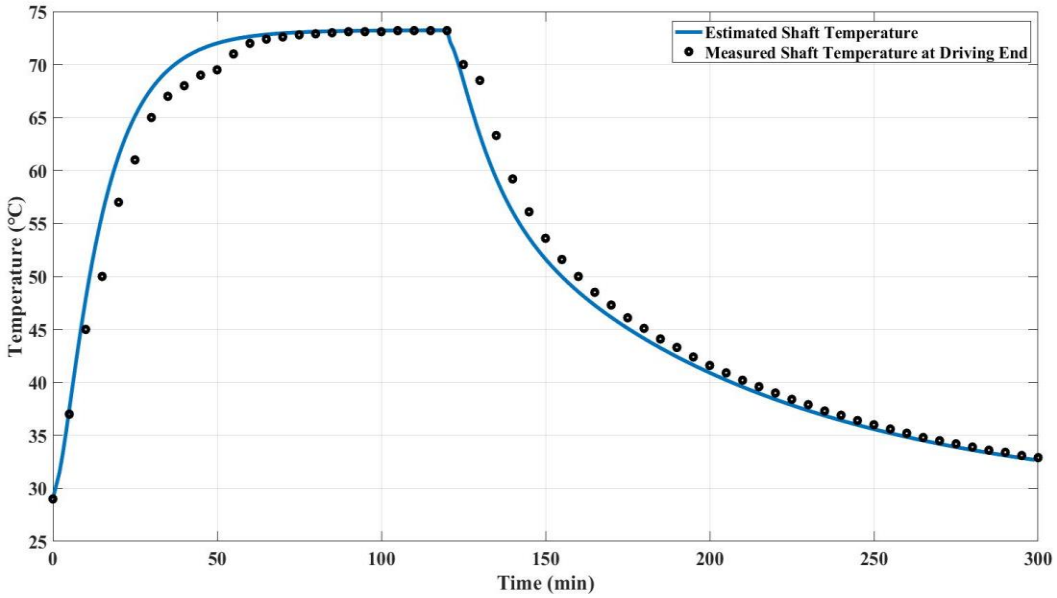

Fig. 7.11. Comparison of estimated shaft temperature with measured value at driving end.

Fig 7.12 depicts the steady state temperature of all nodes at driving and non-driving end. This estimated temperature distribution pattern shows similar characteristics as described in chapter 6, Fig 6.15, hence exhibits the expected nature.

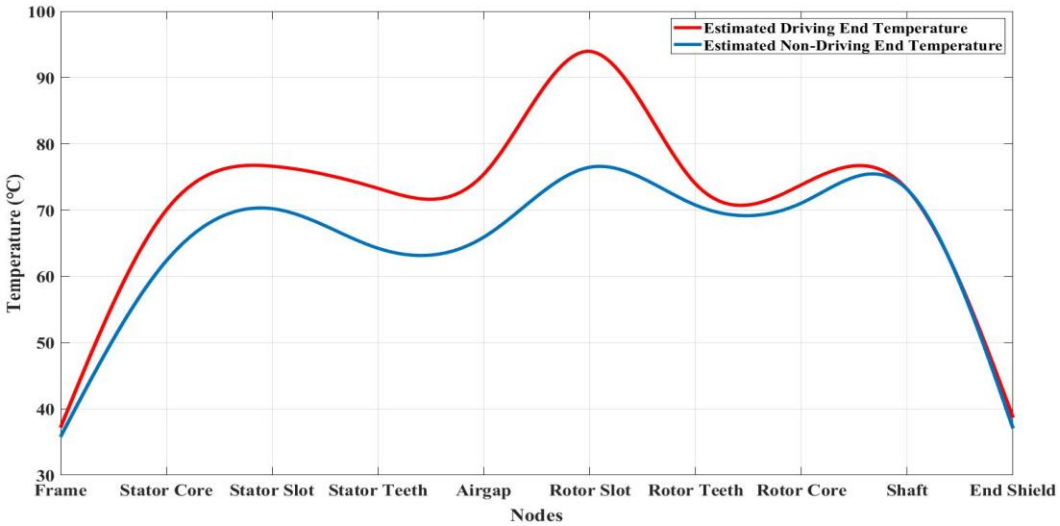

Fig. 7.12. Estimated temperature distribution characteristics of the induction motor at driving end and non-driving end under full load condition.

7.7 Conclusion and scope of future work

This work has successfully addressed the critical challenges associated with temperature estimation that includes the estimation of inner dimension of the induction motor. The development and extension of the proposed temperature estimation scheme have proven to be instrumental in accurately predicting temperature distributions across various motor components.

For practical solution of temperature estimation of induction motors, it is necessary to develop a specialized estimation scheme, that can predict the inner motor dimensions, because, dimensional data is neither readily available, nor can be measured easily, without completely dismantling the machine. From the performance characteristics and frame size of the induction motor, the extended scheme offers a real-world solution to this longstanding challenge.

Furthermore, the research is not only focused on achieving precise temperature estimates but also identifies the critical design considerations. The comparative analysis of estimated and measured performance indicators, utilizing machine design equations, has allowed for the identification and implementation of design parameters that align optimally with the actual motor performance.

This work signifies a step forward in the domain of temperature estimation for induction motors, offering a complete approach that combines theoretical models with practical applications. The insights derived from this study provide a valuable foundation for future advancements in the field, contributing to the ongoing evolution of motor design and temperature management techniques.

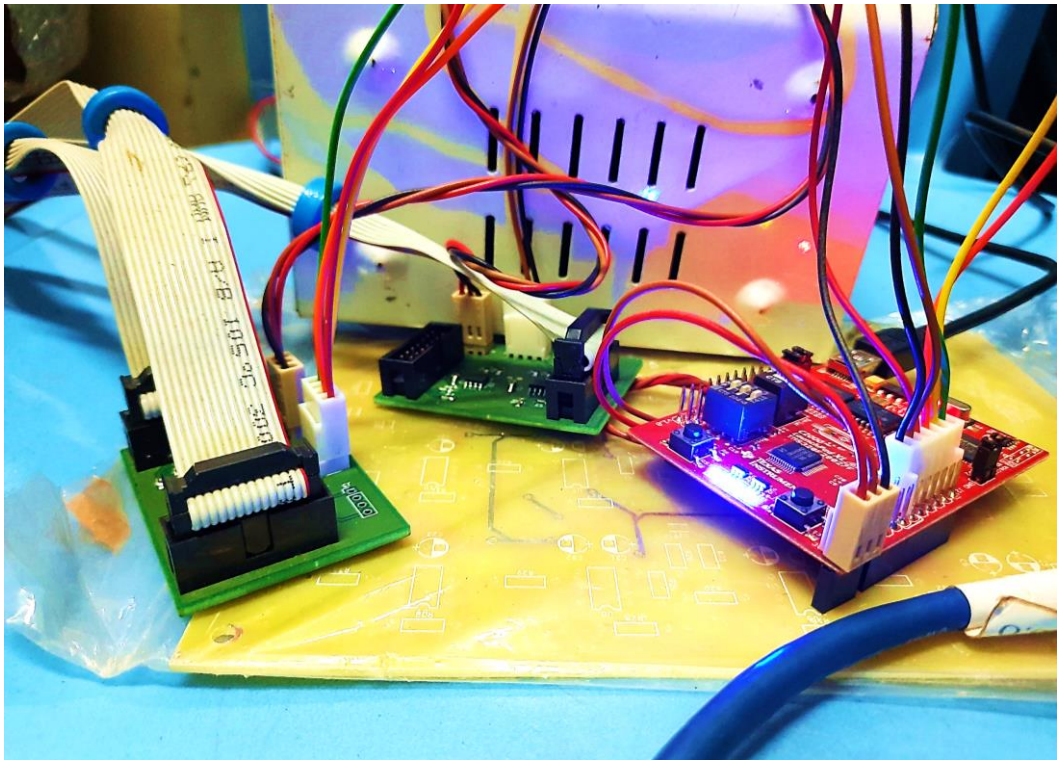

CHAPTER 8

Conclusion and Future Work

The integration of equivalent circuit parameters, loss estimation, and a comprehensive thermal model represents a significant leap forward in induction motor temperatire estimation. The proposed technique can be further explored to assess its contribution in the domain of temperature based predictive condition monitoring of induction motor. This holistic approach offers a deeper understanding of motor behavior, enabling proactive maintenance, extended lifespan, and improved efficiency. By building upon this foundation and exploring further advancements, the optimal performance and longevity of induction motors can be assured, contributing to a more sustainable and efficient future for motor-driven systems.

8.1 Conclusion

The equivalent circuit model provides a fundamental framework for understanding induction motors operation. Accurate estimation of circuit parameters such as resistance, leakage reactance, magnetising reactance and core loss resistance, provides valuable insights into the motor's dynamic response under varying operating conditions. Quantifying losses gives a comprehensive assessment of motor efficiency and performance. A robust assessment of motor parameters and losses is thus crucial for in-depth analysis of motor behaviour, enhancing motor lifespan and optimizing motor performance.

While electrical parameters offer valuable insights into motor performance, they do not fully capture the thermal dynamics that influence motor health. Overheating is a common cause of motor failure, leading to insulation degradation, bearing wear, resulting in catastrophic breakdowns. By simulating temperature profiles of the motor under various operating conditions, thermal models provide crucial information for preventing overheating and predicting potential failures.

The integration of equivalent circuit parameters, loss estimation, and thermal modelling offers a holistic approach in the field of temperature estimation of induction motor. The methodology begins by estimating equivalent circuit parameters and losses of the motor, by analyzing collected performance data applying suitable optimization techniques. The equivalent circuit parameters, loss estimation, and thermal modelling components are integrated with a thermal model for prediction of motor temperature. The integrated monitoring system will enable operators to plan proactive maintenance strategies. The developed methodology offers a versatile, robust and simple approach. The scheme can be applied across

various industries, with proper problem specific modifications. A well-designed system is able to handle variations in operating conditions and environmental factors and will allow the operators to identify potential issues. It will minimize downtime, reduce energy consumption, and prolong the lifespan of induction motors, leading to cost savings and environmental benefits resulting in sustainable industrial processes.

8.2 Future work

This work serves as a foundation for further advancements in the field of induction motor condition monitoring. Under the laboratory environment, the results look promising; however, validating the accuracy and reliability of the integrated system under different industrial environmental circumstances, for motors with different specifications, is essential for ensuring its effectiveness in real-world applications. Future research may focus on validating the system across different industrial processes, improving its performance.

Advanced and more efficient newly developed optimization techniques may be applied to improve the developed system. This work also opens up opportunities for incorporating advanced technologies such as artificial intelligence (AI) and machine learning (ML) in the field of motor condition monitoring. The integration of an IoT-based online monitoring mechanism can be explored to facilitate real-time condition monitoring of induction motors. This system will require a computationally efficient estimation algorithm such as Recursive Least Squares (RLS) or Extended Kalman Filters (EKF) that can be feasibly implemented in real-time, to ensure timely and accurate parameter estimation without overwhelming the processing capabilities of IoT devices.

Utilizing emerging sensor technologies like wireless sensors and development of cloud-based system can provide more advanced data handling and storage scheme for in-depth analysis.

Developing standardized protocols, guidelines, and best practices are also essential to facilitate the implementation of the integrated monitoring systems and its widespread adoption across industries.

References

[1] L. Zhao, J. Huang, J. Chen and M. Ye, "A Parallel Speed and Rotor Time Constant Identification Scheme for Indirect Field Oriented Induction Motor Drives," IEEE Transactions on Power Electronics, vol. 31, no. 9, pp. 6494-6503, Sept. 2016, doi: 10.1109/TPEL.2015.2504399.

[2] M. Carraro and M. Zigliotto, "Automatic Parameter Identification of Inverter-Fed Induction Motors at Standstill," IEEE Transactions on Industrial Electronics, vol. 61, no. 9, pp. 4605-4613, Sept. 2014, doi: 10.1109/TIE.2013.2289903.

[3] M. Al-Badri, P. Pillay and P. Angers, "A Novel In Situ Efficiency Estimation Algorithm for Three-Phase IM Using GA, IEEE Method F1 Calculations, and Pretested Motor Data," IEEE Transactions on Energy Conversion, vol. 30, no. 3, pp. 1092-1102, Sept. 2015, doi: 10.1109/TEC.2015.2421288.

[4] E. Laroche and M. Boutayeb, "Identification of the Induction Motor in Sinusoidal Mode," IEEE Transactions on Energy Conversion, vol. 25, no. 1, pp. 11-19, March 2010, doi: 10.1109/TEC.2009.2035512.

[5] Hamoudi Abdallah, Kouadri Benatman., "Stator winding inter-turn short-circuit detection in induction motors by parameter identification," IET Electric Power Applications, Volume 11, Issue 2, p. 272 – 288, February 2017. DOI: 10.1049/iet-epa.2016.0432.

[6] X. Liang, M. Z. Ali and H. Zhang, "Induction Motors Fault Diagnosis Using Finite Element Method: A Review," in IEEE Transactions on Industry Applications, vol. 56, no. 2, pp. 1205-1217, March-April 2020, doi: 10.1109/TIA.2019.2958908.

[7] P. Balakrishna and U. Khan, "An Autonomous Electrical Signature Analysis-Based Method for Faults Monitoring in Industrial Motors," IEEE Transactions on Instrumentation and Measurement, vol. 70, pp. 1-8, 2021, Art no. 3512008, doi: 10.1109/TIM.2021.3059466.

[8] J. E. Garcia-Bracamonte, J. M. Ramirez-Cortes, J. de Jesus Rangel-Magdaleno, P. Gomez-Gil, H. Peregrina-Barreto and V. Alarcon-Aquino, "An Approach on MCSA-Based Fault Detection Using Independent Component Analysis and Neural Networks," IEEE Transactions on Instrumentation and Measurement, vol. 68, no. 5, pp. 1353-1361, May 2019, doi: 10.1109/TIM.2019.2900143.

[9] M. R. Barusu and M. Deivasigamani, "Non-Invasive Vibration Measurement for Diagnosis of Bearing Faults in 3-Phase Squirrel Cage Induction Motor Using Microwave Sensor," IEEE Sensors Journal, vol. 21, no. 2, pp. 1026-1039, 15 Jan.15, 2021, doi: 10.1109/JSEN.2020.3004515.

[10] J. Du, Y. Li, Z. Yu and Z. Wang, "Research on Radial Electromagnetic Force and Vibration Response Characteristics of Squirrel-Cage Induction Motor Fed by PWM Inverter," IEEE Transactions on Applied Superconductivity, vol. 31, no. 8, pp. 1-4, Nov. 2021, Art no. 5205304, doi: 10.1109/TASC.2021.3096501.

[11] P. Pescetto, S. Ferrari, G. Pellegrino, E. Carpaneto and A. Boglietti, "Winding Thermal Modeling and Parameters Identification for Multithree Phase Machines Based on Short-Time Transient Tests," IEEE Transactions on Industry Applications, vol. 56, no. 3, pp. 2472-2480, May-June 2020, doi: 10.1109/TIA.2020.2969643.

[12] J. de Pelegrin, U. J. Dreyer, J. P. Bazzo and J. C. C. d. Silva, "Faults Diagnosis in Induction Motors Through Thermal Mapping Produced by the RDTS System," IEEE Sensors Journal, vol. 21, no. 18, pp. 20061-20068, 15 Sept.15, 2021, doi: 10.1109/JSEN.2021.3097940.

[13] IEEE Standard Test Procedure for Polyphase Induction Motors and Generators, IEEE Std. 112, 2004.

[14] Keun Lee, Stephen Frank, and Pankaj K. (PK) Sen, et.al, "Estimation of Induction Motor Equivalent Circuit Parameters from Nameplate Data", North American Power Symposium (NAPS), 9-11 Sept. 2012, DOI: 10.1109/NAPS.2012.6336384.

[15] S. R. P. Reddy and U. Loganathan, "Offline Recursive Identification of Electrical Parameters of VSI-Fed Induction Motor Drives," IEEE Transactions on Power Electronics, vol. 35, no. 10, pp. 10711-10719, Oct. 2020, doi: 10.1109/TPEL.2020.2978932.

[16] S. A. Odhano, P. Pescetto, H. A. A. Awan, M. Hinkkanen, G. Pellegrino and R. Bojoi, "Parameter Identification and Self-Commissioning in AC Motor Drives: A Technology Status Review," IEEE Transactions on Power Electronics, vol. 34, no. 4, pp. 3603-3614, April 2019, doi: 10.1109/TPEL.2018.2856589.

[17] M. H. Haque, "Determination of NEMA Design Induction Motor Parameters from Manufacturer Data," IEEE Transactions on Energy Conversion, vol. 23, no. 4, pp. 997-1004, Dec. 2008, doi: 10.1109/TEC.2008.2001451.

[18] Manuel Gomez-Gonzalez, Francisco Jurado & I. Perez, (2012). "Shuffled frog-leaping algorithm for parameter estimation of a double-cage asynchronous machine", Electric Power Applications, IET. 6. 484-490. 10.1049/iet-epa.2011.0262.

[19] A. Boglietti, A. Cavagnino and M. Lazzari, "Computational Algorithms for Induction-Motor Equivalent Circuit Parameter Determination—Part I: Resistances and Leakage Reactances," IEEE Transactions on Industrial Electronics, vol. 58, no. 9, pp. 3723-3733, Sept. 2011, doi: 10.1109/TIE.2010.2084974.

[20] A. Boglietti, A. Cavagnino and M. Lazzari, "Computational Algorithms for Induction Motor Equivalent Circuit Parameter Determination—Part II: Skin Effect and Magnetizing Characteristics," IEEE Transactions on Industrial Electronics, vol. 58, no. 9, pp. 3734-3740, Sept. 2011, doi: 10.1109/TIE.2010.2084975.

[21] S. Lee, A. Yoo, H. Lee, Y. Yoon and B. Han, "Identification of Induction Motor Parameters at Standstill Based on Integral Calculation," IEEE Transactions on Industry Applications, vol. 53, no. 3, pp. 2130-2139, May-June 2017, doi: 10.1109/TIA.2017.2650141.

[22] M. Stender, O. Wallscheid and J. Böcker, "Accurate Torque Control for Induction Motors by Utilizing a Globally Optimized Flux Observer," IEEE Transactions on Power Electronics, vol. 36, no. 11, pp. 13261-13274, Nov. 2021, doi: 10.1109/TPEL.2021.3080129.

[23] D. M. Reed, H. F. Hofmann and J. Sun, "Offline Identification of Induction Machine Parameters With Core Loss Estimation Using the Stator Current Locus," IEEE Transactions on Energy Conversion, vol. 31, no. 4, pp. 1549-1558, Dec. 2016, doi: 10.1109/TEC.2016.2601781.

[24] A. Accetta, F. Alonge, M. Cirrincione, F. D'Ippolito, M. Pucci and A. Sferlazza, "GA-based off-line parameter estimation of the induction motor model including magnetic

saturation and iron losses," in 2017 IEEE Energy Conversion Congress and Exposition (ECCE), 2017, pp. 2420-2426, doi: 10.1109/ECCE.2017.8096466.

[25] M. Perin, L. A. Pereira, L. F. A. Pereira and G. Nicol, "Estimation of Parameters of Five-Phase Induction Motors Using Step Voltage at Standstill," in IEEE Transactions on Energy Conversion, vol. 36, no. 4, pp. 3491-3501, Dec. 2021, doi: 10.1109/TEC.2021.3085221.

[26] H. Kojooyan-Jafari, L. Monjo, F. Córcoles and J. Pedra, "Parameter Estimation of Wound-Rotor Induction Motors From Transient Measurements," IEEE Transactions on Energy Conversion, vol. 29, no. 2, pp. 300-308, June 2014, doi: 10.1109/TEC.2014.2300236.

[27] K. S. Huang, Q. H. Wu and D. R. Turner, "Effective identification of induction motor parameters based on fewer measurements," IEEE Transactions on Energy Conversion, vol. 17, no. 1, pp. 55-60, March 2002, doi: 10.1109/60.986437.

[28] Z. Masoumi, B. Moaveni, M. Khorshidi, J. Faiz and S. M. M. Gazafrudi, "Experimental Parameter Estimation of Induction Motor Based on Transient and Steady-State Responses in Synchronous and Rotor Reference Frames," IEEE Transactions on Energy Conversion, vol. 37, no. 1, pp. 145-152, March 2022, doi: 10.1109/TEC.2021.3094521.

[29] S. Yang, D. Ding, X. Li, Z. Xie, X. Zhang and L. Chang, "A Novel Online Parameter Estimation Method for Indirect Field Oriented Induction Motor Drives," IEEE Transactions on Energy Conversion, vol. 32, no. 4, pp. 1562-1573, Dec. 2017, doi: 10.1109/TEC.2017.2699681.

[30] J. Benzaquen, J. Rengifo, E. Albánez and J. M. Aller, "Parameter Estimation for Deep-Bar Induction Machines Using Instantaneous Stator Measurements From a Direct Startup," IEEE Transactions on Energy Conversion, vol. 32, no. 2, pp. 516-524, June 2017, doi: 10.1109/TEC.2017.2657647.

[31] S. Foti, A. Testa, S. De Caro, T. Scimone and M. Pulvirenti, "Rotor Flux Position Correction and Parameters Estimation on Sensorless Multiple Induction Motors Drives," IEEE Transactions on Industry Applications, vol. 55, no. 4, pp. 3759-3769, July-Aug. 2019, doi: 10.1109/TIA.2019.2906862.

[32] O. Rodríguez-Abreo, J. M. Hernandez-Paredes, A. F. Rangel, C. Fuentes-Silva and F. A. C. Velásquez, "Parameter Identification of Motors by Cuckoo Search Using Steady-State Relations," IEEE Access, vol. 9, pp. 72017-72024, 2021, doi: 10.1109/ACCESS.2021.3078578.

[33] S. Khadar, H. Abu-Rub and A. Kouzou, "Sensorless Field-Oriented Control for Open-End Winding Five-Phase Induction Motor With Parameters Estimation," IEEE Open Journal of the Industrial Electronics Society, vol. 2, pp. 266-279, 2021, doi: 10.1109/OJIES.2021.3072232.

[34] G. B. Reddy, G. Poddar and B. P. Muni, "Parameter Estimation and Online Adaptation of Rotor Time Constant for Induction Motor Drive," IEEE Transactions on Industry Applications, vol. 58, no. 2, pp. 1416-1428, March-April 2022, doi: 10.1109/TIA.2022.3141700.

[35] M. Reza Feyzi and M. Sabahi, “Online dynamic parameter estimation of transformer equivalent circuit,” in Proc. 5th. IEEE Int. Conf. Power Electron. Motion Control, 2006, vol. 2, pp. 1–5.

[36] Y. Koubaa, "Recursive identification of induction motor parameters," Journal of Simulation Modeling Practice and Theory, Vol. 12, Issue 5, pp. 363-381, August 2004.

[37] Zhang Hu, Gong Shu-juan, Dong Zi-zhao, "On-Line Parameter Identification of Induction Motor Based On RLS Algorithm", 2013 International Conference on Electrical Machines and Systems, Oct. 26-29, 2013 , Busan, Korea.

[38] Ebrahim Rahimpour, Mehdi Bigdeli, "Simplified transient model of transformer based on geometrical dimensions used in power network analysis and fault detection studies", 2009 International Conference on Power Engineering, Energy and Electrical Drives, March 18-20, 2009.

[39] P. S. Szczepaniak and M. Rudnicki, "Soft-computing methods for diagnosis and design of electrical devices", Africon, 1999, IEEE Volume:2, 28 Sep-01 Oct, 1999.

[40] Mehdi Bigdeli, Ebrahim Rahimpour, "Estimation of simplified transient model parameters using genetic algorithm", 2010 18th Iranian Conference on Electrical Engineering, 11-13 May 11-13, 2010.

[41] S. Subramanian and S. Padma, "Bacterial foraging algorithm-based parameter estimation of three winding transformer," Energy Power Eng. J., vol. 3, pp. 135–143, 2011.

[42] Mohamed I. Mossad, Mohamed Azab, and A. Abu-Siada,"Transformer Parameters Estimation From Nameplate Data Using Evolutionary Programming Techniques", IEEE Transactions on Power Delivery, vol. 29, no. 5, October 2014.

[43] Nangsue P, Pillay P, Conry S. "Evolutionary Algorithms for Induction Motor Parameter Determination". IEEE Transactions Energy Conversion.1999. 14(3), pp:447-453.

[44] Hong-yu Zhu, Wan-sheng Cheng, Zhu-zhi Jia, Wei-Gang Hou, "Parameter estimation of induction motor based on chaotic ant swarm algorithm" 2nd International Conference on Information Science and Engineering, Dec 4-6, 2010.

[45] Burak Tekgun, Yilmaz Sozer, Senior Member, IEEE, and Igor Tsukerman, "Modeling and Parameter Estimation of Split-Phase Induction Motors", IEEE Transactions on Industry Applications, Vol. 52, No. 2, March/April 2016.

[46] Ali Karimi, Muhammad A. Choudhry, Ali Feliachi, "PSO-based Evolutionary Optimization for Parameter Identification of an Induction Motor", 39th North American Power Symposium, 2007. NAPS '07. Sept. 30 2007-Oct. 2 2007, pp.659 - 664.

[47] Hassan M. Emara, Wesam Elshamy, A. Bahgat, "Parameter identification of induction motor using modified Particle Swarm Optimization algorithm", 2008 IEEE International Symposium on Industrial Electronics, June 30 2008-July 2 2008, pp.841 – 847.

[48] P. Tavner, L. Ran, J. Penman and H. Sedding, Condition Monitoring of Rotating Electrical Machines, London, United Kingdom, IET Power and Energy Series 56, The Institution of Engineering and Technology, ISBN 978-0-86341-739-9, 2008.

[49] J. Xiaochun, Y. Geng, W. Yunfei, "A parameter identification method for general inverter-fed induction motor drive", 2006 CES/IEEE 5th International Power Electronics and Motion Control Conference, 14-16 Aug. 2006.

[50] Y. He, Y. Feng, Y. Wang, "Estimating the electrical parameters of induction motors at standstill using RLS method", The 2nd International Symposium on Power Electronics for Distributed Generation Systems, 16-18 June 2010.

[51] A. G. Yepes, J. A. Riveros, J. Doval-Gandoy, F. Barrero, Ó. Lopez, B. Bogado, M. Jones, E. Levi, "Parameter identification of multiphase induction machines with distributed windings—Part 1: Sinusoidal excitation methods", IEEE Transactions on Energy Conversion, Volume: 27 , Issue: 4 , Dec. 2012, Page(s): 1056 – 1066.

[52] P. N. Phuc, D. Bozalakov, H. Vansompel, K. Stockman and G. Crevecoeur, "Rotor Temperature Virtual Sensing for Induction Machines Using a Lumped-Parameter Thermal Network and Dual Kalman Filtering," in IEEE Transactions on Energy Conversion, vol. 36, no. 3, pp. 1688-1699, Sept. 2021, doi: 10.1109/TEC.2021.3060478.

[53] H. Zhao et al., "Parameter Identification Based Online Noninvasive Estimation of Rotor Temperature in Induction Motors," in IEEE Transactions on Industry Applications, vol. 57, no. 1, pp. 417-426, Jan.-Feb. 2021, doi: 10.1109/TIA.2020.3039940.

[54] S. Makkena and K. S. Sandhu, "Temperature estimation of induction motor fed with unbalanced supply," 2015 International Conference on Energy, Power and Environment: Towards Sustainable Growth (ICEPE), Shillong, India, 2015, pp. 1-5, doi: 10.1109/EPETSG.2015.7510133.

[55] X. Liang, "Temperature Estimation and Vibration Monitoring for Induction Motors and the Potential Application in Electrical Submersible Motors," in Canadian Journal of Electrical and Computer Engineering, vol. 42, no. 3, pp. 148-162, Summer 2019, doi: 10.1109/CJECE.2018.2875111.

[56] A. Boglietti, A. Cavagnino, M. Lazzari and M. Pastorelli, "A simplified thermal model for variable-speed self-cooled industrial induction motor," in IEEE Transactions on Industry Applications, vol. 39, no. 4, pp. 945-952, July-Aug. 2003, doi: 10.1109/TIA.2003.814555.

[57] Z. Gao, R. S. Colby and L. Turner, "Supply Frequency Tracking in Resistance-Based Induction Motor's Rotor Temperature Estimation," in IEEE Transactions on Industry Applications, vol. 50, no. 5, pp. 3161-3172, Sept.-Oct. 2014, doi: 10.1109/TIA.2014.2301863.

[58] K. -H. Seong, J. Hwang, J. Shim and H. -W. Cho, "Investigation of Temperature Rise in an Induction Motor Considering the Effect of Loading," in IEEE Transactions on Magnetics, vol. 50, no. 11, pp. 1-4, Nov. 2014, Art no. 8206304, doi: 10.1109/TMAG.2014.2327112.

[59] L. He, S. Cheng, Y. Du, R. G. Harley and T. G. Habetler, "Stator Temperature Estimation of Direct-Torque-Controlled Induction Machines via Active Flux or Torque Injection," in IEEE Transactions on Power Electronics, vol. 30, no. 2, pp. 888-899, Feb. 2015, doi: 10.1109/TPEL.2014.2310902.

[60] N. Z. Popov and S. N. Vukosavic, "Estimator of the Rotor Temperature of Induction Machine Based on Terminal Voltages and Currents," in IEEE Transactions on Energy Conversion, vol. 32, no. 1, pp. 155-163, March 2017, doi: 10.1109/TEC.2016.2609502.

[61] W. Pawlus, H. Van Khang and M. Rygaard Hansen, "Temperature Rise Estimation of Induction Motor Drives Based on Loadability Curves to Facilitate Design of Electric

Powertrains," in IEEE Transactions on Industrial Informatics, vol. 13, no. 3, pp. 985-994, June 2017, doi: 10.1109/TII.2016.2641454.

[62] D. D. Reigosa, J. M. Guerrero, A. B. Diez and F. Briz, "Rotor Temperature Estimation in Doubly-Fed Induction Machines Using Rotating High-Frequency Signal Injection," in IEEE Transactions on Industry Applications, vol. 53, no. 4, pp. 3652-3662, July-Aug. 2017, doi: 10.1109/TIA.2017.2684742.

[63] Y. Zhang, J. Ruan, T. Huang, X. Yang, H. Zhu and G. Yang, "Calculation of Temperature Rise in Air-cooled Induction Motors Through 3-D Coupled Electromagnetic Fluid-Dynamical and Thermal Finite-Element Analysis," in IEEE Transactions on Magnetics, vol. 48, no. 2, pp. 1047-1050, Feb. 2012, doi: 10.1109/TMAG.2011.2174433.

[64] A. Boglietti, E. Carpaneto, M. Cossale and S. Vaschetto, "Stator-Winding Thermal Models for Short-Time Thermal Transients: Definition and Validation," in IEEE Transactions on Industrial Electronics, vol. 63, no. 5, pp. 2713-2721, May 2016, doi: 10.1109/TIE.2015.2511170.

[65] A. Choudhary, D. Goyal and S. S. Letha, "Infrared Thermography-Based Fault Diagnosis of Induction Motor Bearings Using Machine Learning," in IEEE Sensors Journal, vol. 21, no. 2, pp. 1727-1734, 15 Jan.15, 2021, doi: 10.1109/JSEN.2020.3015868.

[66] E. G. Armando, A. Boglietti, E. Carpaneto, A. Castagnini and M. Seita, "Thermal Performances of Induction Motors for Applications in Washdown Environment," in IEEE Transactions on Industry Applications, vol. 55, no. 5, pp. 4578-4584, Sept.-Oct. 2019, doi: 10.1109/TIA.2019.2917419.

[67] Y. Xia, Y. Xu, M. Ai and J. Liu, "Temperature Calculation of an Induction Motor in the Starting Process," in IEEE Transactions on Applied Superconductivity, vol. 29, no. 2, pp. 1-4, March 2019, Art no. 5201304, doi: 10.1109/TASC.2019.2895313.

[68] S. Moon and S. Lee, "High-Reliable Temperature Prediction Considering Stray Load Loss for Large Induction Machine," in IEEE Transactions on Magnetics, vol. 55, no. 6, pp. 1-5, June 2019, Art no. 8201905, doi: 10.1109/TMAG.2019.2901862.

[69] S. Nategh, H. Zhang, O. Wallmark, A. Boglietti, T. Nassen and M. Bazant, "Transient Thermal Modeling and Analysis of Railway Traction Motors," in IEEE Transactions on Industrial Electronics, vol. 66, no. 1, pp. 79-89, Jan. 2019, doi: 10.1109/TIE.2018.2821619.

[70] J. L. Gonzalez-Cordoba, R. A. Osornio-Rios, D. Granados-Lieberman, R. d. J. Romero-Troncoso and M. Valtierra-Rodriguez, "Thermal-Impact-Based Protection of Induction Motors Under Voltage Unbalance Conditions," in IEEE Transactions on Energy Conversion, vol. 33, no. 4, pp. 1748-1756, Dec. 2018, doi: 10.1109/TEC.2018.2834487.

[71] J.Kennedy and R.Eberhart, “Particle swarm optimization,” in Proc.IEEE Int. Conf.Neural Netw., Perth, Australia, 1995, vol. IV, pp.1942-1948.

[72] Konstantinos E. Parsopoulos, Michael N. Vrahatis, “Particle Swarm Optimization and Intelligence: Advances and Applications”, Information Science Publishing (IGI Global), Hershey, PA, U.S.A., ISBN-13: 978-1-61520-666-7, DOI: 10.13140/2.1.3681.1206.

[73] Aleksandar Lazinica, Particle Swarm Optimization, In-tech Publications, Austria, 2009.

[74] Hamid Reza Mohammadi, Ali Akhavan, "Parameter Estimation of Three-Phase Induction Motor Using Hybrid of Genetic Algorithm and Particle Swarm Optimization", Journal of Engineering, vol. 2014, Article ID 148204, 6 pages, 2014. https://doi.org/10.1155/2014/148204

[75] E. M. Tofighi, A. Mahdizadeh and M. R. Feyzi, "Online estimation of induction motor parameters using a modified particle swarm optimization technique," IECON 2013 - 39th Annual Conference of the IEEE Industrial Electronics Society, Vienna, Austria, 2013, pp. 3645-3650, doi: 10.1109/IECON.2013.6699715.

[76] D.C. Huynh, M.W. Dunnigan, "Parameter estimation of an induction machine using advanced particle swarm optimisation algorithms", IET Electric Power Applications, Volume 4, Issue 9, 748 – 760, 10.1049/iet-epa.2009.0296.

[77] Diarra, M.N.; Yao, Y.; Li, Z.; Niasse, M.; Li, Y.; Zhao, H, "In-Situ Efficiency Estimation of Induction Motors Based on Quantum Particle Swarm Optimization-Trust Region Algorithm (QPSO-TRA)", Energies 2022, 15(13), 4905, https://doi.org/10.3390/en15134905.

[78] Mohamed Saïd Naït Saïd and Mohamed El Hachemi Benbouzid, "H–G Diagram Based Rotor Parameters Identification for Induction Motors Thermal Monitoring", IEEE Transactions on Energy Conversion, vol 15, no1, March 2000, p 14.

[79] Dr. S Kar Chowdhury, S Maulik, "Estimation of Speed and Equivalent Circuit Parameters of Three Phase Induction Motor from Voltage and Current", Journal of The Institution of Engineers (India), Volume 90, June 2009.

[80] Wang, Jin Jiang, et al. "Concordia Transform-Based Current Analysis for Induction Motor Diagnosis." Key Engineering Materials, vol. 569–570, Trans Tech Publications, Ltd., July 2013, pp. 481–488.

[81] J. F. Martins, V. Ferno Pires and A. J. Pires, "Unsupervised Neural-Network-Based Algorithm for an On-Line Diagnosis of Three-Phase Induction Motor Stator Fault," in IEEE Transactions on Industrial Electronics, vol. 54, no. 1, pp. 259-264, Feb. 2007, doi: 10.1109/TIE.2006.888790.

[82] P. C. Krause and C. H. Thomas, "Simulation of Symmetrical Induction Machinery," IEEE Transactions on Power Apparatus and Systems, vol. 84, no. 11, pp. 1038-1053, Nov. 1965, doi: 10.1109/TPAS.1965.4766135.

[83] Paul C. Krause; Oleg Wasynczuk; Scott D. Sudhoff, "Reference-Frame Theory," Analysis of Electric Machinery and Drive Systems, IEEE, 2002, pp.109-140, doi: 10.1109/9780470544167.ch3.

[84] Paul C. Krause; Oleg Wasynczuk; Scott D. Sudhoff, "Symmetrical Induction Machines," Analysis of Electric Machinery and Drive Systems, IEEE, 2002, pp.141-190, doi: 10.1109/9780470544167.ch4.

[85] F. Zidani, M. E. H. Benbouzid, D. Diallo and M. S. Nait-Said, "Induction motor stator faults diagnosis by a current Concordia pattern-based fuzzy decision system," IEEE Transactions on Energy Conversion, vol. 18, no. 4, pp. 469-475, Dec. 2003, doi: 10.1109/TEC.2003.815832.

[86] Amr M. Amin and Omar T. Hegazy, "Swarm Intelligence Applications in Electric Machines", Particle Swarm Optimization, Aleksandar Lazinica, Intech Open, 2009, pp.11-48, doi: 10.5772/6739.ch2.

[87] Stephen J Chapman, "Induction Motors," Electric machinery fundamentals, 4th ed. New York, NY, USA: McGraw-Hill, 2005, pp. 394–401.

[88] V.P. Sakthivel, R. Bhuvaneswari, S. Subramanian, "Multi-objective parameter estimation of induction motor using particle swarm optimization," Engineering Applications of Artificial Intelligence, vol. 23, Issue 3, pp. 302-312, 2010, doi: 10.1016/j.engappai.2009.06.004.

[89] L. Haoguang, Y. Yunhua and S. Xuefeng, "Load parameter identification based on particle swarm optimization and the comparison to ant colony optimization," in 2016 IEEE 11th Conference on Industrial Electronics and Applications (ICIEA), Hefei, China, 2016, pp. 545-550, doi: 10.1109/ICIEA.2016.7603644.

[90] B. K. Bose, Modern Power Electronics and AC Drives, Prentice Hall PTR, Upper Saddle River, NJ 07458, ISBN: 0-13-016743-6, 2002.

[91] L. Yousfi, A. Bouchemha, M. Bechouat, A. Boukrouche, "Induction machine parameter identification: A comparison between GAs and PSO approaches", 2013 Eighth International Conference and Exhibition on Ecological Vehicles and Renewable Energies (EVER), 27-30 March 2013.

[92] S. K. Chowdhury and P. K. Baski, "A simple lumped parameter thermal model for electrical machine of TEFC design," *2010 Joint International Conference on Power Electronics, Drives and Energy Systems & 2010 Power India*, New Delhi, India, 2010, pp. 1-7, doi: 10.1109/PEDES.2010.5712385.

Diptarshi Bhowmick.
19/02/2024